Relevant changes

The selection and order of figures have changed as follows:

ACPD	Revised	ACPD	Revised	ACPD	Revised
1	**1**		S4cd	S9	*B3abc*
2abcdef	**4abcdef**	**7ab**	**2ac**	S10	*B3def*
2gh	**5ab**		**2bd**	S11	S9
3ab	**4gh**	**8**	S14	S12, S13, S14	
3cdef	*B1abcd*	**9**	S16	S15	S17
3gh	**5cd**	**10**	**7**	S16abce	S5abcd
	5efgh	**11**	**8**	S16dh	S6ab
4abc	**3abc**	*A1*	*A1*		S6cd
5abc	**3def**	*A2*	*A3*	S16fg	S7ab
6abce	S2abcd	*A3*	*A4*		S7cd
6dh	S3ab	S1, S2, S3, S4, S5, S6			**6**
	S3cd	S7	*B2*		*A2*
6fg	S4ab	S8	S8		S1, S10, S11, S12, S13, S15

- Highlighted figures are new or have been modified compared to their respective ACPD versions. Most modifications are related to using different vertical coordinates. Other figures include additional panels or features.
- The paper has been restructured. The markup-version of the manuscript might be a bit misleading, because copy and paste of sections shows up as new or removed text. There is new text and there is removed text, but most snippets are largely unchanged.
- Supplement and accompanying paper are less heavily referenced. Readers should now be able to go through the main text without looking into the supplement.
- Discussion extended for: Photochemical O3 production, LiNOx, vertical coordinates
- Convection and uplift of CO: The discussion has been extended not only compared to the ACPD version, but the revised manuscript also contains an additional aspect that has been missing in the open discussion.
- More validation for lightning and nitrogen oxides
- Focus shifted towards processes in the ASMA
- Detailed discussion of NOy put in a new appendix. The strategy to shorten the main text is explained in the detailed responses to the referees.
- Shortened the text despite additional content, striving to make it more concise.

Updated reply to Anonymous Referee #1

Major comments:

Presentation: - parts of the paper are too long and divert the reader from the main and strong elements brought by the paper. In particular, some rather general and introductory statements are given all along the manuscript (about the emissions, chemistry and dynamics...). It could be good if the authors try to shorten the paper and keep introductory elements to the introduction. Some examples of lengthy parts are mentioned in the detailed comments. - the paper is very often referencing to results from its accompanying paper which makes the reading and understanding somehow difficult. One example about O3 production regime is given below. - the same is true concerning the supplementary material which makes the paper a bit heavy to handle.

We thoroughly restructured the paper, slightly shifting the focus from putting the HALO ESMVal measurements into context towards ASMA O3 and corresponding processes. Parts of the text became obsolete, while the discussion of aspects like photochemical O3 production, LiNOx, convective transport, vertical coordinates and validation was extended.
We strived to make the main text less dependent on references to the supplement or to the accompanying paper. Readers should now be able to go through the main text stand alone. There are still many figures in the supplement, but they are there mainly for documentation and reproducibility. This is also stated in the introduction.
Despite additional contents, the main text (incl. figures) is about 20% shorter now, and hopefully more concise and focused.

LiNOx and O3 production: Fig. 3h displays higher LiNOx production from EMAC in the Tibetan part of the ASMA during spring than during summer as mentioned P10L4-5. Nevertheless, the net O3 production is larger in summer than in spring down to 200 hPa below the tropopause (Fig. 2h). The authors explanation is that (i) in spring lower COV are uplifted by convection resulting in COV limitation and reduced O3 production (ii) LiNOx are produced locally in spring and not in summer. The latest argument also appears in the Annexe about LiNOx (p20L14-16).
Concerning (i) 1/ LiNOx production is linked to deep convection, especially in the models where both parametrization are coupled (in EMAC flashes are linked to convective updraught velocity as mentioned P20L10-11). Therefore more LiNOx should be associated with larger uplift of pollutants. Why EMAC displays more LiNOx with less uplifted COV in spring?

We added a discussion of this very interesting question to the revised manuscript, section 6.2.

2/ Over South and East Asia the season of largest deep convection takes place in summer during the monsoon rather than in spring. Why are there more LiNOx in spring in EMAC?

We added a comparison between EMAC-simulated lightning activity and the corresponding TRMM-LIS/OTD observations to the revised manuscript (section 6.1 and Appendix A). Overall, the agreement is reasonable. In particular, also the observations show a maximum of lightning activity in spring.
The corresponding figure has been put in the supplement, because lightning is not a focus of this paper. It is rather the resulting NOx background that interests here and a corresponding comparison to CARIBIC observations has been added to the revised manuscript (section 2, Appendix A).

Concerning (ii): Looking at Fig. A1 displaying monthly LiNOx at 168 hPa, we see that they are localized over NW and NE India and Pakistan in May while in August they are more over SE India and Himalaya/Tibet. Nevertheless, the source is much stronger in spring. In both cases, the LiNOx emissions are very "patchy" and localized with also in June a single large emission spot over Bangladesh and in July the LiNOx spot localized over northern central India. Therefore, it is difficult to attribute a lower O3 production to more localized LiNOX emissions in spring.

We extended the discussion on photochemical O3 production (section 6.3), which now addresses the above question. Essentially we attribute increased ProdO3 in summer to the combination of two effects: (i) The increased availability of CO; (ii) The decrease of ProdO3 in high-NOx air.

Why are the LiNOx emissions so "patchy" on a monthly scale? The averaging should smooth horizontally the distributions because convection does not always occur at the same place. It could be interesting to compare LIS/OTD distributions of lightnings to EMAC LiNOx distributions.

This has been added to the revised manuscript (section 6.1 and Appendix A).

Finally, in Barret et al. (2016) the LiNOx are not shown but a sensitivity test shows that O3 and NOx produced by LiNOx are the highest during the monsoon season which seems rather logical for the reasons discussed above. This discrepancy between the EMAC and GEOS-Chem models concerning LiNOx should be discussed.

A dedicated comparison would be needed to pinpoint and discuss discrepancies between different model systems. This didn't seem feasible in the context of this paper, which already required shortening. Therefore we added a corresponding statement to the draft (section 6.1) and for now resorted to showing that lightning and NOx are reasonably well represented in our simulation.

The east-west O3 net production gradient is logical as explained in the manuscript (P10L11-12) and in agreement with previous comparable evaluations by e.g. Liu et al. (JGR,2009) and Barret et al. (ACP,2016). Furthermore, the values of Fig. 2 seems in rather good agreement with those of the above mentioned papers for the monsoon season. A comparison and discussion of the EMAC O3 production with these previous studies could be interesting to strengthen and put the results in perspective.

This has been added to section 6.3.

Referring to the accompanying paper, it is mentioned that O3 production at 168 hPa is rather limited by CO than by NOx (P15L12-13). The exact sentence in the accompanying paper is "Net O3 production seems to depend more on CO (and related precursors) than on Nox". The use of "seems" shows that the authors are rather uncertain. I do not really understand how is this possible because of the rather high CO concentrations within the ASMA (70-100 ppbv according to HALO and all references cited in the paper). This statement of a generally CO-limited regime in the ASMA at 168 hPa needs to be demonstrated and is not supported by the literature. For instance, according to Brune (IGAC Isuue 21, 2000), in the upper troposphere, the O3 regime is NOx limited for NOx concentrations lower than some hundreds pptv.

We extended the discussion of photochemical O3 production (section 6.3). In particular we added a figure (Fig. 6) to resolve the mix-up between chemical regimes (e.g. NOx-limited, NOx-saturated) and operating modes of the chemical system.

Tracer-tracer relationships:

This part is very interesting because the 3 tracers document different transport and chemical processes. HCl in particular which is rarely used is good to trace stratospheric air because O3 is photochemically produced in the troposphere. The authors explain that "mixing line with negative CO/O3 slope dominate" in Fig 4c (corresponding to positive slopes in Fig. 5c). They correspond to mixing stratospheric air with photochemically processed tropospheric air. Neverthelesse, in Fig. 5c, we also see some horizontal mixing lines (red and green). According to the discussion in p11 and 12 they correspond to mixing of fresh uplifted pollution (increasing CO, horizontal lines not so clear in Fig. 4c) and stratospheric air (increasing HCl in Fig 5c) with antagonist effects on O3. Another line with O3 decrease / HCl increase in Fig. 5c and O3 decrease / CO increase in Fig. 4c corresponding to mixing of fresh pollution in the UTLS can also be isolated. It is difficult to see whether these mixing lines correspond to important part of the sampled air masses but they could be mentioned.

Explanations for the different types of mixing lines are offered in the context of the hypothetical lines (L1-L5), shown in Figs. 4b and 5b. In the revised manuscript we refer more often to specific hypothetical lines when discussing Figs. 4c and 5c. The discussion of vertical lines in Fig. 5c has been corrected.
A detailed quantification of different processes' contributions to individual measurements would require more sophisticated analyses along back-trajectories.

Details:

Part 3: the description of the different species at beginning of §3.1; 3.2, 3.3 and 3.4 (origin, chemistry etc.) are too close to "textbook" descriptions and should be shorten for readability.

In the revised manuscript we only shortly motivate the selection of tracers in the context of the tracer-tracer correlations (section 4), which is now before the discussion of the annual evolution of tracer profiles (former section 3; now section 5).

Part 5: this part tries to describe the different processes that control the ASMA composition one by one. It is interesting and well documented but rather lengthy and descriptive. For instance, the description of the evolution of the CO and HCL distributions P17L1-15 is very detailed and could be summarized.

~

P17L1-14: the dynamics are very detailed with the evolution of the air masses but is it really necessary to give so much details?

The corresponding figure has been moved to the supplement and the main text now only contains a summary of the splitting event (section 6.6).

Fig2 and 3: the plots are shown in pressure coordinates that makes the region around the tropopause very compact. Readability would be better in logP coordinates

This is now Figs. 4 and 5, given in logP coordinates. A short discussion on the selection of vertical coordinate systems has also been added (end of section 3).

(altitude plots are provided in the supplement but it makes the reading uncomfortable and could be simply removed).

The altitude plots have been removed, but the extension of Figs. 4 and 5 to five years is still given in the supplement. Those supplemental figures are in isentropic coordinates, just for documenting that the general picture remains similar to logP coordinates.

p5l13: why choose PV = 3.5 for the tropopause in the extratropics? Most studies choose 2 or 1.5.

This is the standard tropopause definition of EMAC in the extratropics, as introduced by Jöckel et al. (2006).

P5l27: Fig.1 is referenced after Fig 2 and 3.

The figures have changed, and also their numbering. The numbering of figures is determined by the order of where they are mainly discussed, rather than by their first mentioning in the text. For example, a side aspect ("ridge line") of Fig. 7 is briefly mentioned in the context of defining the ASMA region in section 3., but Fig. 7 is not really discussed before section 6.4.

p9l5: "indicates that relatively: : :"

Reformulated (now p10l17).

Updated reply to Anonymous Referee #2

Major comments:

General:
This is very interesting and important paper which is worth to be published. The most important finding is the explanation of high ozone within the Asian summer monsoon anticyclone. The authors show that photochemical ozone production in the circulating air masses as well isentropic in-mixing from the stratosphere are key processes defining ozone. In this picture the anticyclone can be understood as a photochemically active and not well-isolated reactor. In this reactor there are two parts: "convectively driven" eastern (Tibetian) part and more "chemistry driven" western (Iranian) part. Although the paper is well-written, it suffers from an inadequate presentation (see major points). Because of this, the paper needs a major revision.

1. As you show in many places, isentropic mixing between the stratospheric air (you call it TP layer) and the interior of the anticyclone is an important process in your chain of arguments. In Fig. 7 you show how such isentropes connecting the extratropical lower stratosphere intersect the tropopause (some almost perpendicular) and penetrate into the anticyclone itself. The mixing (stirring) happens on such isentropes and is almost a 2d process. So I do not understand, why you do not show the respective tracer distributions at such isentropes. I guess θ = 360 K would be the right choice instead of using the 168hPa level (e.g. Fig. 8, Fig 9 or Fig. 10). I would recommend to show Fig. 7 much earlier in the text (e.g. as the second figure of your paper) and than use much more isentropic analysis. As you mentioned, such isentropes are tilded in pressure space, but transport occurs much more on such isentropes.

We added a short discussion on vertical coordinates at the end of section 3. Figure 7 has been moved to the beginning (now Fig. 2, see table on the first page of this document) and we revised the discussion accordingly throughout the paper. Several figures are now in isentropic coordinates. The 355 K level was chosen as a compromise between representing the HALO ESMVal measurements and little intersection with the TP near the equator.

2. For me it is unreasonable to include 16 figures into the supplement! If your story exceeds something like 10-12 main figures and 2-5 figures of your appendix, you should divide the story into two parts or make your story shorter. The last point seems for me to be more your case. Your abstract roughly describes your main results (see also my general comments). So maybe, you can go through the text and remove everything what is not supportive for your main results (see also my minor points).

Several figures have been removed, but new content also required new figures. In summary the main text is considerably shorter now. The focus of the paper has shifted towards O3 and related processes in the ASMA. There are still many figures in the appendices and the supplement. However, the main text is more stand-alone now. We note in the introduction that the supplement is mainly for documenting side aspects and throughout the text try not to encourage readers to visit the supplement. However, we prefer to publish these supplemental figures with the paper for the reproducibility of our arguments.
The situation is less clear for the appendices. As a compromise between brevity and completeness, detailed discussions of LiNOx and NOy are put there, i.e. closer to the main text. Summaries of the findings in the main text should be sufficient for understanding our chain of arguments, but we feel that

some readers will be interested in the details. Since nitrogen oxides play an integral role in the ASMA, we would prefer to publish them with this rather than spawning a separate paper.

Minor Points:

1. P 1/L 18-19

"contrasted by...in autumn and winter" - ASM anticyclone does not exist in autumn and winter. Why we should talk about it.

This phrase was removed when shortening the abstract. However, throughout the paper we still highlight the specific features of the monsoon by comparing it to other seasons.

2. P 1/L 20

"is regularly entrained a the eastern flank" - This is the isentropic in-mixing mentioned in my major point and not correctly described in your paper

Starting from Fig. 2, the representation of isentropic in-mixing has been modified throughout the paper. We also note that the details of this process are a topic of ongoing research.

3. P 1/L 24

"by northerly" - I think "by southerly"

Corrected. We mean "winds from the south".

4. P 1/L 24

"Although..." - this sentence is not clear for me. I would remove it

We removed the above sentence and now state at the beginning of the abstract that the measurements reflect the main processes acting throughout the monsoon season. It is one of the main objectives of the paper to put the HALO ESMVal measurements in the ASMA into perspective.

5. P 2/L 11

I think that also "the eastward propagation of eddy shedding" is important now (Dethof et al.„ 1999; Vogel et al., 2014).

Agree. We mentioned eastward eddy shedding only later in the paper, and have added the above recommendation to section 1.

6. P 2/L 15

"the associated heat low" - do not understand what you mean

This has been reformulated in the revised draft. In short: Overall upwelling in the eastern part of the ASMA is accompanied by large scale subsidence in the western part. UT subsidence results in mostly

clear skies, heating up the landmass of the Arabian Peninsula. The hot air rises, generating a thermal low near the ground and an anticyclone in the outflow region in the mid troposphere.

7. P 3/L7-34

I would recommend to focus the attention of the reader on ozone (observation very high in the core, but why, you will discuss it in the paper, also in the interannual context, etc). Instead of this you talk here too much about general aspects...

The focus of the paper has been shifted towards O3.

8. P 5/L1-6

For me this is the main motivation for the paper and it should roughly replace the part in P 3/L7-34 !

Section 1 has been revised accordingly.

9. P 5/L14-16

"The extratropics are dominated..." - this sentence is unnecessary.

Removed.

10. P 5/L24

...dominate the averages in the chosen regions.

Revised.

11. P 5/L29-32

too much. I can only recommend to remove this material

Most of those supplemental figures have been removed (see table on the first page of this document).

12. Figure 1, caption

dynamical proxy of what.... I do not see any gray parts of the flight. "Panel a additionally shows..."????

- Changed to: "… dynamical proxy to delimit the ASMA …"
- There is a grey section over the coast of Oman, which might be hard to see. Since the flight track has been discussed in the accompanying paper, we removed this information here.
- Panels are now denoted with brackets, e.g. (a), (b), …

13. P 7/L21-24

"slowly descending HCl..." - this feature is very strange. Typically, during the considered season (JJA) there is a strong diabatic upwelling in the UTLS region confined by the anticyclone. Maybe you should explain it with model or remove it...

As noted above, there is overall upwelling in the eastern part of the ASMA, and large scale subsidence in the UT over the Arabian Peninsula. For instance, Nützel et al. (2016) show a corresponding figure.

14. P 8/L7

"...differ between the summer monsoon season and the rest of the year.." – I would say the strong difference is during AMJJA and not only during JJA

Changed to: "Simulated NO_y profiles in the ASMA region from April to September differ to the rest of the year (Figs. 3cd), but the monsoon season is also distinct: …"

15. P 8

The main part of NOy in the stratosphere should be HNO3, so I expect a much stronger correlation with HCl. Please comment.

Apart from stratospheric contributions, NOy also contains LiNOx and uplifted pollutants. HCl is just related to stratospheric air.

16. P 8-9

Section 3.4 contains for me too much information. I would reduce it by considering only the ozone-relevant NOx, NOy features.

We consider the discussion of C- vs E-shaped NOy profiles interesting in itself, but agree that it is only a side aspect regarding ozone. The discussion of reactive nitrogen is now mostly in appendix B.

17. P 10, L5

NOx, typo

Corrected

18. P 10

Section 4 is a very important and novel part of the paper. It combines in situ observations (tracer-tracer correlations) with the model. It shows in a very nice way the interaction between the photochemical ozone production and stratospheric in-mixing. Because it does not use so much the observed NOx, NOy features, it is the next motivation to shorten section 3.4.

Ok, thank you.

19. P 12, L23

"because HCl ...are decreased" - with the vertical mixing lines you argue that HCl should be constant. Maybe you should reformulate

Corrected to: “There are also a few almost vertical mixing lines in Fig. 5c, indicating case L3 described above.”

20. P 13, L20-31 and P 14

Here you show how important is the isentropic transport (mixing between the stratospheric and tropospheric air) on tilted isentropes. Here is also the origin for my major points.

21. On the following pages there are to many references to the supplement (see my major point) I can only recommend to shorten the following sections.

Points 20 and 21 have already been addressed in the “Major comments” section.

References

Lelieveld, J., Hoor, P., Jöckel, P., Pozzer, A., Hadjinicolaou, P., Cammas, J.-P., and Beirle, S.: Severe ozone air pollution in the Persian Gulf region, Atmos. Chem. Phys., 9, 1393-1406, 2009.

Nützel, M., Dameris, M., and Garny, H.: Movement, drivers and bimodality of the South Asian High, Atmospheric Chemistry and Physics, 16, 14755-14774, 10.5194/acp-16-14755-2016, 2016.

Rodwell, M. J., and Hoskins, B. A.: Monsoons and the dynamics of deserts, Q. J. R. Meteorol. Soc., 122, 1385-1404, 10.1002/qj.49712253408, 1996.

Dynamics and composition of the Asian summer monsoon anticyclone

Klaus-D. Gottschaldt[1], Hans Schlager[1], Robert Baumann[1], Duy S. Cai[1], Veronika Eyring[1], Phoebe Graf[1], Volker Grewe[1,2], Patrick Jöckel[1], Tina Jurkat-Witschas[1], Christiane Voigt[1,3], Andreas Zahn[4] and Helmut Ziereis[1]

[1]Deutsches Zentrum für Luft- und Raumfahrt (DLR), Institut für Physik der Atmosphäre, Oberpfaffenhofen, Germany
[2]Delft University of Technology, Aerospace Engineering, Delft, The Netherlands
[3]Johannes Gutenberg-Universität, Institut für Physik der Atmosphäre, Mainz, Germany
[4]Karlsruher Institut für Technologie (KIT), Institut für Meteorologie und Klimaforschung, Karlsruhe, Germany

Correspondence to: Klaus-D. Gottschaldt (klaus-dirk.gottschaldt@dlr.de)

Abstract. This study places HALO research aircraft observations in the upper-tropospheric Asian summer monsoon anticyclone (ASMA) obtained during the Earth System Model Validation (ESMVal) campaign in September 2012 into the context of regional, intra-annual variability by hindcasts with the ECHAM/MESSy Atmospheric Chemistry (EMAC) model. Observed and simulated tracer-tracer relations reflect photochemical O_3 production, as well as in-mixing from the lower troposphere and the tropopause layer. ~~-~~The simulations demonstrate that tropospheric trace gas profiles in the monsoon season are distinct from the rest of the year, and the measurements reflect the main processes acting throughout the monsoon season. ~~Air uplifted from the lower troposphere to the tropopause layer dominates the eastern part of the ASMA's interior, while the western part is characterised by subsidence down to the mid-troposphere. Soluble compounds are being washed out when uplifted by convection in the eastern part, where lightning simultaneously replenishes reactive nitrogen in the upper troposphere.~~ Net photochemical O_3 ~~ozone~~ production is significantly enhanced in the ASMA, where uplifted precursors meet increased NO_x, mainly produced by lightning. ~~, contrasted by an ozone depleting regime in the mid-troposphere and more neutral conditions in autumn and winter.~~

An analysis of multiple monsoon seasons in the simulation shows that stratospherically influenced tropopause layer air is regularly entrained at the eastern ASMA flank, and then transported in the southern fringe around the interior region. Radial transport barriers of the circulation are effectively overcome by subseasonal dynamical instabilities of the anticyclone, which occur quite frequently, and are of paramount importance for the trace gas composition of the ASMA. Both, the isentropic entrainment of O_3-rich air and the photochemical conversion of uplifted O_3-poor air tend to increase O_3 in the ASMA outflow. ~~Observed and simulated tracer-tracer relations reflect photochemical O_3 production, as well as in-mixing from the lower troposphere and the tropopause layer.~~ ~~The simulation additionally shows entrainment of clean air from the equatorial region by northerly winds at the western ASMA flank. Although the in situ measurements were performed towards the end of summer, the main ingredients needed for their interpretation are present throughout the monsoon season.~~

Formatted: Font color: Red

Formatted: Subscript

Formatted: Subscript

Formatted: Subscript

Formatted: Subscript

Formatted: Subscript

~~A transition between two dynamical modes of the ASMA took place during the HALO ESMVal campaign. Transport barriers of the original anticyclone are overcome effectively when it splits up. Air from the fringe is stirred into the interiors of the new anticyclones and vice versa. Instabilities of this and other types occur quite frequently. Our study emphasises their paramountcy for the trace gas composition of the ASMA and its outflow into regions around the world.~~

1 Introduction

The Asian monsoon system is one of the largest and dominating atmospheric features on Earth. It is stronger than other monsoon systems because of the topography of the region, which insulates warm, moist air over South Asia from the cold and dry extratropics (Boos and Kuang, 2010). This leads to a global maximum of surface moist static energy at the south-western flank of the Himalayas (Boos and Hurley, 2013), which drives deep convective updrafts during northern hemispheric summer. Elevated surface heating over the Tibetan plateau (Flohn, 1960; Fu et al., 2006), predominantly northward surface winds plus orographic uplifting at the southern/southwestern slopes of the Himalayas (Li et al., 2005; Liu et al., 2009b), and deep convection over the Bay of Bengal (Park et al., 2009; Nützel et al., 2016) - ~~all Episodic deep convection (Hoskins and Rodwell, 1995) related to the northwards shifted inter-tropical convergence zone (Lawrence and Lelieveld, 2010), elevated surface heating over the Tibetan plateau (Flohn, 1960; Fu et al., 2006), and orographic uplifting at the southern/southwestern slopes of the Himalayas (Li et al., 2005; Liu et al., 2009b)~~ additionally contribute to an overall ascending air current. This drives an anticyclonic circulation, centred at 200 to 100 hPa (Dunkerton, 1995; Randel and Park, 2006; Garny and Randel, 2015).

Location, shape and strength of the ASMA strongly vary on intra-seasonal, inter-annual and longer timescales (Dunkerton, 1995; Lin et al., 2008; Kunze et al., 2010; Pokhrel et al., 2012), which is subject to ongoing discussion (Pan et al., 2016; Nützel et al., 2016). An elliptical vortex is intrinsically unstable (Hsu and Plumb, 2001; Popovic and Plumb, 2001), thus prone to splitting up and ~~and mostly westward~~ eddy shedding to the west and east (Dethof et al., 1999; Vogel et al., 2014). Variable forcing by convection (Randel and Park, 2006; Garny and Randel, 2013), sub-seasonal oscillations (Lin et al., 2008; Goswami, 2012), the interaction with Rossby waves or mid-latitude synoptic disturbances (Dethof et al., 1999) add further complexity. The overall upwelling~~In particular, the Rossby wave response to convection~~ in the eastern ASM region is accompanied by ~~results in~~ large-scale subsidence in the western part ~~over the Arabian Peninsula~~ (Rodwell and Hoskins, 1996), making the Arabian Peninsula~~it~~ one of the warmest and driest regions on Earth. The ~~associated~~ heat low associated with the hot desert conditions in summer supports itself an anticyclone (Lelieveld et al., 2009), which interacts ~~intermittently merges~~ with the ASMA. ~~If both anticyclones are separated, the western and eastern parts will be denoted "Iranian" and "Tibetan", respectively. "ASMA" will be used for the Tibetan anticyclone, or the whole system when merged. Based on reanalysis data of the National Centers for Environmental Prediction – NCEP1 (Kalnay et al., 1996) it was suggested that the core of the anticyclone oscillates between Iranian and Tibetan mode on a quasi-biweekly timescale(Tao and Zhu, 1964)~~

Formatted: Font color: Auto
Formatted: Font color: Auto
Formatted: Font color: Auto
Field Code Changed
Formatted: Font color: Auto
Field Code Changed
Formatted: Font color: Auto
Formatted: Font color: Auto
Formatted: Font color: Auto
Field Code Changed
Field Code Changed
Field Code Changed
Formatted: Font color: Auto

~~Zhang et al. (2002). However, amongst 6 re-analyses such a bimodality is only found in NCEP1 and to a lesser degree in its successor (Nützel et al., 2016).~~

The interplay of the above dynamical ingredients makes the Asian summer monsoon a switch yard and mixing vessel for air masses of different origin and with different composition, including the exchange between troposphere and stratosphere. Monsoon air is received by regions around the globe (Rauthe-Schöch et al., 2016), and was for instance shown to affect the tropospheric chemical composition in the Mediterranean (Lelieveld et al., 2001; Lelieveld et al., 2002; Scheeren et al., 2003). A mid-tropospheric (400-500 hPa) summertime O_3 maximum over the eastern Mediterranean / Middle East region (Li et al., 2001; Lelieveld et al., 2009; Schuck et al., 2010; Akritidis et al., 2016) is enhanced by Asian monsoon outflow (Liu et al., 2009b; Richards et al., 2013; Barret et al., 2016)., but it is not clear, if O_3 in the ASMA plume is generally enhanced or depleted (Lawrence and Lelieveld, 2010). ~~Furthermore, the UT anticyclone is important for the exchange of air masses between the stratosphere and the troposphere. It episodically drags stratospherically influenced air from the tropopause layer (TL) into the troposphere . Eddy shedding is also a means to transport tropospheric ASMA air into the stratosphere (Ungermann et al., 2016).~~

In the following "TL" refers to the mixing zone at the tropopause, where cross-tropopause exchange of air masses on average creates a gradient between stratospheric to tropospheric trace gas signatures. The TL is also denoted ExTL in the extratropics and TTL in the tropics, reflecting that the dominating physical processes change at about the 30° circles of latitude. There are no rigid boundaries, but rather stratospheric influence decreases towards the troposphere over a range of several kilometres (Gettelman et al., 2011). In contrast, "upper troposphere" (UT) is used here to describe the altitude region that is dominated by the ASMA. Despite its importance for redistributing trace gases between boundary layer, troposphere and lower stratosphere, the highly variable composition of the ASMA and the processes behind it are not well understood yet (Randel et al., 2016).

In situ measurements were conducted in the ASMA during the ESMVal field experiment with the High Altitude and LOng Range (HALO) research aircraft in September 2012. A sudden enhancement of measured O_3 when HALO entered the ASMA from the south triggered the accompanying paper (Gottschaldt et al., 2017), since those measurements contrast the presumption of decreased O_3 in the ASMA. It was shown that the ASMA filament(s) encountered during that flight were associated with entrainments of lower-/mid-tropospheric air at the eastern ASMA flank, as well as with stratospherically influenced TL air.

Here we put the specific situation observed during the HALO ESMVal campaign into a regional, seasonal and multi-annual perspective, which is provided by global chemistry climate simulations with the EMAC model.

Recent papers discussed climatological trace gas distributions in the monsoon region (Santee et al., 2017), CO distributions in the context of daily ASMA dynamics (Pan et al., 2016), and monthly budgets of CO and O_3 (Barret et al., 2016)~~(Santee, 2017 #204)~~. Building on the ASMA observations during the HALO-ESMVal campaign, the second objective of our study is

Field Code Changed
Field Code Changed
Field Code Changed
Field Code Changed
Field Code Changed
Field Code Changed
Field Code Changed
Formatted: Font color: Auto
Formatted: Font color: Auto
Field Code Changed
Field Code Changed
Field Code Changed

to complement these papers by considering additional tracers on a 10-hourly scale to characterise key processes relevant for the O_3 distribution in the monsoon region.

~~Gottschaldt et al. (2017) identified key processes for the interpretation of the in situ data from selected flight segments and we refer to that study as "accompanying paper" in the following. Those processes include the entrainment of stratospherically influenced air at the eastern flank and its transport in the fringe around the interior of the ASMA, intermittent mixing of uplifted lower tropospheric with UT air, net photochemical O_3 production, and the splitting up of the anticyclone into a Tibetan and an Iranian part. In the present study the specific situation observed during the HALO ESMVal campaign is put into a regional, seasonal and multi annual perspective, which is provided by global chemistry climate simulations with the EMAC model. We examine, if the above processes are important beyond individual flight segments and for the ASMA composition in general. This touches several key aspects of the UT monsoon system: dynamical and chemical coupling with convection, composition/reactive chemistry in the monsoon region, the relative importance of different reactive nitrogen sources, mixing of higher latitude lower stratospheric air into the tropical TL by the ASMA – all of which are only poorly understood (Randel et al., 2016).~~

~~A recent paper of Pan et al. (2016) discussed CO distributions in the monsoon region in the context of daily ASMA dynamics. Another paper (Barret et al., 2016) focused on monthly budgets of CO and O_3, confined within the ASMA. Building on the ASMA observations during the HALO ESMVal campaign, our study complements these papers by considering additional tracers on a 10-hourly scale to characterise key processes relevant for the O_3 distribution in the monsoon region. Section 2 briefly summarises the data used here, i.e. the in situ measurement techniques for selected tracers during the HALO ESMVal campaign, and the global chemistry climate simulations and trajectory calculations used for the interpretation of the observations. Those methodological aspects are described in further detail in the accompanying paper.~~ From all the observed and simulated tracers available, a subset is chosen for the present study. We discuss the intra-annual variability of these tracers in the ASMA region in section 3 by analysing the year 2012 of an EMAC simulation. In section 4 observed tracer-tracer relations are put in the context of simulated ones. The latter are not limited to the flight track of the HALO ESMVal campaign, but provide a wider view on the prevailing trace gas relations in the Asian monsoon region in September 2012. Section 5 is dedicated to the interplay of the processes that contributed to the observed trace gas signatures and their relevance beyond the specific situation observed during the HALO ESMVal campaign. By analysing multiple monsoon seasons in the EMAC simulation we show that those processes occur frequently, discuss their implications for composition and transport in the ASMA, and note remaining open questions. We first briefly summarize the data used here, then discuss the EMAC-simulated intra-annual variability of selected tracers in the ASMA region for the year of the HALO ESMVal campaign, put observed tracer-tracer relations in the context of simulated ones, discuss the interplay of the processes that contributed to the observed trace gas signatures, and also show in the context of multiple monsoon seasons that the specific situation observed during the HALO ESMVal campaign was not exceptional. For brevity the main text provides only summarizing statements about lightning NO_x ($LiNO_x$) and reactive nitrogen (NO_y) in the ASMA, and we refer to two appendices for details. Additional figures in the supplement are provided for documentation and reproducibility.

Formatted: Font color: Auto
Formatted: Font color: Auto
Formatted: Font color: Auto
Formatted: Font color: Auto
Formatted: Font color: Auto
Formatted: Font color: Auto
Formatted: Subscript
Formatted: Subscript
Formatted: Subscript
Formatted: Font color: Auto

2 Data

We focus on the analyses of O_3, CO, hydrogen chloride (HCl) and reactive nitrogen (NO, NO_x, NO_y), as those tracers reflect the processes most relevant for the interpretation of in situ measurements in the ASMA during the ESMVal flight from Male (Maldives) to Larnaca (Cyprus) on 18 September 2012. All in situ measurements used here are based on a data set with 10 s time resolution, which is available from the HALO database (https://halo-db.pa.op.dlr.de). The corresponding measurement techniques are described in the accompanying paper, and in more detail in publications about the individual instruments: CO (Hoor et al., 2004; Schiller et al., 2008; Müller et al., 2016), HCl (Jurkat et al., 2014; Voigt et al., 2014), NO/NO_y (Ziereis et al., 2000), O_3 (Zahn et al., 2012). Among those tracers, only HCl mixing ratios were at the instrument's detection limit during the considered flight (Jurkat et al., 2016).

The transport pathways of air parcels before being encountered by HALO were calculated with the Lagrangian HYSPLIT model (Draxler and Hess, 1998; Draxler and Rolph, 2015). Although ~~That analysis is published~~described in the accompanying paper, those analyses are a basis for this study. ~~It led to a pragmatic classification of the observations into 7 periods of interest (POI), which is also adopted here. The periods of interest number 3, 5 and 6 ("ASMA filament" in the following) were shown to be part of an UT air filament that was entrained by lower /mid tropospheric air at the eastern ASMA flank. This filament is part of the ASMA circulation and associated with the entrainment of air from the TL. POI1 and POI7 cover ascent and descent, respectively. During POI2 HALO was flying in the UT south of the ASMA, and dived into the lower troposphere during POI4.~~

In the following a~~A~~ll simulation data ~~of this paper~~ stem from global chemistry climate simulations with the EMAC model (Jöckel et al., 2010), performed within the ESCiMo (Earth System Chemistry integrated Modelling) project (Jöckel et al., 2016) and the DLR-internal ESMVal project. Our reference simulation has been described and generally evaluated as RC1SD-base-10a by Jöckel et al. (2016). Its set-up is designed for best possible comparability to observations by nudging of the dynamics to ECMWF ERA-Interim (Dee et al., 2011) reanalysis data and covers the period 1980 – 2013 (excluding spin-up). Convection is not resolved in the simulation, but its effects are captured by a parameterisation in EMAC. LiNO$_x$ emissions are parameterized on top of the convection parameterization. Given the above uncertainties, simulated lightning activity compares acceptably to satellite observations (Appendix A).

NO_x background mixing ratios are crucial for O_3 photochemistry, as will be discussed in more detail in section 6.3. In-situ measurements are the most accurate in the UT. We have shown in the accompanying paper that this simulation reproduces the measured trace gas mixing ratios along the HALO flight track of 18 September 2012 reasonably well~~—~~, but this comparison is rather limited spatially and temporally. Therefore we compare simulated NO and NO_y to one of the most comprehensive observational datasets available for reactive nitrogen in the UT (Stratmann et al., 2016): IAGOS-CARIBIC (In-service Aircraft for a Global Observing System - Civil Aircraft for the Regular Investigation of the atmosphere Based on an Instrument Container; Brenninkmeijer et al. (2007), www.caribic-atmospheric.com). Our comparisons are based on the output of the EMAC S4D submodel (Jöckel et al., 2010), i.e. along the given IAGOS-CARIBIC flight tracks each model

Field Code Changed
Field Code Changed
Field Code Changed
Field Code Changed
Field Code Changed
Field Code Changed
Formatted: Font color: Auto
Field Code Changed
Field Code Changed
Field Code Changed
Field Code Changed
Formatted: Subscript
Formatted: Font color: Auto
Formatted: Subscript
Formatted: Subscript
Formatted: Font color: Auto
Formatted: Font color: Auto
Formatted: Font color: Auto
Formatted: Font color: Auto
Formatted: Font color: Auto,
Formatted: Font color: Auto
Formatted: Font color: Auto
Formatted: Font color: Auto
Formatted: Font color: Auto
Formatted: Font color: Auto
Formatted: Font color: Auto
Formatted: Font color: Auto
Formatted: Font color: Auto
Formatted: Font color: Auto
Formatted: Font color: Auto
Formatted: Font color: Auto
Formatted: Font color: Auto

time step (Δt = 12 min). The agreement between simulated NO and corresponding IAGOS-CARIBIC observations is remarkable, particularly in the ASMA region (Appendix B). Further comparisons between the EMAC RC1SD-base-10a simulation and IAGOS-CARIBIC are shown by Jöckel et al. (2016) for O_3, CO and others, based on 10-hourly simulation output.

Ten-year averages of simulated O_3 reproduce the low-O_3 ASMA interior of satellite climatologies, as well as increased O_3 found by HALO ESMVal at slightly lower potential temperatures (supplement, Fig. S1).

~~In the following we analyse the results of the reference simulation for the ASMA region (Fig. 1) on three timescales: (i) September 2012 to elucidate the synoptic situation during the flight; (ii) the entire year 2012 to discuss the peculiarities of the monsoon season with respect to other seasons; (iii) 5 consecutive years (2010 – 2014), either entirely or the monsoon months July to September. The goal of the longer analyses (ii, iii) is to put the in situ observations into an intra- and inter-annual context.~~ Additional EMAC simulations were performed in quasi chemistry transport model mode (Deckert et al., 2011; Gottschaldt et al., 2013) to test the impact of ~~lightning NO_x (LNO_x~~$LiNO_x$~~)~~. Those are described in Appendix A and referred to always by their acronyms. ~~For brevity,~~ "~~S~~simulation" without further specification refers to RC1SD-base-10a in the following.

3 The ASMA region

As noted in the introduction, ~~(Boos and Hurley, 2013)(Boos and Kuang, 2010)~~the ASMA is driven by a large scale updraft originating from the south-western flank of the Himalayas on the one hand, and by smaller scale tropical deep convection events on the other hand. The latter correlates with a maximum of Outgoing Longwave Radiation (OLR), which ~~(Hurley and Boos, 2013)(Hoskins and Rodwell, 1995)~~expands from the Bay of Bengal towards the Tibetan plateau and back in the course of a monsoon season (Nützel et al., 2016). In contrast, the large scale updraft is tied to geographical features (maximum of moist static energy in the Indo-Gangeatic plain, heating of the Tibetan plateau, orographic forcing of the Himalayas). The inland thermodynamic conditions of the Arabian Peninsula support the mid tropospheric anticyclone in the west. It may intermittently merge with the ASMA, but we presume that the composition of the UT in the west is determined mainly by the air transported in the eastern-driven circulation. We denote ~~If both anticyclones are separated,~~ the western and eastern parts ~~will be denoted~~ "Iranian" and "Tibetan", respectively. "ASMA" unspecifically refers to the ~~will be used for the Tibetan anticyclone, or the~~ whole system ~~when merged~~.

The regions' delimitations (Fig. 1) for separate analyses of the different parts were chosen by eye, considering the following: (i) For putting the measurements into perspective, the regions shall capture the synoptic situation during the HALO ESMVal campaign; (ii) Both parts shall be equally sized; (iii) The variability of the ASMA's location and extent shall be covered. The chosen meridional range of 15°N to 35°N covers the simulated ASMA ridgeline for most of the monsoon season (shown in Fig. 7b). The zonal ranges are 30°E to 65°E and 65°E to 100°E for Iranian and Tibetan regions, respectively. For

Formatted: Font color: Auto
Formatted: Font color: Auto
Formatted: Font color: Auto
Formatted: Font color: Auto
Formatted: Font color: Auto
Formatted: Font color: Auto
Formatted: Font color: Auto,
Formatted: Font color: Auto
Formatted: Subscript
Formatted: Subscript
Formatted: Subscript
Field Code Changed
Formatted: Subscript
Formatted: Font color: Auto
Formatted: Font:

comparison, Yan et al. (2011) classified anticyclonic centres between 50°E and 67.5°E as Iranian mode, and between 80°E and 92.5°E as Tibetan mode.

We decided not to adapt the regions dynamically to the actual ASMA, because the boundary definitions we are aware of (Ploeger et al., 2015; Barret et al., 2016; Pan et al., 2016) emphasise the concept of a closed ASMA volume or transport barriers on monthly or seasonal timescales. However, the ASMA boundaries are not always well defined, particularly during transitions between different dynamical modes. Our pre-fixed regions allow an unbiased view on the effects of complex, 10-hourly dynamics. This comes at the price that features from outside the ASMA might contribute to the analyses occasionally. We can not rule out that concurrent but geographically distinct features feign correlations between different species, but monsoon-related features should mostly dominate the lateral averages in the chosen regions. Our approach detects differences between Iranian and Tibetan parts, because the corresponding circulation is tied to geographical features of the respective regions. Enhanced CO is considered to be a chemical characteristic of the ASMA (Pan et al., 2016), and increased geopotential height (GPH) is a dynamical proxy (Barret et al., 2016). Simulated seasonal mean distributions of both proxies indicate that our regions well capture the ASMA of 2012 (Fig. 1).

Large scale transport occurs mainly on isentropes, unlike convective transport. Pressure and isentropic vertical coordinates are similar in the UTLS in the tropics of the Tibetan region (Fig. 2a). In the EMAC simulation the TP has been diagnosed by a potential vorticity of 3.5 PVU in the extratropics and by the WMO definition between 30°N and 30°S (Jöckel et al., 2006). It is almost parallel to one isentrope in the tropics and to a lower one in the extratropics, but intersects isentropes around 360 K almost perpendicularly in the transition region at about 30°N. This facilitates isentropic inmixing from the lower stratosphere or the TL, but only in combination with southward wind components. If winds follow the TP (e.g. subtropical jet), it is still a transport barrier. The latter aspect is relevant for stratosphere-to-troposphere trace gas gradients and captured by coordinates relative to the TP (used for Fig. 4). The barrier effect of the TP is also relevant for convective transport (TP following coordinates also used for Fig. 5). Isentropic coordinates account for the seasonal evolution of potential temperature (θ, Fig. 2b), and best capture isentropic transport (used for Fig. 7, but also for the supplementary 5-year-equivalents to Figs. 4, 5).

Field Code Changed

Field Code Changed

Field Code Changed

Field Code Changed

Field Code Changed

Formatted: Font color: Auto

4 Tracer-tracer relations in September 2012

The distribution of points in a tracer-tracer diagram provides hints on the origin and evolution of air masses. A short primer for the interpretation of such diagrams is provided in Appendix C.

4.1 Selected tracers

Here we focus on CO versus O_3 and HCl versus O_3 (Fig. 3), while NO_x versus O_3 and NO_x versus NO_y are shown in Appendix B (Fig. B3).

Enhanced O_3 mixing ratios in the TL exhibit a strong vertical gradient. Given a chemical lifetime in the order of weeks, this reflects the degree of mixing between O_3-poor UT air and O_3-rich air from the lowermost stratosphere (Sprung and Zahn, 2010). That general picture might not hold in the ASMA though, where –depending on the availability of precursors- enhanced photochemical O_3 production is superimposed on isentropic inmixing from the stratosphere.

Enhanced CO is a tracer of boundary layer pollution and an O_3 precursor in the troposphere. Oxidation with the hydroxyl radical (OH) prevails under stratospheric conditions, and CO mixing ratios decrease by about an order of magnitude across the tropopause (Hoor et al., 2002).

As tracer for stratospheric air we use HCl, which in the UT has no significant photochemical sources and a lifetime similar to O_3 (Marcy et al., 2004). Wet scavenging in clouds effectively prevents convective transport of HCl to the UT, and no injections of HCl from volcanic activity affected the ESMVal flight from Male to Larnaca. Together this makes HCl a viable tracer of stratospheric O_3 entrainments, until it is selectively removed by wet scavenging.

NO_x ($NO + NO_2$) is an O_3 precursor and part of NO_y (see Appendix B for details). NO_x primarily characterises fresh emissions. Only NO was measured during the HALO ESMVal campaign, but daytime NO is a good proxy for NO_x.

4.2 Ranges covered by observed and simulated tracer-tracer distributions

In order to place the observed tracer-tracer relations into context, we plot the measured samples together with grid-cell samples from the EMAC simulation. Simulation output along the flight track is too sparse for a meaningful comparison (10 s resolution of measurements versus 12 min for the simulation). Therefore 5000 simulated samples per panel are chosen randomly, from the entire month of September 2012 and from throughout the ASMA region (Fig. 1: Tibetan plus Iranian parts). Plotting all corresponding samples form the EMAC simulation would impair the visibility of clustering. Two different vertical ranges are chosen. The range from 50 hPa above to 100 hPa below the actual EMAC tropopause (Figs. 3ad) provides a zoom-out view of possible tropospheric and stratospheric tracer mixing ratios and tracer-tracer relations for the time of year and region of the measurements. Zooming-in to the altitude range of measurements, we choose tropospheric tracers from the pressure altitude range 200 hPa to 100 hPa (Figs. 3be). The observations from the entire flight without ascend and descent are shown in (Figs. 3cf).

Measurements south of the ASMA are marked by dark blue dots in Figs. 3cf and are clearly distinct from the measurements in the ASMA filament (orange boxes). The ranges covered by the measurements are also given in the corresponding panels with simulated data, but are adjusted for model biases there. Those biases were estimated according to comparisons by eye, of measured versus simulated trace gas mixing ratios along the flight track in the ASMA filament (shown in the accompanying paper). All measured ranges fit into the simulated monthly averages for September 2012 in the ASMA region, thus the simulation captures this aspect well and the measurements are unlikely to represent an exceptional situation. We also note that all measurements clearly fall into the tropospheric regions of the respective simulated tracer-tracer spaces. This is no surprise: all HALO ESMVal measurements considered here were taken well within the troposphere.

Field Code Changed

Field Code Changed

Formatted: Font color: Auto

Field Code Changed

Formatted: Font color: Auto

Formatted: Subscript

Formatted: Not Superscript/ Subscript

Formatted: Font color: Auto

Formatted: Font color: Auto,

Formatted: Font color: Auto

4.3 In situ photochemistry, tropospheric and TL contributions

The colour code of the observations (Figs. 3cf) corresponds to measurement time. Similar colours indicate spatial and temporal proximity, a prerequisite for mixing lines. Schematic lines L1-L5 (Figs. 3be) and their parallels indicate special, hypothetical cases for the evolution of air masses, which are discussed next.

CO versus O_3 (Figs. 3abc): O_3 and CO display opposite gradients across the tropopause, and globally have lifetimes of several months in the UT (IPCC, 2013). Thus mixing lines in a CO versus O_3 scatter plot are generally suited to identify stirring and mixing processes in the UT that occur on timescales of days to weeks, including cross-tropopause mixing (Fischer et al., 2000). The well known L-shape (Hoor et al., 2002; Pan et al., 2004; Müller et al., 2016) is reproduced by the simulation in the CO vs. O_3 diagram for the UTLS (Fig. 3a), consisting of a CO-poor & O_3-rich stratospheric branch, connected by UTLS mixing lines to a CO-rich & O_3-poor tropospheric branch.

However, the above studies (Hoor et al., 2002; Pan et al., 2004; Müller et al., 2016) focused on the extratropics. The ASMA is mostly situated in the tropics, where trace gas mixing ratios are controlled by different processes (Gettelman et al., 2011). The ASMA in particular constitutes a special atmospheric situation, because a continuous resupply of rapidly uplifted lower tropospheric air impedes UT photochemical equilibrium there. O_3 is photochemically produced in the ASMA at a net rate of almost 4 nmol/mol/day (Barret et al. (2016); and Fig. 5b, which will be discussed in section 6). Only 2 weeks are needed to increase O_3 mixing ratios by 50 nmol/mol, i.e. to produce the O_3 enhancement observed at the southern ASMA edge. This is not much longer than the advection timescale (~10 days) discussed in the context of the HALO ESMVal campaign. Thus photochemical production needs to be considered as an alternative to stratospheric in-mixing for explaining enhanced O_3 in the ASMA. Photochemical ageing increases O_3 and depletes CO here.

Mixing lines with negative slopes in CO vs. O_3 space dominate the UT observations (black dotted in Fig. 3c). Such mixing lines in the troposphere could result from one or a combination of the following: (i) mixing between stratospherically and tropospherically influenced air masses; (ii) mixing between photochemically aged and freshly uplifted lower tropospheric air; (iii) an O_3 depleting photochemical regime (Baker et al., 2011). While the latter is unlikely in the ASMA (Fig. 5b), we need to consider additional tracers to disentangle stratospheric influence and photochemical ageing.

HCl versus O_3 (Figs. 3def): HCl is a proxy for stratospheric entrainment and CO marks tropospheric influence. Consider the hypothetical case of constant HCl (lines L1 and parallels in Figs. 3be): increasing O_3 corresponds to increasing CO then. The trace gas gradients along that hypothetical line reflect a gradient in net O_3 production rather than differences with respect to stratospheric influence between two reservoirs. Now consider the opposite case, i.e. constant CO (lines L2): increasing O_3 corresponds to increasing HCl, indicating a gradient of stratospheric influence. CO mixing ratios decrease for increasing HCl in the special case of constant O_3 and different HCl mixing ratios (lines L3). This indicates mixing between a tropospheric and a stratospheric reservoir, where two opposite effects lead to almost constant O_3 mixing ratios: increased net O_3

Field Code Changed
Field Code Changed
Field Code Changed
Field Code Changed
Field Code Changed
Field Code Changed

production in air with decreased HCl, versus both increased O_3 and HCl in the more stratospheric components. In intermediate cases the trace gas gradients in the tracer-tracer plots reflect a combination of gradients of in-mixing as well as in situ photochemistry. Spatial gradients of photochemical O_3 production dominate over gradients of stratospheric influence (i.e. in-mixing from the TL or stratosphere) within the sampled air mass, if increasing O_3 correlates with increasing CO and decreasing HCl (lines L4). In contrast, gradients of stratospheric or TL in-mixing dominate, if increasing O_3 correlates with increasing HCl and decreasing CO (lines L5).

The measurements (Figs. 3cf) mostly – but not exclusively - show the latter case (L5): neighbouring points form negatively sloped lines in CO vs. O_3 space (black dotted in Fig. 3c), corresponding to horizontal to positively sloped lines in HCl vs. O_3 space (black dotted lines in Fig. 3f). Thus, observed trace gas gradients are mostly due to gradients of stratospheric influence on some well mixed UT background. This could either be entrainment of tropospheric air into a more stratospheric background, or entrainment of TL air into a more tropospheric background. There are also a few almost vertical mixing lines in Fig. 3f, indicating case L3 described above. Systematic HCl gradients – like across the tropopause - are not expected in convectively uplifted air. O_3 variability in such air masses is at least partly due to different amounts of in situ produced O_3. However, mixing between aged and young tropospheric air alone cannot explain the observations.

We further note that mixing lines in Fig. 3f cover similar ranges of HCl, but are separated by different levels of O_3. The corresponding background air had seen similar amounts of stratospheric influence, but different O_3 production. As long as all points of an individual mixing line are subject to similar O_3 production, the entire line will be shifted to different O_3 levels. The O_3 ranges covered by individual mixing lines are similar to the offsets between different lines. Individual mixing lines in the measurements cover timescales of about 20 minutes (Fig. 3c), corresponding to 300 km at typical HALO speeds. The flight track in the ASMA filament altogether covers more than 3000 km and multiple mixing lines were found on that scale.

Summarizing, our observations of O_3, HCl and CO in an ASMA filament show that: (i) Both, photochemical production and TL/stratospheric in-mixing contribute to increased O_3 in the observed ASMA filament; (ii) small-scale gradients of stratospheric influence are superimposed on background regions that are rather homogeneous on small scales (hundreds of kilometres), but differ in their amounts of photochemically produced O_3 on larger scales (thousands of kilometres).

Formatted: Font color: Auto

5~~3~~ Simulated intra-annual variability of trace gas dynamics in the monsoon region

~~A sudden enhancement of measured O_3 when HALO entered the ASMA from the south triggered the accompanying paper and this study, since those measurements contrast the presumption of decreased O_3 in the ASMA. The other tracers considered here shall help to understand the corresponding O_3 dynamics and photochemistry.~~ In this section we discuss the evolution of simulated trace gas profiles ~~in the ASMA region and their evolution~~ throughout the year 2012, separately for lateral averages over the western (Iranian) and eastern (Tibetan) ASMA regions (Fig. 1). ~~Some features and processes that distinguish the monsoon season are highlighted.~~

Figures 2 and 3 show the simulated evolution of trace gas profiles relative to the EMAC tropopause throughout 2012, laterally averaged separately for the western (Iranian) and eastern (Tibetan) ASMA region (Fig. 1), respectively. The regions' delimitations were chosen by eye, considering the following: (i) For putting the measurements into perspective, the regions shall capture the synoptic situation during the HALO ESMVal campaign (see the accompanying paper for details); (ii) Both parts shall be equally sized; (iii) The variability of the ASMA's location and extent shall be covered. The chosen meridional range of 15°N to 35°N covers the simulated ASMA ridgeline for most of the monsoon season (Fig. 10b). We note that the EMAC tropopause is diagnosed by a potential vorticity of 3.5 PVU in the extratropics and by the WMO definition between 30°N and 30°S (Jöckel et al., 2006). The extratropics are dominated by baroclinic wave activity and downward stratospheric circulation, the tropics by radiative-convective balance and upward stratospheric circulation (Gettelman et al., 2011). The zonal ranges are 30°E to 65°E and 65°E to 100°E for Iranian and Tibetan regions, respectively. For comparison, Yan et al. (2011) classified anticyclonic centres between 50°E and 67.5°E as Iranian mode, and between 80°E and 92.5°E as Tibetan mode.

We decided not to adapt the regions dynamically to the actual ASMA, because the boundary definitions we are aware of (Ploeger et al., 2015; Barret et al., 2016; Pan et al., 2016) emphasise the concept of a closed ASMA volume or transport barriers on monthly or seasonal timescales. However, the ASMA boundaries are not always well defined, particularly during transitions between different dynamical modes. Our pre-fixed regions allow an unbiased view on the effects of complex, 10-hourly dynamics. This comes at the price that features from outside the ASMA might contribute to the analyses occasionally, but we are confident that monsoon-related features dominate the lateral averages. Our approach detects differences between Iranian and Tibetan parts, because the corresponding circulation is tied to geographical features of the respective regions. Enhanced CO is considered to be a chemical characteristic of the ASMA (Pan et al., 2016), and increased GPH is a dynamical proxy (Barret et al., 2016). Simulated seasonal mean distributions of CO and GPH at 168 hPa are shown in Fig. 1 for comparison, indicating that our regions well capture the ASMA of 2012.

Corresponding plots of the seasonal mean distribution at 168 hPa in the ASMA region of the other tracers considered here are available in the supplementary material (Figs. S1 – S3). In the following all simulated profiles are given in vertical coordinates relative to the tropopause, as pressure (Figs. 2, 3) or distance (Fig. 6, supplementary material, Figs. S4 – S8, S16).

53.1 Ozone

Enhanced O_3 mixing ratios in the TL exhibit a strong vertical gradient, which reflects the degree of mixing between O_3-poor UT air and O_3-rich air from the lowermost stratosphere. Due to its long chemical lifetime, O_3 fluctuations in the TL are generally determined by transport on timescales of days. It takes 1 or 2 weeks in the lowermost stratosphere to smooth out short timescale fluctuations and adopt the mean signature corresponding to a certain vertical distance to the tropopause (Sprung and Zahn, 2010). However, this might not hold under the particular photochemical UT conditions of the ASMA.

Formatted: Highlight

Field Code Changed

~~O_3 is subject to complex photochemical production and loss processes, which in the UT are masked even by small stratospheric entrainment.~~ Steep vertical gradients across the tropopause dominate O_3 profiles in the monsoon regions (Figs. 4~~2~~ef), but the profiles also show temporal fluctuations of various timescales. Note that our lateral averaging regions are rather large and smaller-scale structures get smoothed out, e.g. when an O_3-poor interior is combined with an O_3-rich fringe.

There is increased influx from the stratosphere in spring, enhancing O_3 in the UT. This is in accordance with the study of Cristofanelli et al. (2010), but in contrast to their study there are non-negligible O_3 enhancements connected to the stratosphere during the monsoon season (Fig. 4~~2~~f, circled). In this respect our simulation is however consistent with trace gas budget considerations for the ASMA (Barret et al., 2016) and the TTL (Konopka et al., 2010). Entrainment from the TL rather than deep from the stratosphere could reconcile the different findings. No other stratospheric contributions were found for the ~~In the accompanying paper TL entrainment is considered to be the source of~~ stratospherically influenced trace gas signatures in the HALO ESMVal ASMA observations.

Field Code Changed

Field Code Changed

Field Code Changed

Enhanced O_3 prints through in the averaged profiles of the eastern ASMA part only from the tropopause to about 200 hPa below the tropopause, while the mid-troposphere in the Tibetan part is dominated by particularly O_3 poor air during the monsoon season (Fig. 4~~2~~f). The latter is consistent with the findings of Safieddine et al. (2016). O_3 depletion in the mid-troposphere of the eastern part is contrasted by enhanced O_3 in the mid-troposphere during the monsoon season in the western part (Fig. 4~~2~~e, circled), marking the well known summertime O_3 maximum there.

Field Code Changed

5~~3~~.2 Carbon monoxide

Formatted: Font color: Auto

~~Enhanced CO is produced in combustion and thus a good tracer of boundary layer pollution, which is spatially and temporally rather heterogeneous. In the troposphere it is an O_3 precursor. CO is also a product of the oxidation of methane (CH_4) and higher hydrocarbons with the hydroxyl radical (OH). It has its predominant sink in a reaction with OH. Without tropospheric entrainment the sink dominates under stratospheric conditions, and CO mixing ratios decrease by about an order of magnitude across the tropopause (Hoor et al., 2002).~~ This is reflected in the evolution of CO profiles in the ASMA region in 2012 (Figs. 4~~2~~cd). CO-poor air dominates in the UT during spring, consistent with the stratospheric influx indicated by O_3.

CO-rich air rises throughout the troposphere of the eastern part during the monsoon season (Fig. 4~~2~~d, circled). On the western side there is a conspicuous CO depleted zone 200 to 300 hPa below the tropopause during the monsoon season (Fig. 4~~2~~c, circled), while CO is episodically enhanced in the UT. Uplifted air with enhanced CO mixing ratios hardly reaches higher than to 450 hPa below the tropopause in summer.

This difference between CO profiles in the Tibetan and the Iranian parts is consistent to the findings of Pan et al. (2016). Occasional horizontal transport in the UT from the eastern to the western part of the ASMA is an explanation for spatio-temporal evolution of CO mixing ratios, indicating that trace gas signatures in the Iranian part are dominated by the UT outflow of the Tibetan part of the ASMA.

Field Code Changed

53.3 Hydrochloric acid

~~As tracer for stratospheric air we use HCl. There are no significant HCl sources in the UT, apart from stratospheric entrainment (Marcy et al., 2004). Marine boundary layer sources for the ASMA are small (Randel et al., 2010; Bergman et al., 2013), wet scavenging in clouds effectively prevents convective transport of HCl to the UT, and no injections of HCl from volcanic activity affected the ESMVal flight from Male to Larnaca. Like O_3, HCl has a photochemical UT lifetime of the order of weeks (Marcy et al., 2004). This makes HCl a viable tracer of stratospheric O_3 entrainments, until it is selectively removed by wet scavenging.~~ As expected for a stratospheric tracer, ~~Consequently~~ the simulated HCl profiles (Figs. 42ab) show a strong anti-correlation with CO in the UT, with increased HCl in times of stratospheric influx (e.g. Fig. 42b, blue circle), and decreased HCl in the monsoon season. Stratosphere-to-troposphere exchange is pronounced during spring, consistent with the seasonality of the Brewer-Dobson circulation (Holton et al., 1995).

Field Code Changed

Field Code Changed

~~HCl is also emitted by the sea.~~ HCl plumes in the Iranian part rise to about 400 hPa below the tropopause in summer (Fig. 42a, circled), just like CO. Predominantly dry conditions in the western part prevent HCl from being washed out. However, CO and HCl are temporally anti-correlated in the mid-troposphere. Since HCl is emitted by the sea, w~~W~~e attribute this to alternating marine and continental origins in the uplifted air (Figs. 42ac).

Some HCl is ~~also slowly~~ descending from the tropopause into the mid-troposphere, as indicated by tilted patterns of enhanced HCl, which start at the tropopause and propagate downward (marked by an arrow in Fig. 42a). Similar tell-tale signs of descent also print through in other species in the Iranian part during summer.

There is almost no HCl in the Tibetan part throughout the monsoon season (Fig. 42b, black circle), except for the UT. Convection and thunderstorms are galore during the monsoon season in South Asia (~~see~~ Fig. 5d~~3h and the supplementary material of the accompanying paper~~)). Washing out does not affect CO, but effectively prevents transport of HCl to higher altitudes. ~~Thus enhanced HCl in the UT indicates stratospheric influence.~~ Predominantly continental origins also contribute to an increased CO/HCl ratio in the rising plumes of the eastern part.

53.4 Reactive nitrogen

~~Mixing ratios and the distribution of total reactive nitrogen (NO_y; comprising NO, NO_2, HNO_3, PAN, HONO, N_2O_5, HO_2NO_2, NO_3 as the most abundant species) are controlled by a variety of natural and anthropogenic sources, such as lightning, stratospheric input, soil microbiology, biomass burning, air traffic emissions and other fossil fuel combustion. The apportionment of NO_y sources varies between different parts of the atmosphere. Nitrogen oxides are key parameters in atmospheric chemistry, partly controlling the ozone production in the troposphere and lower stratosphere. In the UTLS, enhanced NO_y originates both from tropospheric and from stratospheric sources. In the lower troposphere odd nitrogen species are co-emitted with carbon monoxide in combustion processes, resulting in a strong correlation between both species. In the stratosphere HNO_3 is the main component of the NO_y family. It is mainly produced from N_2O photo-oxidation.~~

Simulated NO_y profiles in the ASMA region distinctively differ between the summer monsoon season and the rest of the year (Figs. 3cd): during summer there is more NO_y in the UTLS and mid-troposphere in both, the Tibetan and Iranian regions (Figs. 3cd, S5cd, S6). Episodes of enhanced NO_y (~1.5 nmol/mol) in the UT are frequent in the Tibetan part during summer, and alternate with periods of decreased NO_y (~1.0 nmol/mol). However, the altitude region just above the tropopause is hardly affected by this UT variability and maintains an average mixing ratio of ~1.2 nmol/mol NO_y (Figs. 3cd; for a better resolved UTLS see also the supplementary material, Fig. S5). NO_y mixing ratios generally increase with altitude in the lower stratosphere, but reach 1.6 nmol/mol only at about 15 hPa above the tropopause. E-shaped NO_y-profiles dominate the Tibetan part, with maxima in the lower troposphere, in the UT and in the lower stratosphere (see supplementary material for an example, Figs. S5cd, S6g, S7b). Less NO_y is simulated in many profiles for the mid-troposphere and just above the tropopause transport barrier (see also the supplementary material, Figs. S5, S7). E-shaped NO_y profiles were also reported by the NOXAR measurement campaign in the northern mid-latitudes and corresponding modelling studies (Grewe et al., 2001). The E-shape in northern mid-latitudes was in part attributed to aviation NO_x emissions (Rogers et al., 2002), but aviation effects are much smaller in the tropics (Gottschaldt et al., 2013). Instead of aviation emissions, in situ production of lightning NO_x in the prevalent thunderstorms of the monsoon season increases NO_y in the UT over South Asia (Fig. 3h, see also Appendix A). Thus a possible explanation for the E-shaped NO_y-profiles in the eastern ASMA part during the monsoon season is as follows: NO_y from boundary layer sources' pollution is uplifted, and solvable NO_y-components (e.g. HNO_3, N_2O_5) become increasingly washed out (Fig. 3d). At about 400 hPa below the tropopause only non-solvable components (e.g. NO_x) are left. Episodes of increased NO_y in the UT are well correlated with increased lightning NO_x emissions (Figs. 3d, 3h). NO_y mixing ratios however increase with altitude above the tropopause, due to increased photochemical production of HNO_3 in the stratosphere. With little in situ production and not much transport from above or below, NO_y mixing ratios in the region between the tropopause and 15 hPa above the tropopause are often smaller than in the adjacent altitudes.

Profiles in the western, i.e. Iranian ASMA part (Fig. 3c) have a different history of origins, and with just one minimum in the mid-troposphere are mostly C-shaped (supplementary material, Figs. S5, S7). During summer the Arabian Peninsula is dry. Convection (as indicated by lightning NO_x emissions in Fig. 3g) is mainly localised near the Bab al-Mandab Strait (Fig. A1), i.e. at the edge of the region we defined for calculating profiles of the Iranian part of the ASMA. Washing out is negligible throughout most of the Iranian region (Fig. A1, see also satellite pictures in the supplementary material of the accompanying paper), and therefore NO_y can rise to about 400 hPa below the tropopause (circled in Fig. 3c). Downward transport (as indicated by anti-clockwise tilted signals, one example marked by an arrow in Fig. 3c) dominates above that altitude, preventing further uplift. With little in situ production of lightning NO_x over the Arabian Peninsula in summer (Figs. 3g and A1), UT NO_y in the Iranian part is dominated by the outflow of the Tibetan part.

NO_x ($NO + NO_2$) is part of NO_y, but characterises young emissions. Only NO was measured during the HALO-ESMVal campaign, but daytime NO is a good proxy for NO_x:

Both, NO_x and NO_y increase with altitude above the tropopause. Recycling of stratospheric NO_y additionally increases NO_x in the troposphere. Stratospheric influx contributes to increased NO_x mixing ratios in the UT in spring (blue circles in Figs. 4bh), but enhanced UT NO_x during the monsoon (Figs. 4gh, black circles) is rather due to lightning NO_x emissions in the Tibetan part than to stratospheric entrainments (compare Figs. 4bh).

There is less NO_x in the mid-troposphere than in the UT ~~above or~~and in the lower troposphere, and l~~below (Figs. 2ab, S5ab). This indicates that that relatively i~~ittle NO_x rises to the UT from the lower troposphere -~~,~~ in both parts and throughout the year. -The conversion of non-solvable NO_x into solvable NO_y components facilitates subsequent loss by washing out. ~~The conversion of non-solvable NO_x into solvable NO_y components facilitates the subsequent loss by washing out.~~

~~Both, NO_x and NO_y increase with altitude above the tropopause, and recycling of stratospheric NO_y additionally increases NO_x in the troposphere. Therefore stratospheric influx contributes to increased NO_x mixing ratios in the UT (blue circles in Figs. 2b and 3b). Note that the timing of most enhanced LNO_x emissions during spring in Fig. 3h does not match the timing of most enhanced NO_x in the circled period in Fig. 3b. Enhanced UT NO_x during the monsoon (Figs. 3ab, black circles) is rather due to lightning NO_x emissions in the Tibetan part than to stratospheric entrainments. As a combination of the different effects affecting NO_x and NO_y, the NO_x/NO_y ratio maintains a broad maximum in the TL throughout the year (Figs. 3ef). The monsoon season is characterised by particularly little fluctuations of NO_x/NO_y (Figs. 3ef, circles). During the monsoon, the NO_x/NO_y ratio in the UTLS is higher in the western than in the eastern ASMA part. This indicates preferential export of high-NO_x air from the Tibetan part, or is an artefact of the possible dominance of a single source of LNO_x in the Iranian averaging region (Fig. A1). Only NO was measured during the HALO ESMVal campaign, but daytime NO is a good proxy for NO_x.~~

~~3.5 Photochemical ozone production~~

~~The net photochemical O_3 production rate (Figs. 2gh) is derived from the difference of EMAC simulated diagnostic tracers ProdO3 and LossO3 (Jöckel et al., 2016). Here we take into account effective ozone production and loss terms following (Crutzen and Schmailzl, 1983) and extended by Grewe et al. (2017, see their supplement). We note that the origin of high O_3 biases in the simulation (Jöckel et al., 2016) is not resolved yet. Uncertainties in the chemical mechanism (Gottschaldt et al., 2013) also impose uncertainties onto the net photochemical O_3 production rate. In contrast to the other tracers, there is no equivalent tracer in the HALO ESMVal measurements that could be used for independent evaluation of the photochemical O_3 production.~~

~~More O_3 is produced than destroyed in the ASMA, signalled by a pronounced maximum of net O_3 production in the UT during the monsoon season (Figs. 2h, circled). This is accompanied by net ozone destruction during the monsoon season 300 hPa below the tropopause and lower. At the tropopause and slightly above there is a local minimum of net O_3 production, followed by increased net O_3 production in the stratosphere.~~

~~O_3 photochemistry is dominated by photolytic cycles in the stratosphere, and catalytic cycles in the troposphere. Net O_3 production by the latter non-linearly depends on the availability of precursors like NO_x, CO and hydrocarbons. For instance,~~

net O_3 production is at maximum at roughly 0.3 nmol/mol NO_x, but the optimum NO_x mixing ratio depends on several other parameters (Grooß et al., 1998; Jaeglé et al., 1999). We consider CO (Fig. 2d) not only as an ozone precursor in itself, but also as a proxy for co-emitted hydrocarbons (volatile organic compounds, VOCs).

The simulated profiles of Fig. 2h show that enhanced net O_3 production in the ASMA has two prerequisites: enhanced UT NO_x meeting an enhanced supply of uplifted other precursors. We note that net O_3 production is enhanced during the spring periods of enhanced lightning NO_x (circled in Fig. 3h), but still about 3 nmol mol^{-1} day^{-1} smaller than during summer (see also supplementary material, Figs. S8cd): there is less CO in the UT during spring (Fig. 2d) and lightning NO_x is available only locally (Fig. A1: compare April vs. August). The local minimum of net O_3 production at the tropopause is due to missing uplifted O_3 precursors, while the decreasing net O_3 production 200 hPa below the tropopause and lower is due to missing NO_x. Note that in contrast to these conclusions from laterally averaged profiles, O_3 production in any specific air mass might still be limited by either NO_x or CO.

Both, NO_x and other precursors are more abundant in the Tibetan part UT, resulting in higher photochemical O_3 production than in the Iranian part (Figs. 2gh; see also supplementary material, Fig. S8 for time averaged profiles). O_3 depleting conditions prevail in the mid troposphere over the Arabian Peninsula throughout the summer (Fig. 2g, circled). Thus increased O_3 there (Fig. 2e) must be due to transport. Increased net photochemical O_3 production certainly contributes to relatively high O_3 mixing ratios in the ASMA, despite the influx of O_3 poor air linked to the CO rich updraughts. Entrainment of O_3 rich air from the TL additionally enhances O_3 in the ASMA.

4 Tracer tracer relations in September 2012

The distribution of points in a tracer-tracer diagram (i.e. mixing ratios of two species encountered simultaneously) provides hints on the origin and evolution of air masses. Here we focus on CO versus O_3 (Fig. 4) and HCl versus O_3 (Fig. 5), while NO_x versus O_3 and NO_x versus NO_y are shown in the supplementary material (Figs. S9, S10). A short primer for the interpretation of such diagrams is provided in Appendix B.

In order to place the observed tracer-tracer relations into context, we plot the measured samples together with grid-cell samples from the EMAC simulation. Because simulation output along the flight track is too sparse for a meaningful comparison (e.g. POI3: about 180 observations correspond to only 3 simulated samples). Therefore 5000 simulated samples per panel are chosen randomly, from the entire month of September 2012 and from throughout the ASMA region, as shown in Fig. 1 (Tibetan plus Iranian parts). Plotting all corresponding samples form the EMAC simulation would impair the visibility of clustering. Two different vertical ranges are chosen. The range from 50 hPa above to 100 hPa below the actual EMAC tropopause (Figs. 4a, 5a, S9a, S10a) provides a zoom-out view of possible tropospheric and stratospheric tracer mixing ratios and tracer-tracer relations for the time of year and region of the measurements. Zooming in to the altitude range of measurements, we choose tropospheric tracers from the pressure altitude range 200 hPa to 100 hPa (Figs. 4b, 5b, S9b, S10b).

Field Code Changed

Formatted: Subscript

Formatted: Font color: Auto

The observations from the beginning of POI2 to the end of POI6 are shown in (Figs. 4c, 5c, S9c, S10c), where colouring corresponds to measurement time. Similar colours indicate spatial and temporal proximity, a prerequisite for mixing lines.

4.1 Ranges covered by observed and simulated tracer-tracer distributions

POI2 is marked by dark blue dots in Figs. 4c, 5c, S9c, S10c, and is clearly distinct from the measurements in the ASMA filament (orange boxes). The ranges covered by the measurements are also given in the corresponding panels with simulated data, but are adjusted for model biases there. Those biases were estimated according to comparisons by eye, of measured versus simulated trace gas mixing ratios along the flight track in the ASMA filament (see accompanying paper). All measured ranges fit into the simulated monthly averages for September 2012 in the ASMA region, so the simulation captures this aspect well and the measurements are unlikely to represent an exceptional situation. We also note that all measurements clearly fall into the tropospheric regions of the respective simulated tracer-tracer spaces. This is no surprise: all HALO ESMVal measurements considered here were taken well within the troposphere, and tropospheric trace gas signatures are expected to dominate the distribution of points in the tracer-tracer diagrams.

4.2 In situ photochemistry, tropospheric and TL contributions

CO versus O_3 (Fig. 4): O_3 and CO display opposite gradients across the tropopause, and globally have lifetimes of several months in the UT (IPCC, 2013). Thus mixing lines in a CO versus O_3 scatter plot are generally suited to identify stirring and mixing processes in the UT that occur on timescales of days to weeks, including cross-tropopause mixing (Fischer et al., 2000). The well known L shape (Hoor et al., 2002; Pan et al., 2004; Müller et al., 2016) is reproduced by the simulation in the CO vs. O_3 diagram for the UTLS (Fig. 4a), consisting of a CO-poor & O_3-rich stratospheric branch, connected by UTLS mixing lines to a CO-rich & O_3-poor tropospheric branch.

Field Code Changed

However, the above studies (Hoor et al., 2002; Pan et al., 2004; Müller et al., 2016) focused on the extratropics. The ASMA is mostly situated in the tropics, where trace gas mixing ratios are controlled by different processes (Gettelman et al., 2011). The ASMA in particular constitutes a special atmospheric situation, because a continuous resupply of rapidly uplifted lower tropospheric air impedes UT photochemical equilibrium there. O_3 is photochemically produced in the ASMA at a net rate of almost 4 nmol/mol/day (Fig. (Barret et al., 2016)2h). Only 2 weeks are needed to increase O_3 mixing ratios by 50 nmol/mol, i.e. to produce the O_3 enhancement observed at the beginning of POI3. This is not much longer than the advection timescales (~10 days) discussed in the context of the HALO ESMVal campaign. Thus photochemical production needs to be considered as an alternative to stratospheric in mixing for explaining enhanced O_3 in the ASMA. Photochemical ageing increases O_3 and depletes CO here.

Field Code Changed

Mixing lines with negative slopes in CO vs. O_3 space dominate the UT observations (black dotted in Fig. 4c). Such mixing lines in the troposphere could result from one or a combination of the following: (i) mixing between stratospherically and tropospherically influenced air masses; (ii) mixing between photochemically aged and freshly uplifted lower tropospheric

air; (iii) an O_3 depleting photochemical regime (Baker et al., 2011). While the latter is unlikely in the ASMA (Fig. 2h), we need to consider additional tracers to disentangle stratospheric influence and photochemical ageing.

HCl versus O_3 (Fig. 5): As discussed in the context of Fig. 2, HCl is a proxy for stratospheric entrainment and CO marks tropospheric influence. Consider the hypothetical case of constant HCl (indicated by schematic line L1 and parallels in Figs. 4b, 5b): increasing O_3 corresponds to increasing CO then. The trace gas gradients along that hypothetical line reflect a gradient in net O_3 production rather than differences with respect to stratospheric influence between two reservoirs. Now consider the opposite case, i.e. constant CO (hypothetical line L2 in Figs. 4b, 5b): increasing O_3 corresponds to increasing HCl, indicating a gradient of stratospheric influence. CO mixing ratios decrease for increasing HCl in the special case of constant O_3 and different HCl mixing ratios (hypothetical line L3 in Figs. 4b, 5b). This indicates mixing between a tropospheric and a stratospheric reservoir, where two opposite effects lead to almost constant O_3 mixing ratios: increased net O_3 production in air with decreased HCl, versus both increased O_3 and HCl in the more stratospheric components. In intermediate cases the trace gas gradients in the tracer-tracer plots reflect a combination of gradients in in-mixing as well as in situ photochemistry. Spatial gradients of photochemical O_3 production dominate over gradients of stratospheric influence (i.e. in-mixing from the TL or stratosphere) within the sampled air mass, if increasing O_3 correlates with increasing CO and decreasing HCl (hypothetical line L4 in Figs. 4b, 5b). In contrast, gradients of stratospheric or TL in-mixing dominate, if increasing O_3 correlates with increasing HCl and decreasing CO (hypothetical line L5 in Figs. 4b, 5b).

The measurements (Figs. 4c, 5c) mostly –but not exclusively- show the latter case: neighbouring points form negatively sloped lines in CO vs. O_3 space (black dotted in Fig. 4c), corresponding to horizontal to positively sloped lines in HCl vs. O_3 space (black dotted in Fig. 5c). Thus observed trace gas gradients are mostly due to gradients of stratospheric influence on some well-mixed UT background. This could either be entrainment of tropospheric air into a more stratospheric background, or entrainment of TL air into a more tropospheric background. There are also a few almost vertical mixing lines in Fig. 5c, mostly at the lower end of observed HCl mixing ratios. We interpret those vertical components as a result of mixing between young and aged lower tropospheric air, because HCl mixing ratios in convectively uplifted air masses are decreased. Systematic HCl gradients –like across the tropopause- are not expected in convectively uplifted air. O_3 variability in such air masses is at least partly due to different amounts of in situ produced O_3. However, mixing between aged and young tropospheric air alone cannot explain the observations.

We further note that mixing lines in Fig. 5c cover similar ranges of HCl, but are separated by different levels of O_3. The corresponding background air had seen similar amounts of stratospheric influence, but different O_3 production. As long as all points of an individual mixing line are subject to similar O_3 production, the entire line will be shifted to different O_3 levels. The O_3 ranges covered by individual mixing lines are similar to the offsets between different lines. Individual mixing lines in the measurements cover timescales of about 20 minutes (Fig. 4c), corresponding to 300 km at typical HALO speeds. The flight track in the ASMA filament altogether covers more than 3000 km and multiple mixing lines were found on that scale.

Summarizing, our observations of O_3, HCl and CO in an ASMA filament show that: (i) Both, photochemical production and TL/stratospheric in-mixing contribute to increased O_3 in the observed ASMA filament; (ii) small-scale gradients of

Formatted: Subscript

~~stratospheric influence are superimposed on background regions that are rather homogeneous on small scales (hundreds of kilometres), but differ in their amounts of photochemically produced O_3 on larger scales (thousands of kilometres).~~

~~6~~5 P~~Discussion of~~rocesses and their ~~the~~ interplay ~~of dynamics and composition~~ in the ASMA ~~beyond the HALO ESMVal campaign~~

In this section the observed and simulated trace gas signatures are related to simulated photochemical, transport and mixing properties of the ASMA. The term "interplay" is thereby used in a neutral sense regarding the direction of feedbacks between different processes: It subsumes mostly one-way interactions (e.g. emissions affecting O_3 production, dynamics affecting trace gas distributions) here. ~~for timescales beyond the HALO ESMVal campaign by analysing selected processes in the EMAC simulation for 5 consecutive monsoon seasons (2010 – 2014).~~ We note upfront that the intra-annual variability of trace gas dynamics in the Tibetan and Iranian ASMA regions as discussed ~~in detail~~ for the year 2012 in section ~~5~~3 is largely similar in the other considered years (supplement, Figs. S2-~~6~~S7, include the parameters shown in Figs. 4, 5; ~~supplementary material, Fig. S16~~). ~~Building on that, we discuss additional aspects of the following processes: (1) Entrainment of O_3-rich TL air at the northern or eastern edge of the anticyclone; (2) Photochemical in situ O_3 production that also contributed to the increased O_3 observed during our campaign; (3) Radial stratification in the ASMA circulation; (4) Stirring related to dynamical instabilities of the anticyclone. Finally we consider the interplay of those processes and the implications for trace gas distributions in the ASMA and its outflow.~~ ~~The term "interplay" is thereby used in a neutral sense regarding the direction of feedbacks between different processes: It subsumes mostly one-way interactions (e.g. emissions affecting O_3 production, dynamics affecting trace gas distributions) here.~~

6.1 Lightning NO_x

In our EMAC simulations, $LiNO_x$ is released based on a parameterisation that links flash frequency to updraft velocity in - also parameterised - convection. It is difficult to narrow down $LiNO_x$ emissions (Schumann and Huntrieser, 2007), and both parameterizations are a notorious source of uncertainty in global models. The parameterizations for convection (Tiedtke, 1989; Nordeng, 1994; Tost, 2006) and lightning (Grewe et al., 2001) used in our simulations have been tested in several studies (Tost et al., 2007; Grewe, 2009; Lopez, 2016) and appear to be state of the art. EMAC-simulated lightning activity matches the corresponding TRMM-LIS/OTD observations (Cecil, 2006) reasonably well, temporally and spatially (Appendix A). Simulated and observed NO along the HALO ESMVal flight track agree remarkably well within the ASMA region (accompanying paper). The same is true for comparisons of IAGOS-CARIBIC measurements of NO and our simulation's output along the IAGOS-CARIBIC flight tracks, where the agreement is particularly noticeable for the monsoon season in the ASMA region (Appendix A). There is no proof that EMAC is right for the right reasons, and a dedicated comparison to other models is desirable. For the current study, however, the above comparisons provide some confidence that $LiNO_x$ emissions have been captured well by the simulation.

Formatted: Font color: Auto
Formatted: Font color: Auto
Formatted: Not Highlight
Formatted: Not Highlight
Formatted: Not Highlight
Formatted: Not Highlight
Formatted: Subscript
Formatted: Subscript
Formatted: Subscript
Field Code Changed
Field Code Changed
Field Code Changed
Field Code Changed
Field Code Changed
Formatted: Subscript

Simulated $LiNO_x$ emission rate profiles for 2012 show prominent maxima for the eastern and western ASMA regions during spring (Figs. 5cd). Overall, $LiNO_x$ emissions are much stronger in the Tibetan part. The emissions reach up to the tropopause throughout the year, implying that $LiNO_x$ is emitted at higher potential temperatures during the monsoon season (Fig. 2b). Despite higher emission rates in the laterally averaged profiles (Fig. 2d), lightning activity in the Tibetan part is more sporadic and localized in spring than in summer (Appendix A). During the monsoon season, $LiNO_x$ is constantly replenished in the ASMA throughout the region. Sensitivity simulations show that UT NO_x (Fig. 4h) is mainly $LiNO_x$ during the monsoon season (Appendix A).

6.2 Entrainment of lower tropospheric air

The uplift of lower tropospheric air to the UT is a well known characteristic of the ASMA (Pan et al., 2016). Simulated CO profiles in the Tibetan region show episodes of such uplift not only for 2012 (Fig. 4d), but for every monsoon season 2010 – 2014 (supplement, Fig. S2b). This is consistent with the HALO ESMVal measurements, since the trace gas gradients observed in the ASMA can be explained by mixing between lower tropospheric air and stratospherically influenced air.

CO uplift to the UT and $LiNO_x$ emissions are both related to convection and it is remarkable that there is a much stronger correlation between the two in summer than in spring (Figs. 4d, 5d). We attribute this to three effects: (i) The large scale uplift at the south-western flank of the Himalayas is only active during the monsoon season and not exclusively driven by deep convection (see sections 1, 3). It has been suggested as the main transport pathway of pollutants to the UT (Bergman et al., 2013; Pan et al., 2016), which is supported by our simulation (supplement, Fig. S11) and the location of maximum moist static energy (Boos and Hurley, 2013). Back-trajectory calculations in the accompanying paper identified this pathway as the source of enhanced CO in some of the HALO ESMVal measurements, despite that the underlying reanalysis does not account for (small scale) convection; (ii) In the UT the ASMA is an – although leaky - transport barrier, allowing some accumulation of the uplifted pollutants (Pan et al., 2016). There is no such transport barrier in spring; (iii) The spatial and temporal match of deep convection and increased CO at different altitudes reflects the potential for entrainment and subsequent convective transport of CO (Figs. 5gh). It is clearly increased in summer. More detailed analyses (supplement, Figs. S12, S13) show that convection is localized over the coastal regions of Western Bengal and Bangladesh in April 2012. In contrast, during August 2012 convection is ubiquitous throughout the Tibetan region. It is most persistent at the south-western flank of the Himalayas and over the Tibetan plateau. This coincides with the highest CO mixing ratios, which are accumulated there by the prevalent south-westerly winds during the monsoon season. Consequently, more CO is transported through the troposphere in the Tibetan region during summer.

6.3 Photochemical O_3 production and ageing

The net photochemical O_3 production rate (Figs. 5ab) is derived from the difference of EMAC simulated diagnostic tracers $ProdO_3$ and $LossO_3$ (Jöckel et al., 2016). Here we take into account effective O_3 production and loss terms following (Crutzen and Schmailzl, 1983) and extended by Grewe et al. (2017, see their supplement). There are known high-O_3 biases

Formatted: Subscript
Formatted: Subscript
Formatted: Font color: Auto
Formatted: Font color: Auto,
Formatted: Font color: Auto
Formatted: Font color: Auto
Formatted: Subscript
Formatted: Subscript
Formatted: Subscript
Field Code Changed
Formatted: Subscript
Formatted: Not Highlight
Field Code Changed
Formatted: Font color: Auto
Formatted: Font color: Auto
Formatted: Font color: Auto
Formatted: Font color: Auto
Formatted: Font color: Auto
Formatted: Font color: Auto
Formatted: Font color: Auto
Formatted: Font color: Auto
Formatted: Font color: Auto
Formatted: Font color: Auto
Formatted: Font color: Auto
Formatted: Font color: Auto
Formatted: Font color: Auto
Formatted: English (U.K.)
Formatted: Font color: Auto
Formatted: Font color: Auto
Formatted: Font color: Auto,
Formatted: Font color: Auto
Formatted: Font color: Auto,
Formatted: Font color: Auto
Formatted: Font color: Auto
Formatted: Font color: Auto
Formatted: Subscript
Formatted: Font color: Auto

in the simulation (Jöckel et al., 2016), and uncertainties in the chemical mechanism (Gottschaldt et al., 2013) also impose uncertainties onto O_3 photochemistry. Nevertheless our simulated net O_3 production rates in the ASMA (Fig. 5b) agree remarkably well with the independent estimate of Barret et al. (2016).

O_3 photochemistry is dominated by catalytic cycles in the troposphere and affected by a variety of parameters, e.g. ambient mixing ratios of H_2O, O_3, CO and NO_x (Ehhalt and Rohrer, 1994; Grooß et al., 1998; Jaeglé et al., 1998; Seinfeld and Pandis, 1998). We focus on NO_x and CO for illustration (Fig. 6). Photochemical O_3 production[1] ($ProdO_3$) non-linearly depends on ambient NO_x mixing ratios: It increases proportional to NO_x in the NO_x-limited regime, is almost independent of NO_x variations at higher NO_x mixing ratios, and a further increase of NO_x even leads to decreasing $ProdO_3$ (NO_x-saturated regime). Increasing CO increases $ProdO_3$ and shifts the point of maximum $ProdO_3$ to higher NO_x. Increasing H_2O impacts $ProdO_3$ qualitatively similar as increasing CO. Decreasing O_3 leads to higher $ProdO_3$, but NO_x at the point of maximum $ProdO_3$ is lowest for medium O_3 mixing ratios.

The simulation shows the superposition of the above effects, amongst others within the full complexity of the chemical mechanism. As a result, a net O_3 producing photochemistry prevails in the ASMA throughout the monsoon season (circled in Figs. 5ab). This is accompanied by net O_3 destruction during the monsoon season 300 hPa below the tropopause and lower. At the tropopause and slightly above, there is a local minimum of net O_3 production, followed by increased net O_3 production in the stratosphere. Net O_3 production is at maximum in the altitude range, where uplifted young air (enriched in CO and co-emitted volatile, organic O_3 precursors) mixes with NO_x-rich UT air (Figs. 4dh, 5b).

$ProdO_3$ per NO_x shows a strong gradient at the altitude of maximum net O_3 production (circled in Figs. 5bf). This indicates the transition from the NO_x-limited to the NO_x-saturated regime (Fig. 6), but is superimposed by gradients of CO and other O_3 precursors. The maximum corresponds to about 300 pmol/mol NO_y (circled in Fig. 3h), and variations of NO_x in that region have a relatively little effect on net O_3 production ("2" in Fig. 6).

Going down from the TP in the ASMA, NO_x and O_3 generally decrease, while CO and H_2O increase (Fig. 4, H_2O not shown). It's a multi-dimensional problem. CO (among others) determines the curve in the NO_x-vs-$ProdO_3$ diagram, and NO_x determines the operating point on the curve. Considering typical ranges of CO and NO_x in different parts of the ASMA, an area on the surface in $ProdO_3$-NO_x-CO space is termed "operating mode of the chemical system" in the following. Different chemical regimes (e.g. NO_x-limited or NO_x-saturated) are allowed within one operating mode. The non-linear dependence of $ProdO_3$ on ambient trace gas mixing ratios leads to the simulated maximum within the opposite gradients of those trace gases (NO_x decreases below the TP, while CO increases) in the UT ASMA. Going down from the TP, the chemical system goes from operating mode "3" to "2" to "1" (Fig. 6). In principle, all those operating modes could be in the NO_x-limited regime and still lead to a maximum of net O_3 production in the UT. However, our simulations also show the NO_x-saturated regime (supplement, Fig. S15).

[1] Net O_3 production in the UT is determined rather by $ProdO_3$ than by $LossO_3$ (supplement, Figs. #+S4, #+S7, #+S15), so it is sufficient to analyze $ProdO_3$ in this context.

Formatted: Subscript
Field Code Changed
Formatted: Font color: Auto
Field Code Changed
Formatted ... [1]
Formatted ... [2]
Formatted ... [3]
Formatted ... [4]
Formatted ... [5]

Periods of enhanced lightning NO_x in spring (circled in Fig. 5d) correspond to increased net O_3 production (Fig. 5b), but despite higher LiNO_x emissions in spring, net O_3 production is at maximum in the ASMA. The main differences between the seasons are that there is less CO in the UT during spring (Fig. 4d) and lightning NO_x is available only locally (section 6.1. and Appendix A). More CO in the UTLS in summer increases ProdO_3 and the maximum possible O_3 production (Fig. 6). Too high NO_x in spring does not help ProdO_3 – or even pushes the system into the NO_x-saturated regime ("3" in Fig. 6). NO_x close to maximum ProdO_3 conditions ("2" in Fig. 4) throughout the region in summer leads to higher ProdO_3 in the lateral average.

Both, NO_x and other precursors are more abundant in the Tibetan part UT, resulting in larger photochemical O_3 production than in the Iranian part (Figs. 5ab). This is consistent to other studies (Liu et al., 2009a; Barret et al., 2016), which also found such an asymmetry. O_3 depleting conditions prevail in the mid-troposphere over the Arabian Peninsula throughout the summer (Fig. 5a, circled). Thus increased O_3 there (Fig. 4e) must be due to transport.

Confinement in the ASMA circulation allows the mixed air to age, i.e. to produce O_3. CO is being depleted in the process of ageing, and NO_x is transferred to NO_y. The other source of aged air is entrainment from the TL, which is however enriched in HCl (at least within the photochemical lifetime of HCl). O_3 is produced in the ASMA at a net rate of about 4 nmol mol^{-1} day^{-1} (Fig. 5b), and simulated O_3 mixing ratios in the UT of the ASMA region vary by about 120 nmol/mol (Fig. 3b). It would take 30 days to cover that range by photochemical O_3 production alone. The observed values in the ASMA filament cover a range of about 48 nmol/mol (Fig. 3c), corresponding to 12 days of photochemical O_3 production. According to the trajectory calculations in the accompanying paper, this is about the time needed to circle the ASMA. The above O_3 variability of course includes different amounts of O_3 from the TL, and O_3 productivity varies too. Neglecting these uncertainties, it takes one or two rotations of the ASMA to transform O_3-depleted, freshly uplifted air into aged, O_3-enhanced air. O_3-depletion in the ASMA relative to the regional average can only be maintained by frequent replenishment of young air.

6~~5~~.4~~1~~ Entrainment of tropopause layer~~lower tropospheric and TL~~ air

~~The uplift of lower tropospheric air to the UT is a well known characteristic of the ASMA (see section 1 and references therein). We consider enhanced CO in the ASMA as a marker for air of lower tropospheric origin. Simulated CO profiles in the Tibetan region show episodes of such uplift in every monsoon season 2010 – 2014 (Fig. 6b), and particularly throughout the monsoon season of 2012 (Fig. 2d). This is consistent with the HALO-ESMVal measurements, since the trace gas gradients observed in the ASMA can be explained by mixing between lower tropospheric air and stratospherically influenced air (section 4 and accompanying paper).~~

Here we focus on the less well known entrainment of stratospheric or TL air into the free troposphere, which is supported by the unique thermodynamic conditions over the Tibetan plateau in summer (Fig. 1). ~~The heating of the plateau mainly initiates and maintains the ASMA. Thereby PV surfaces are lifted to form domes above the Tibetan plateau, while potential temperature surfaces form wells at the same time. Furthermore, the transition from the extratropics to the tropics occurs at~~

Formatted: Font color: Auto
Formatted: Font color: Auto
Formatted: Font color: Auto
Formatted: Font color: Auto
Formatted: Font color: Auto
Formatted: Font color: Auto
Formatted: Font color: Auto
Formatted: Font color: Auto,
Formatted: Font color: Auto
Formatted: Font color: Auto
Formatted: Font color: Auto,
Formatted: Font color: Auto
Formatted: Font color: Auto
Formatted: Font color: Auto,
Formatted: Font color: Auto
Formatted: Font color: Auto
Formatted: Font color: Auto,
Formatted: Font color: Auto
Formatted: Font color: Auto
Formatted: Font color: Auto
Formatted: Font color: Auto
Field Code Changed
Formatted: Font color: Auto
Formatted: Font color: Auto
Formatted: Font color: Auto
Formatted: Font:

~~the same latitude range and is accompanied by a steeply inclined tropopause (Fig. 7). The dominating physical processes differ between the extratropics and the tropics (Gettelman et al., 2011), resulting in a generally higher tropopause in the tropics. An isocontour of potential vorticity (PV) is commonly used to diagnose the tropopause in the extratropics, e.g. at 3.5 PVU in EMAC. Flows in the atmosphere, as a first-order approximation, tend to follow isentropic surfaces. Between 20°N and 30°N, isentropes from the extratropical lower stratosphere intersect the tropopause, some almost perpendicular (Fig. 7).~~

The prevailing northerly winds (Kunze et al., 2010) of the eastern ASMA flank (Fig. 1) tend to transport high-PV (stratospheric or TL, Fig. 2c) air along the isentropic surfaces into the troposphere (Ren et al., 2014; Kunz et al., 2015). This effect was also detected by Konopka et al. (2010) as enhanced horizontal transport of O_3-rich air from the extratropics into the TTL. Such transport from the TL or even the extratropical lower stratosphere into the free tropical troposphere may not leave a tell-tale signature of increased potential temperature ~~(Tpot)~~ in the corresponding air masses in the tropics. This includes the 350 K – 370 K isentropes that were encountered during the HALO ESMVal campaign in the tropics (Fig. 2~~7~~; θ estimates for the measurements are shown in the supplement~~ary material~~, Fig~~s~~. S~~9~~11, S12).

Additional stratospheric or TL contributions at~~to~~ the outer ASMA edge~~fringe~~ other than at the eastern flank are also plausible. The eastern Mediterranean and Central Asian region is a global hot spot of tropopause folding activity (Tyrlis et al., 2014), which is related to ASMA dynamics and generates enhanced O_3 levels through stratosphere-troposphere exchange (Akritidis et al., 2016). If the ASMA circulation encompasses that tropopause folding hotspot, it may pick up stratospheric entrainments ~~(see also supplementary material, Fig. S13). Lawrence and Lelieveld (2010) already suggested that O_3 rich air masses might be swept around the ASMA.~~

A stratospheric influence is manifested in our measurements by increased HCl mixing ratios in combination with other tracers (~~see~~ section 4.3~~2~~). ~~Furthermore the detailed analyses of POI3 in the accompanying paper show entrainment of TL air into the ASMA circulation at the eastern flank of the UT anticyclone. No indication for other stratospheric contributions was found. The stratospheric influence in the observed ASMA filament is consistent with recent TL entrainment at the eastern ASMA flank, but also with earlier entrainments of TL or stratospheric air. In the latter case stratospherically influenced air was already circling in the ASMA fringe before arriving at the eastern flank.~~

Did the HALO ESMVal campaign encounter an exceptional situation, or does TL entrainment at the eastern ASMA flank occur more often? The synoptic situation in question is characterized by a filament of enhanced HCl that is carried along the south-eastern ASMA flank, around a HCl-depleted ASMA interior. Here we analyse the evolution of simulated HCl mixing ratios at θ = 355 K, on a meridional (N-S) transect at 90°E, throughout the monsoon seasons of 2010 to 2014. The transition between eastward and westward winds indicates the location of the ASMA centre on the meridional transect, which wobbles around 30°N (white “ridgeline” in Fig. 7b). Enhanced tropospheric HCl mixing ratios south of the ridgeline serve as an indicator of TL entrainment (Fig. 7c). Caution with this interpretation is only needed at times when the ASMA is shifted to the West (compare Fig. 7a), because the transect in Fig. 7c may then be too far within the eastern ASMA flank. Episodes of increased HCl in the southern or eastern ASMA flank cover at least half of the time axis, showing that entrainment of TL air into the ASMA circulation is quite a common process. One horizontal slice from each analysed month is shown in the

Field Code Changed
Field Code Changed
Field Code Changed
Formatted: Not Highlight
Formatted: Font color: Auto
Field Code Changed
Formatted: Font color: Auto
Field Code Changed
Formatted: Font color: Auto
Formatted: Font color: Auto

supplement (Fig. S14), indicating that filaments of enhanced HCl often protrude from a TP trough of a Rossby wave at the eastern ASMA flank. The association of this mixing process with planetary wave breaking events is a topic of ongoing research (Lubis and Nakamura, 2017). We use HCl as a tracer for TL entrainment in the altitude range of the measurements in the simulation. Indeed situations similar to the one seen in September 2012 occur quite regular in the monsoon season. Figure 8 shows a collection of snapshots of the corresponding simulated synoptic distributions of HCl: one HALO ESMVal campaign like situation was selected from each month of the monsoon seasons (July – September) of the years 2010 – 2014. In each panel (Fig. 8) the south-eastern ASMA flank is marked by a filament of enhanced HCl, which often protrudes from a tropopause trough at the eastern flank. HCl mixing ratios steeply decrease towards the ASMA interior in all snapshots, which can be explained by HCl-poor upwellings. Those lower tropospheric upwellings are the main driver of the ASMA circulation and mostly located in the eastern part of the Tibetan anticyclone (Nützel et al., 2016).

A more continuous exploration of the frequency of TL entrainment in the simulation is given in Fig. 10. Figure 10b shows the zonal wind fraction ($u/\sqrt{u^2+v^2}$) along a meridional (N-S) transect throughout the monsoon seasons of 2010 to 2014. The UT transect is located at 90°E, i.e. approximately through the centre of the Tibetan anticyclone. This is a proxy for the meridional location of the ASMA. The pattern corresponds to an anticyclone, with its centre (zero = white = "ridgeline") moving north and south around 30°N. Enhanced tropospheric HCl mixing ratios south of the ridgeline serve as an indicator of TL entrainment (Fig. 10c). Caution with this interpretation is only needed at times when the ASMA is shifted to the West (compare Fig. 10a), because meridional transects in Fig. 10c may then be too far within the eastern ASMA flank. Episodes of increased HCl in the southern or eastern ASMA flank cover at least half of the time axis, showing that entrainment of TL air into the ASMA circulation is quite a common process.

5.2 Photochemical O_3 production and ageing

A net O_3 producing photochemical regime prevails in the ASMA throughout the monsoon season (Figs. 2gh), and thus observed O_3 mixing ratios are partly due to in situ production (see section 4.2). O_3 production may be limited by the availability of precursors, namely NO_x and CO (and co-emitted, other volatile organic compounds). Furthermore, net O_3 production non-linearly depends on NO_x mixing ratios, being at maximum at about 300 pmol/mol (see section 3.5). NO_x and CO distribution show opposite vertical gradients in the ASMA: NO_x mostly decreases from the stratosphere towards the UT, CO decreases from the UT towards the tropopause (Figs. 2d, 3b). Lightning produces NO_x in the ASMA (Fig. 3gh, Appendix A) and some NO_x of stratospheric origin gets entrained from the TL. CO and co-emitted precursors are uplifted from the lower troposphere. The net O_3 production is at maximum in the altitude range, where uplifted young air mixes with NO_x-rich UT air. It was shown in the accompanying paper that the simulated net O_3 production at 168 hPa is rather limited by the availability of CO than by too much or too less NO_x. However, NO_x mixing ratios of 300 pmol/mol are abundant in the ASMA (Figs. 3ab), facilitating increased O_3 production.

Formatted: Font color: Auto

Formatted: Font color: Auto

Formatted: Font color: Auto

Formatted: Font color: Auto

Formatted: Font color: Auto

~~Confinement in the ASMA circulation allows the mixed air to age, i.e. to produce O_3. CO is being depleted in the process of ageing, and NO_x is transferred to NO_y. The other source of aged air is entrainment from the TL, which is however enriched in HCl. There is no appreciable HCl in uplifted air, and none is produced during ageing in the UT. The distinction between aged uplifted and entrained TL air is not always clear, since HCl in the UT is being depleted through oxidation by OH (see Appendix A).~~

~~We attribute some larger scale trace gas gradients in the measurements to different photochemical O_3 production (section 4). There are positive correlations between NO & O_3 and NO & NO_y (Fig. S9c and Fig. S10c), but not between CO & O_3 (Fig. 4c). This combination indicates that the measurements show a NO_x limited photochemical regime.~~

~~O_3 is produced in the ASMA at a net rate of about 4 nmol mol^{-1} day^{-1} (Fig. 2h). Simulated O_3 mixing ratios in the UT of the ASMA region vary by about 120 nmol/mol (Fig. 4b). It would take 30 days to cover that range by photochemical O_3 production alone. The observed values in the ASMA filament cover a range of about 48 nmol/mol (Fig. 4c), corresponding to 12 days of photochemical O_3 production. This is about the time needed to circle the ASMA (see accompanying paper). The above O_3 variability of course includes different amounts of O_3 from the TL, and O_3 productivity varies too. Ignoring these uncertainties, it takes one or two rotations of the ASMA to transform O_3 depleted, freshly uplifted air into aged, O_3 enhanced air. O_3 depletion in the ASMA relative to the regional average can only be maintained by frequent replenishment of young air.~~

~~6~~5.~~5~~3 Radial stratification and patchy trace gas distributions

Deep convection from the lower troposphere discharges more towards the ASMA interior, as shown by studies that report relatively young air there (Li et al., 2005; Randel and Park, 2006; Park et al., 2008; Liu et al., 2009b; Kunze et al., 2010; Liu et al., 2011; Santee et al., 2017) and also by our simulation (section 6.4~~Fig. 8~~). In contrast, trace gas signatures in a belt of outer streamlines are dominated by a combination of photochemically aged lower tropospheric air and entrainments of UT air surrounding the ASMA. In this schematic of an undisturbed anticyclone, interior trace gas signatures are generally characterised by lower O_3 mixing ratios than fringe signatures then.

Such radial zoning in the ASMA is an expression of almost closed circulation, and was observed in IAGOS-CARIBIC ~~(http://www.caribic-atmospheric.com)~~ in situ data of flights between Chennai, India and Frankfurt, Germany (Baker et al., 2011; Rauthe-Schöch et al., 2016). ~~ICARIBIC data show i~~ncreased O_3 mixing ratios were found in the northern part of the ASMA, and decreased levels towards the southern end of the flights. ~~This was tentatively attributed to differences in the time available for O_3 production there (Lawrence and Lelieveld, 2010), which is supported by corresponding differences in photochemical age (Baker et al., 2011; Rauthe-Schöch et al., 2016). Those observations are consistent with the above scenario of preferential replenishment of young air in the ASMA's interior, while the outermost streamlines are less affected by upwellings and photochemical ageing may proceed for longer. Furthermore, TL entrainment affects the ASMA fringe, enhancing the aged-air (increased O_3) signatures. It was even pointed out by Baker et al. (2011) that the aged-air signatures~~

Field Code Changed

Field Code Changed

Field Code Changed

~~can also be explained by stratospheric contributions, which they could only rule out along the CARIBIC flight tracks through the north-western ASMA flank.~~

Radial stratification is counteracted by t~~T~~he general on-off nature of TL entrainment, upwellings from the lower troposphere and lightning. Still considering only undisturbed ASMA circulation, all those effects lead~~s~~ to patches of air with different trace gas signatures ~~in the UT ASMA circulation~~. Each of these patches might again receive contributions from any of the above sources. In principle all sorts of combinations are possible, generating heterogeneity. In contrast, mixing and photochemical ageing are homogenizing effects. In combination with closed streamlines the preferential positions of the different sources might still ~~should~~ print through as radial stratification in the ASMA, or show up in individual situations (section 6.4).

However, neither the HALO ESMVal measurements, nor various ~~the~~ sequences of ~~corresponding~~ simulated snapshots (supplement) ~~or monthly mean values in the accompanying paper~~ show a clear stratification. The idealised picture that the ASMA circulation is dominated by stationary, closed streamlines is certainly not realistic - at least not on the timescales of the homogenizing effects.

~~6~~5.~~6~~4 Splitting-up and stirring

Transient streamlines, particularly eddy shedding or splitting of the ASMA, effectively overcome radial transport barriers. Whether stratified or patchy – any trace gas distribution in the ASMA might be subject to effective stirring then. There is an ongoing discussion about different dynamical modes of the ASMA (Nützel et al., 2016; Pan et al., 2016). ~~The study of Pan et al. (2016) distinguishes 4 phases: Tibetan plateau phase, Iranian plateau phase, longitudinally elongated phase, double centre phase.~~

Field Code Changed

Field Code Changed

A splitting-up event occurred just during the HALO ESMVal campaign, ~~, as consistently indicated by backward-trajectories, structure of the probed filament, and the simulated synoptic situation (see Fig. 9, Fig. 10, supplementary material and accompanying paper). It~~ correspond~~ings~~ to the transition from a~~n~~ longitudinally elongated phase to a double centre phase in the nomenclature of Pan et al. (2016). A sequence of simulated streamlines and tracer distributions shows that fringing parts of the elongated anticyclone become part of the interiors of both resulting anticyclones after the splitting, and interior parts are diverted into the fringes (supplement, Fig. S16). Even if not all possible cases are covered by the example, it is easily conceivable that fringing parts may also stay in the fringes and interior parts in the interiors. For a given location and timing of eddy shedding or splitting, the final trace gas distribution simply depends on the initial distribution of different patches. The redistribution of different parts of the anticyclone guarantees a high variability for outflow and interior, whenever the closed circulation breaks down.

Field Code Changed

~~We use the terms Iranian or Tibetan part/eddy/anticyclone to describe the splitting of one big into two smaller anticyclones. A sequence of simulated streamlines and tracer distributions illustrates that event (Fig. 9). Although patchy, CO mainly marks the ASMA interior and HCl serves as a proxy to track the ASMA fringe. The sequence starts with an elongated anticyclone on 16 September 2012 (Figs. 9ab). Then a tropopause trough (marked as "T_1" in Fig. 9) evolves from the west~~

~~along the northern ASMA flank. The elongated and thus inherently unstable anticyclone succumbs to the perturbation and splits up. A part of the initially compact increased CO interior region ("1") is entrained by the outer streamlines of the Iranian part ("1$_i$"), while the rest of the patch is diverted into the interior of the Tibetan anticyclone ("1$_t$"). A patch of increased HCl ("2" in Fig. 9b) dominates the northern interior part of the intact ASMA at start, which is partly diverted into the interior of the Iranian ("2$_i$") and partly into the fringe and interior of the Tibetan part ("2$_t$"). The majority of an HCl filament ("3") that marks TL entrainment is diverted to the Tibetan part. We also note entrainment of tropospheric air by southerly winds at the western flank ("4" in Fig. 9h).~~

~~The above example shows that fringing parts of an elongated anticyclone may become part of the interiors of both resulting anticyclones after the splitting. Interior parts may be diverted into the fringes. Even if not all possible cases are covered by the example, it is easily conceivable that fringing parts may also stay in the fringes and interior parts in the interiors. For a given location and timing of eddy shedding or splitting, the final trace gas distribution simply depends on the initial distribution of different patches. The redistribution of different parts of the anticyclone guarantees a high variability for outflow and interior, whenever the closed circulation breaks down.~~ How often does this happen? Splitting and eddy shedding mainly occur in zonal (E-W) direction, where the transition from northward wind in the west to southward wind in the east indicates the centre of an anticyclone or eddy. We analyse the evolution of meridional winds at θ = 355 K, on a wide (15°N – 35°N) zonal transect, throughout the monsoon seasons of 2010 to 2014 (Fig. 7a).

~~Figure 10a gives an impression of the variability of the ASMA during 5 consecutive monsoon seasons at 168 hPa. The meridional wind fraction is a proxy for the zonal (E-W) location of the anticyclone(s). It is calculated as $v/\sqrt{u^2+v^2}$, with meridional velocity v, and zonal velocity u.~~ The pattern at the given altitude is consistent with one dominating anticyclone, centred at about 90°E. While the northerly winds east of 90°E are relatively persistent, episodes of entirely southerly winds in the western part of the one-piece ASMA alternate with episodes of smaller, secondary anticyclones. Smaller anticyclones also occur regularly east of the Tibetan anticyclone, corresponding to eddy shedding to the East. The splitting event that occurred during the HALO ESMVal campaign is clearly visible in Fig. 7~~10~~a, too. Such instabilities occur approximately twice a month. This coincidentally corresponds to the timescale needed to photochemically erase O_3-depleted signatures in young air masses. ~~, which have ended up in parts of the ASMA that do not receive additional entrainments.~~

~~Open questions remain with regards to the controls of ASMA instabilities and the stirring associated with other transitions between the different dynamical modes. Consistent to the discussion in section 1 we just note that there is an independently sustained, mid-tropospheric anticyclone over the Arabian peninsula (supplementary material, Fig. S14). Whether or not coupling between the mid-tropospheric and UT systems plays a role for triggering ASMA splitting is not further analysed here.~~

~~5.5 ASMA outflow~~

Formatted: Font color: Auto

Formatted: Font color: Auto

Formatted: Normal

~~It was shown in the previous sections that entrainment of TL air and dynamical instabilities of the ASMA occur quite frequently in the simulation. Air is uplifted from the lower troposphere in the eastern part of the ASMA (indicated by CO: Fig. 2d) and a net O_3 producing photochemical regime prevails (Figs. 2gh), both throughout the monsoon season. Thus the main ingredients needed for the interpretation of our measurements are relevant beyond the HALO ESMVal campaign case.~~

~~First we discuss some implications for the question of Lawrence and Lelieveld (2010), whether O_3 in the monsoon outflow is enhanced or depleted. This is relevant for understanding the observed mid-tropospheric summer O_3 maximum over the Arabian Peninsula, i.e. one of the questions raised in section 1. ASMA contributions and transport pathways for the Arabian O_3 maximum have already been established (Liu et al., 2011; Richards et al., 2013; Garny and Randel, 2015) and are also seen in our simulation (section 3). Preferential export of fringe air with enhanced O_3 to the Arabian Peninsula is plausible because the secondary anticyclones or shed eddies tend to be smaller than the Tibetan anticyclone (Fig. 10a). The enhancement of fringe over interior air in the smaller eddies of ASMA outflow is a simple geometrical effect: the ratio of circumference (fringe) to area (interior) is inversely proportional to the size (radius) of the vortex. Even the export of younger, precursor-rich air (Liu et al., 2009a; Richards et al., 2013) from the ASMA interior would contribute to increased O_3 within a week due to photochemical net O_3 production. Both scenarios are consistent with a climatologically decreased O_3 interior in the UT ASMA and at the same time increased O_3 over the Arabian peninsula. However, at least in the simulation transport of O_3 dominates over in situ production in the mid troposphere of the Iranian part. Enhanced O_3 in the ASMA outflow would follow even more straightforward from climatologically enhanced O_3 throughout the ASMA.~~

~~We note that the entrainment of O_3 poor air by northerly winds at the western ASMA flank ("4" in Fig. 9; supplementary material, Fig. S15) counteracts the O_3 enrichment in the western ASMA region. However, there is an asymmetry: processes increasing O_3 dominate in the eastern part of the ASMA, which dynamically dominates the western part in the UT.~~

~~Dynamical instabilities of the ASMA also have contributed to the enhanced O_3 ASMA interior simulated for mid-September 2012. Larger fractions of the O_3 rich fringe were entrained during splitting up events (supplementary material, Fig. S15). The sequence of snapshots (Fig. S15) covers almost half a monsoon season and episodic O_3 poor upwellings over the Tibetan plateau are smaller and shorter lived than O_3 rich regions at 168 hPa. This is consistent with the corresponding monthly mean distributions, which show increased O_3 in the ASMA (accompanying paper).~~

~~However, longer periods of stability seem to strengthen lower tropospheric signatures in the ASMA interior. It was found that the residence time in the ASMA is crucial for the probability to enter the stratosphere (Garny and Randel, 2015). So this interrelation could lead to preferential transport of certain trace gas signatures from the ASMA into the stratosphere, but is not further analysed here.~~

~~7~~6 Summary

This study complements a detailed analysis of in situ trace gas measurements in the ASMA, obtained during the ESMVal campaign with the research aircraft HALO in September 2012 (Gottschaldt et al., 2017). The measurements are put in the

Formatted: Font: Bold

Formatted: Font: Bold

Formatted: Normal

Formatted: Font: Bold

Formatted: Font color: Auto

Field Code Changed

context of the EMAC simulated annual evolution of trace gas profiles in the ASMA region and simulated tracer-tracer relations. This led to the following qualitative understanding of the interplay of processes that determine the trace gas distributions in the ASMA and its outflow (Fig. 8~~11~~):

Air from the steeply inclined TL is entrained by outer ASMA streamlines at the eastern and possibly northern ASMA flank, defining a fringing zone. Tropopause troughs facilitate the entrainment.

~~The TL is characterised by a gradient between stratospheric and tropospheric trace gas signatures.~~ Stratospherically enhanced tracers like HCl and O_3 print through in the entrained air. Thus the fringe is not just a transport barrier, separating the ASMA interior from the respectively surrounding UT. It has a distinct genesis, resulting in air masses with distinct trace gas signatures that may be transported relatively unperturbed over long distances. Deep convection and ~~the upwellings in a~~ conduit of upwelling air over the Tibetan plateau (Bergman et al., 2013) inject lower tropospheric air mainly into the Tibetan part of the ASMA. Enhanced CO is an indicator for this process. Convection is accompanied by in situ production of lightning NO_x, mainly determining mixing ratios of this O_3 precursor in the ASMA.

~~Uplifted air preferentially feeds the ASMA interior, as also indicated by studies that report younger air there (Randel and Park, 2006; Park et al., 2007; Park et al., 2008; Kunze et al., 2010).~~ In the idealised case of one intact anticyclone (Fig. 8~~11~~a) the interior would then be dominated by photochemical ageing of those O_3-poor injections. Net O_3 production dominates in the ASMA, and is particularly enhanced where lower tropospheric O_3 precursors (VOCs) meet UT precursors (NO_x). The preferential positions of convective versus TL entrainments facilitate radial stratification in the ASMA. The intermittent nature of the entrainments, combined with the varying position of the anticyclone lead to patches of air that have different origins and are in different stages of ageing. Mixing and ageing act homogenizing, but each of these patches might again receive fresh entrainments from the TL or by convection plus lightning.

Eddy shedding~~, splitting of the ASMA into an Iranian and a Tibetan part,~~ or transitions between other ~~(Pan et al., 2016)~~ dynamical modes of the ASMA effectively overcome radial transport barriers (Fig. 8~~11~~b, summarizing supplemental Figs. S16, S17). ~~; see also Fig. 9 and supplementary material, Fig. S15).~~ Whether stratified or patchy – any trace gas distribution in the ASMA is subject to effective stirring then. Fringe air can be diverted into the interiors of both anticyclones, and likewise interior air is redistributed throughout the UT in the monsoon region. Remnants of earlier such events gradually lose memory of their origins, leading to a mixed “background” (grey in Fig. 8~~11~~b). ~~It remains an open question, if different dynamical modes of the ASMA are preferentially related to particular trace gas distributions.~~

W~~By analysing 5 consecutive monsoon seasons in the EMAC simulation w~~e found that the processes that led to the curious combination of both enhanced lower tropospheric and TL tracers in the ASMA filaments encountered by the HALO ESMVal campaign are not exceptional: entrainment of TL air and dynamical instabilities of the ASMA occur quite frequently. Deep c~~C~~onvection and thunderstorms are common throughout the monsoon season, accompanied by a net O_3 producing photochemical regime. The alternating interplay of those processes results in highly variable, patchy trace gas distributions in the ASMA. Processes that increase O_3 and its ~~O_3~~ precursors dominate in the Tibetan part of the ASMA. The Iranian part is dynamically dominated by the Tibetan part in the UT. O_3-rich TL entrainments and precursor-rich air, both

Field Code Changed

Formatted: Font color: Auto

Field Code Changed

Formatted: Font color: Auto

Formatted: Subscript

main ASMA components ~~and this asymmetry~~ tend~~s~~ to increase O_3 in the tropospheric ASMA outflow - e.g. ~~, e.g.~~ over the Arabian Peninsula.

Appendix A: Lightning NO_x in the ASMA

~~As noted already in the main text, LNO_x emissions play a major role in UT photochemistry of the ASMA region. At the same time those emissions are subject to considerable uncertainties (Schumann and Huntrieser, 2007). In our EMAC simulations, LNO_x is released based on a parameterisation that links flash frequency to updraught velocity in -also parameterised- convection (Grewe et al., 2001). For simulation RC1SD-base-10a the LNO_x emission rate profiles in the eastern and western ASMA regions for 2012 are shown in Figs. 3gh.~~ The discussion of the evolution of the $LiNO_x$ profile (Fig. 5) is ~~This is~~ supplemented by ~~by Fig. A1, which shows~~ the corresponding lateral distribution of monthly mean ~~LNOx~~$LiNO_x$ emission rates at the altitude of the HALO ESMVal measurements (Fig. A1). We note that there are strong, but localised emissions in the Iranian and Tibetan parts in spring (Fig. A1: Apr-May). ~~LNO_x~~$LiNO_x$ emissions are distributed throughout the Tibetan region in summer (Fig. A1: Jul-Sep). The simulated spatio-temporal emission patterns are similar for 2013 and 2014 (not shown).

Given the uncertainties of the parameterizations for convection and lightning in the model, smoothing and limited detection efficiencies in the observations, our simulated spatial-temporal distribution of lightning activity compares reasonably well to corresponding observations (supplement, Fig. S10). In particular we note that also the observations over South Asia show stronger lightning activity during spring than during the monsoon season. The observed maximum of lightning activity over the coastal areas of Western Bengal and Bangladesh in April also shows up in the simulation.

As noted in section 2, we compare simulated NO and NO_y to the corresponding IAGOS-CARIBIC observations (Fig. A2). ~~(Jöckel et al., 2010)~~Commercial airliners do not fly as high as HALO and the tracks hardly reach the southern ASMA fringe, but the northern ASMA edge and the center of the monsoon region have been sampled multiple times. We evaluated all 345 IAGOS-CARIBIC flights between 19 May 2005 and 9 April 2014, considering the respective latest data versions as of 10 November 2017. In total 86 flights between Frankfurt (IATA code: FRA) and Chennai (MAA) or Guangzhou (CAN) or Bangkok (BKK) transected the ASMA region. 32 of these flights provide NO data there, and 66 flights provide NO_y. Neglecting data below 300 hPa and subsampling to the time resolution of the simulation yields the numbers of comparable data that are given in Figs. A2bd. Given the above uncertainties related to the representation of $LiNO_x$ in the simulation, NO matches the corresponding IAGOS-CARIBIC observations surprisingly well (Fig. A2b). This holds also for the more robust (more data) global comparison (Fig. A2a). Increased $LiNO_x$ emissions in the ASMA region in spring are also consistent to IAGOS-CARIBIC, and the simulation might even slightly underestimate those emissions (Fig. A2b: MAM).

In order to link the ~~LNOx~~$LiNO_x$ emissions to the NO_x burden in the ASMA region, a suite of EMAC sensitivity simulations with modified emission factors was conducted (Figs. A3~~2~~, A4~~3~~). All EMAC analyses in the main text are based on

Formatted: Font color: Auto
Formatted: Subscript
Formatted: Subscript
Formatted: Subscript
Formatted: Font color: Auto
Formatted: Font color: Auto, Not Strikethrough
Formatted: Font color: Auto
Formatted: Font color: Auto,
Formatted: Font color: Auto
Formatted: Font color: Auto
Formatted: Font color: Auto
Formatted: Font color: Auto,
Formatted: Font color: Auto
Formatted: Subscript
Formatted: Font color: Auto
Formatted: Font color: Auto
Formatted: Font color: Auto
Formatted: Font color: Auto,
Formatted: Font color: Auto
Formatted: English (U.S.)
Formatted: Subscript
Formatted: Subscript

simulation RC1SD-base-10a (Jöckel et al., 2016), which is given in Fig. A32 just for comparison. The other simulations discussed in the context of Figs. A32 and A43 here are derived from EMAC simulation RC1SD-base-10, which differs in road traffic emissions and optical properties of stratospheric aerosol (Jöckel et al., 2016) from RC1SD-base-10a. Total ~~LNOx~~LiNO$_x$ emissions in RC1SD-base-10 are 4.6 Tg(N) in 2012 (Jöckel et al., 2016), which is in the realistic range of 2 – 8 Tg(N) yr^{-1} (Schumann and Huntrieser, 2007). RC1SD-base-10 and our base simulation for the ~~LNOx~~LiNO$_x$ sensitivity analysis (b01) are both operated in chemistry-climate model (CCM) mode, i.e. including interactive chemistry with feedback on dynamics. Simulation b01 differs only in the usage of daily (Kaiser et al., 2012) instead of monthly biomass burning emissions and 5 h instead of 10 h output intervals. Feedbacks from chemistry on dynamics in all quasi chemistry-transport model mode (QCTM) (Deckert et al., 2011) simulations are based on identical trace gas time series ~~climatologies~~ from b01. The same dynamics incl. convection is simulated in all QCTM simulations. Differences between a QCTM reference simulation (q01) and sensitivity simulations (s*) are thus exclusively due to chemical perturbations. All QCTM simulations cover June – September 2012, but the first 3 months were discarded for spin-up.

Figure A32 shows that RC1SD-base-10a captures observed O_3, CO, NO and NO_y along the HALO ESMVal flight path slightly better than b01 and q01. We are yet confident that the overall agreement is good enough for the analysis of chemical perturbations. For the QCTM sensitivity analyses it is more important to note that differences between b01 and q01 are negligible.

Figure A43k shows that halving ~~LNOx~~LiNO$_x$ emission factors results in almost halved NO_x in the uppermost troposphere. Doubling of ~~LNOx~~LiNO$_x$ emissions leads to almost doubled NO_x just below the tropopause (Fig. A43m). The biggest relative sensitivity in Fig. A43km almost coincides with the altitude range of the largest NO_x mixing ratios just below the tropopause (Fig. A43j). Thus, in our simulations ~~LNOx~~LiNO$_x$ clearly dominates the NO_x budget from the tropopause to 100 hPa below it. The impact of ~~LNOx~~LiNOx fades out at lower altitude, and almost vanishes at 400 hPa below the tropopause. This is consistent with the profiles of ~~LNOx~~LiNO$_x$ emissions in September 2012, which mainly occur in the Tibetan part of the ASMA (Fig. 5d~~3h~~).

Modifications of NO_x print through on other O_3 precursors mainly via changes to the atmospheric oxidizing capacity (OH: Figs. A43ghi). In response to halved ~~LNOx~~LiNO$_x$, OH decreases 200 hPa below the tropopause and lower, and increases above (Fig. A43h). The effects are reversed for doubled ~~LNOx~~LiNO$_x$ (Fig. A43i). The largest relative effects coincide with largest absolute OH mixing ratios.

CO decreases throughout the shown altitude range for halved ~~LNOx~~LiNO$_x$ (Fig. A43e). Without major production terms in the UT, modifications to CO mixing ratios are dominated by the loss reaction CO + OH → H + CO_2. The rate coefficient of this reaction is proportional to pressure, and otherwise depends only on constants (~~see~~ supplement to Jöckel et al. (2016)). Laterally averaged CO mixing ratios vary little from 50 to 400 hPa below the tropopause (Fig. A43d), but are affected by decreased and increased OH (Figs. A43fg). Decreased OH in the lower half of the domain dominates the overall CO response. CO rises through this region with higher pressures before reaching the UT in the Tibetan part of the ASMA (Fig. 42), which obviously outweighs the CO response to increased OH in the UT of Tibetan and Iranian part combined. Increased

Field Code Changed
Field Code Changed
Formatted: Subscript
Field Code Changed
Field Code Changed
Formatted: Subscript
Field Code Changed
Field Code Changed
Formatted: Subscript
Formatted: Subscript
Formatted: Subscript
Formatted: Subscript
Formatted: Subscript
Formatted: Subscript
Field Code Changed

OH 200 – 500 hPa below the tropopause consequently leads to an overall decrease of CO in response to doubled ~~LNO$_x$~~LiNO$_x$ (Fig. A~~43~~f). The O_3 precursors NO_x and CO display opposite trends in response to Δ~~LNO$_x$~~LiNO$_x$.

Curiously, HCl shows the opposite response to modified ~~LNO$_x$~~LiNO$_x$ (Figs. A~~43~~abc). There is no chemical production of HCl in the UT, and the only loss term in the simulations is HCl + OH → Cl + H_2O. The rate coefficient of this reaction is 1.7E-12 * EXP(-230/Temperature), see supplement to Jöckel et al. (2016). However, the tropospheric response of HCl to ΔOH is dominated rather by the vertical profile of HCl mixing ratios than by lower temperatures towards the tropopause. Almost all HCl in the UT is of stratospheric origin, and HCl mixing ratios steeply increase across the tropopause. Thus the UT response of HCl is dominated by ΔOH near the tropopause: increased OH for halved ~~LNO$_x$~~LiNO$_x$ increases HCl losses, and vice versa for doubled ~~LNO$_x$~~LiNO$_x$.

The response of UT net O_3 production to Δ~~LNO$_x$~~LiNO$_x$ (Figs. A~~43~~qrs) has mostly the same sign as ΔNO_x. As noted already in the context of Fig. ~~42~~, opposite gradients of O_3 precursors NO_x and CO in the UT lead to a broad altitude range of enhanced net O_3 production in the ASMA, centred about 100 hPa below the tropopause. O_3 production is limited by NO_x in lower altitudes and by CO (and other volatile organic compounds) towards the tropopause. NO_x and CO display opposite trends in response to Δ~~LNO$_x$~~LiNO$_x$, but relative changes to NO_x are larger and dominate the overall response of net O_3 production. We note, however, that the largest increase of NO_x at the end of September (circled in Fig. A~~43~~m) decreases net O_3 production to zero or even net loss (circled in Fig. A~~43~~s), indicative of the NO_x-limited photochemical regime. ~~The opposite effect is not seen for halved LNO$_x$ (Fig. A3r). Thus it is most likely due to the non-linearity of net O$_3$ production, which decreases above a certain NO$_x$ concentration threshold that also depends on other parameters (Grooß et al., 1998).~~

O_3 mixing ratios respond to Δ~~LNO$_x$~~LiNO$_x$ essentially like net O_3 production in the UT (Figs. A~~43~~nop). The altitude of maximum relative ΔO_3 is slightly lower than the altitude of maximum absolute changes to net O_3 production. We attribute this effect to upwards increasing absolute O_3 mixing ratios.

~~Appendix B: Primer for tracer-tracer diagrams~~

~~**Sampling of two different air masses that are in the process of mixing is indicated by a mixing line in the tracer-tracer diagram. The slope of the mixing line provides additional clues about the origin of the original air parcels ("end-members"). If the ratios of the end members remain constant over time, the slope of the mixing line is conserved, as long as the mixing process continues. If the mixing processes stops, the mixing lines converge to a single point in the tracer-tracer diagram. If the reservoir of one end-member is bigger than the other, points in the tracer-tracer diagram will be close to the dominating end-member. However, the relative size of the reservoirs does not affect the slope of mixing lines, thus allowing detection of even small entrainments. Slopes change in case of mixing ratio changes over time (e.g. via in situ production or loss) of one or both reservoirs. Different effects may lead to similar tracer-tracer relations, resulting in ambiguity when trying to reconstruct end-members or disentangling**~~

Formatted: Subscript
Formatted: Subscript
Formatted: Subscript
Field Code Changed
Formatted: Subscript
Formatted: Subscript
Formatted: Subscript
Formatted: Subscript
Formatted: Subscript
Formatted: Strikethrough
Formatted: Subscript
Formatted: Font color: Auto

~~mixing and chemical effects. Furthermore, mixing lines in general exist in a multi-dimensional tracer space, and thus lines in a tracer-tracer plot need to be considered as projections onto 2d space. They might also be the result of mixing between more than two reservoirs. Additional dimensions (tracers) need to be considered to reduce ambiguities.~~**Appendix B: Reactive nitrogen in the ASMA**

Nitrogen oxides are key parameters in atmospheric chemistry, partly controlling the O_3 production in the troposphere and lower stratosphere. In the UTLS, enhanced NO_y originates both from tropospheric and from stratospheric sources. In the lower troposphere odd nitrogen species are co-emitted with carbon monoxide in combustion processes, resulting in a strong correlation between both species. NO_y is enhanced in the stratosphere (mainly HNO_3), but it also comprises species with tropospheric sources ($LiNO_x$). Thus it is not a viable tracer for stratospheric air on its own.

The simulation matches IAGOS-CARIBIC NO_y almost perfectly on the global scale (Fig. A2c), and only moderately overestimates it during summer in the ASMA region (Fig. A2d: JJA).

Simulated NO_y profiles in the ASMA region from April to September differ to the rest of the year (Figs. B1ab), but the monsoon season is also distinct: during summer there is more NO_y in the UTLS and mid-troposphere in both, the Tibetan and Iranian regions (Figs. B1ab, 8). Episodes of enhanced NO_y (~1.5 nmol/mol) in the UT are frequent in the Tibetan part during summer, and alternate with periods of decreased NO_y (~1.0 nmol/mol). However, the altitude region just above the tropopause is hardly affected by this UT variability and maintains an average mixing ratio of ~1.2 nmol/mol NO_y (Figs. B1ab). NO_y mixing ratios generally increase with altitude in the lower stratosphere, but reach 1.6 nmol/mol only at about 15 hPa above the tropopause. E-shaped NO_y-profiles dominate the Tibetan part, with maxima in the lower troposphere, in the UT and in the lower stratosphere (Fig. B2b). Less NO_y is simulated in many profiles for the mid-troposphere and just above the tropopause transport barrier (Fig. B3). E-shaped NO_y–profiles were also reported by the NOXAR measurement campaign in the northern mid-latitudes and corresponding modelling studies (Grewe et al., 2001). The E-shape in northern mid-latitudes was in part attributed to aviation NO_x emissions (Rogers et al., 2002), but aviation effects are much smaller in the tropics (Gottschaldt et al., 2013). Instead of aviation emissions, in situ production of lightning NO_x in the prevalent thunderstorms of the monsoon season increases NO_y in the UT over South Asia (Fig. 5d, see also Appendix A). Thus a possible explanation for the E-shaped NO_y-profiles in the eastern ASMA part during the monsoon season is as follows: NO_y from boundary layer sources' pollution is uplifted, and solvable NO_y-components (e.g. HNO_3, N_2O_5) become increasingly washed out (Fig. S4a). At about 400 hPa below the tropopause only non-solvable components (e.g. NO_x) are left. Episodes of increased NO_y in the UT are well correlated with increased lightning NO_x emissions (Figs. S4a, 5d). NO_y mixing ratios however increase with altitude above the tropopause, due to increased photochemical production of HNO_3 in the stratosphere. With little in situ production and not much transport from above or below, NO_y mixing ratios in the region between the tropopause and 15 hPa above the tropopause are often smaller than in the adjacent altitudes.

Profiles in the western, i.e. Iranian ASMA part (Fig. B1a) have a different history of origins, and with just one minimum in the mid-troposphere are mostly C-shaped (Fig. B2). During summer the Arabian Peninsula is dry. Convection (as indicated

Formatted: Subscript
Formatted: Subscript
Formatted: Subscript
Formatted: Subscript
Formatted: Font color: Auto
Formatted: Font color: Auto
Formatted: Font color: Auto

by lightning NO_x emissions in Fig. 5c) is mainly localised near the Bab al-Mandab Strait (Fig. A1), i.e. at the edge of the region we defined for calculating profiles of the Iranian part of the ASMA. Washing out is negligible throughout most of the Iranian region (Fig. A1), and therefore NO_y can rise to about 400 hPa below the tropopause (circled in Fig. B1a). Downward transport (as indicated by anti-clockwise tilted signals, one example marked by an arrow in Fig. B1a) dominates above that altitude, preventing further uplift. With little in situ production of lightning NO_x over the Arabian Peninsula in summer (Figs. 5c and A1), UT NO_y in the Iranian part is dominated by the outflow of the Tibetan part.

As a combination of the different effects affecting NO_x and NO_y, the NO_x/NO_y ratio maintains a broad maximum in the TL throughout the year (Figs. B1cd). The monsoon season is characterised by particularly little fluctuations of NO_x/NO_y (Figs. B1cd, circles). During the monsoon, the NO_x/NO_y ratio in the UTLS is higher in the western than in the eastern ASMA part. This indicates preferential export of high-NO_x air from the Tibetan part, or is an artefact of the possible dominance of a single source of $LiNO_x$ in the Iranian averaging region (Fig. A1).

Simulated O_3 and NO_x increase in the stratosphere with a higher O_3/NO_x ratio than in the troposphere (Fig. B3a). At NO_x mixing ratios of more than 0.7 nmol/mol the corresponding O_3 mixing ratios would allow distinguishing stratospheric influence from tropospheric in situ production, but the range covered by the HALO ESMVal measurements is just at the intersection of stratospheric and tropospheric branch (orange box in Fig. B3a). Similar HCl mixing ratios are simulated throughout the ranges of measured NO_x and O_3 (orange box in Fig. B3b). Measurements of increased NO_x in combination with increased O_3 (upper right corner of the orange boxes in Fig. B3) are compatible with both, increased in situ O_3 production and influence from the stratospheric branch. Consequently almost all measurements in the ASMA filament are well correlated on the scale of all our ASMA measurements (Fig. B3c). As discussed in the accompanying paper, the positive correlation between NO and O_3 is attributed to enhanced O_3 production due to increased NO, if NO also positively correlates with NO_y.

There are three distinct regions in Fig. B3d: a blueish stratospheric branch, a dark TL branch, and a reddish UT region. As a consequence of the local NO_y minimum directly above the tropopause (Figs. B1b, B2), the most decreased NO_y mixing ratios in Fig. B3d also show up in samples taken from near the tropopause. Measured NO and NO_y values in the ASMA filament are well correlated (Fig. B3f), consistent with almost constant NO_x/NO_y ratios in the UT (Figs B1cd). Furthermore, the simulation shows much more scatter in NO_x-vs-O_3 space than the observations. The narrow, linear distribution of the ASMA measurements in Figs. B3cf indicates that all parts of the transected filament had similar sources of reactive nitrogen. This is consistent with Appendix A, where lightning is found to be the dominating source of reactive nitrogen in the ASMA. The filament had seen convection at the eastern ASMA flank three to five days before the measurements. Thus the gradients of NO and NO_y in Figs. B3cf can be explained by different amounts of lightning NO_x of approximately the same age.

We attribute some larger-scale trace gas gradients in the measurements to different photochemical O_3 production (section 4). There are positive correlations between NO & O_3 and NO & NO_y (Figs. B3cf), but not between CO & O_3 (Fig. 3c). This combination indicates that the measurements show a NO_x-limited photochemical regime.

Formatted: Font color: Auto
Formatted: Font color: Auto
Formatted: Font color: Auto,
Formatted: Font color: Auto
Formatted: Font: 10 pt
Formatted: Font: 10 pt
Formatted: Font: 10 pt
Formatted: Font: 10 pt
Formatted: Font: 10 pt
Formatted: Font: 10 pt
Formatted: Font: 10 pt, English (U.K.)
Formatted: Font: 10 pt
Formatted: Font: 10 pt
Formatted: Font: 10 pt
Formatted: Font: 10 pt
Formatted: Font: 10 pt
Formatted: Font: 10 pt
Formatted: Font: 10 pt, Subscript
Formatted: Font: 10 pt
Formatted: Font: 10 pt, Subscript
Formatted: Font: 10 pt
Formatted: Font: 10 pt
Formatted: Font: 10 pt
Formatted: Font: 10 pt
Formatted: Font: 10 pt
Formatted: Font: 10 pt
Formatted: Font color: Auto
Formatted: Font color: Auto

Appendix C: Primer for tracer-tracer diagrams

Tracer-tracer diagrams show mixing ratios of two species encountered simultaneously. Sampling of two different air masses that are in the process of mixing is indicated by a mixing line in the tracer-tracer diagram. The slope of the mixing line provides additional clues about the origin of the original air parcels ("end-members"). If the ratios of the end members remain constant over time, the slope of the mixing line is conserved, as long as the mixing process continues. If the mixing processes stops, the mixing lines converge to a single point in the tracer-tracer diagram. If the reservoir of one end-member is bigger than the other, points in the tracer-tracer diagram will be close to the dominating end-member. However, the relative size of the reservoirs does not affect the slope of mixing lines, thus allowing detection of even small entrainments. Slopes change in case of mixing ratio changes over time (e.g. via in situ production or loss) of one or both reservoirs. Different effects may lead to similar tracer-tracer relations, resulting in ambiguity when trying to reconstruct end-members or disentangling mixing and chemical effects. Furthermore, mixing lines in general exist in a multi-dimensional tracer space, and thus lines in a tracer-tracer plot need to be considered as projections onto 2d space. They might also be the result of mixing between more than two reservoirs. Additional dimensions (tracers) need to be considered to reduce ambiguities.

Formatted: Font color: Auto

Data availability

The simulation results analysed here are archived at the German Climate Computing Center (DKRZ) and are available on request. It is planned to move them to the Climate and Environmental Retrieval and Archive (CERA) database at the German Climate Computing Centre (DKRZ; http://cera-www.dkrz.de/WDCC/ui/Index.jsp). The corresponding digital object identifiers (doi) will be published on the MESSy consortium web page (~~http://~~www.messy-interface.org).

The observational data of the HALO ESMVal flight used here are available from the HALO database (doi:10.17616/R39Q0T)~~: https://halo-db.pa.op.dlr.de/dataset/830~~. ~~Registration is needed to access the data (https://halo-db.pa.op.dlr.de/account/register).~~

Formatted: Font color: Auto

Competing interests

The authors declare that they have no conflict of interest.

Formatted: Font color: Auto

Author contributions

K. Gottschaldt analysed the EMAC and final in situ data, conducted the Lagrangian calculations, produced the plots and drafted the paper. H. Schlager conceived the study, led the HALO ESMVal campaign and interpreted EMAC and in situ

data. R. Baumann wrote and helped with the code that facilitated the HYSPLIT calculations. P. Jöckel led the ESCiMo project, coordinated the preparation of and conducted the EMAC simulations. D. S. Cai and P. Graf prepared a significant part of the boundary conditions, and V. Grewe was responsible for the $ProdO_3$ and $LossO_3$ diagnostics in the ESCiMo simulations. V. Eyring conceived and led the ESMVal project. T. Jurkat, C. Voigt, A. Zahn, and H. Ziereis supplied in situ measurements. All authors contributed to the text.

Acknowledgements

The authors gratefully thank H. Garny and P. Hoor for valuable comments on the manuscript, A. Baker, B. Barret, B. Brötz, J. Crawford, F. Frank, H. Huntrieser, P. Konopka, R. Müller, M. Nützel, L. Pan, R. Ren, M. Santee, M. Schultz, G. Stiller, ~~and~~ B. Vogel for helpful discussions, and the ACAM (Atmospheric Composition and the Asian Monsoon; www2.acom.ucar.edu/acam) activity for providing a forum~~discussions~~.

We thank the German Science Foundation DFG for funding within HALO-SPP 1294 under contracts JU 3059/1-1, SCHL 1857/2-2, SCHL 1857/4-1, VO 1504/2-1 and VO 1504/4-1. The HALO ESMVal aircraft campaign was funded by the DLR-project ESMVal. KG and HS appreciate support by the EU project StratoClim (grant no. 603557) and BMBF project Spitfire (grant no. 01LG1205B). CV and TJ thank financing by the Helmholtz Association under contract no. VH-NG-309 and under contract No. W2/W3-60. In addition we thank the flight department of DLR for their great support during the campaign. P. Hoor and S. Müller contributed to the CO measurements and S. Kaufmann supervised the HCl measurements during the flight.

The EMAC model simulations were performed at the German Climate Computing Centre (DKRZ) through support from the Bundesministerium für Bildung und Forschung (BMBF). DKRZ and its scientific steering committee are gratefully acknowledged for providing the HPC and data archiving resources for the projects 853 (ESCiMo - Earth System Chemistry integrated Modelling) and 854 (ESMVal).

We used the NCAR Command Language (NCL) for data analysis and to create some of the figures of this study. NCL is developed by UCAR/NCAR/CISL/TDD and available on-line: http://dx.doi.org/10.5065/D6WD3XH5.

The article processing charges for this open-access publication were covered by a Research Centre of the Helmholtz Association.

Last but not least we thank the two anonymous reviewers for their insightful comments regarding $LiNO_x$, convective and isentropic transport, which greatly helped to improve the paper.

Formatted: Subscript
Formatted: Subscript
Formatted: Font color: Auto
Formatted: Font color: Auto
Formatted: Font color: Auto
Formatted: Font color: Auto
Formatted: Subscript

Formatted: Font color: Auto

References

Akritidis, D., Pozzer, A., Zanis, P., Tyrlis, E., Škerlak, B., Sprenger, M., and Lelieveld, J.: On the role of tropopause folds in summertime tropospheric ozone over the eastern Mediterranean and the Middle East, Atmospheric Chemistry and Physics, 16, 14025-14039, 10.5194/acp-16-14025-2016, 2016.

Baker, A. K., Schuck, T. J., Slemr, F., van Velthoven, P., Zahn, A., and Brenninkmeijer, C. A. M.: Characterization of non-methane hydrocarbons in Asian summer monsoon outflow observed by the CARIBIC aircraft, Atmospheric Chemistry and Physics, 11, 503-518, 10.5194/acp-11-503-2011, 2011.

Barret, B., Sauvage, B., Bennouna, Y., and Le Flochmoen, E.: Upper-tropospheric CO and O3 budget during the Asian summer monsoon, Atmospheric Chemistry and Physics, 16, 9129-9147, 10.5194/acp-16-9129-2016, 2016.

Bergman, J. W., Fierli, F., Jensen, E. J., Honomichl, S., and Pan, L. L.: Boundary layer sources for the Asian anticyclone: Regional contributions to a vertical conduit, Journal of Geophysical Research: Atmospheres, 118, 2560-2575, 10.1002/jgrd.50142, 2013.

Boos, W. R., and Kuang, Z.: Dominant control of the South Asian monsoon by orographic insulation versus plateau heating, Nature, 463, 218-222, 10.1038/nature08707, 2010.

Boos, W. R., and Hurley, J. V.: Thermodynamic Bias in the Multimodel Mean Boreal Summer Monsoon, Journal of Climate, 26, 2279-2287, 10.1175/jcli-d-12-00493.1, 2013.

Brenninkmeijer, C. A. M., Crutzen, P. J., Boumard, F., Dauer, T., Dix, B., Ebinghaus, R., Filippi, D., Fischer, H., Franke, H., Frieß, U., Heintzenberg, J., Helleis, F., Hermann, M., Kock, H. H., Koeppel, C., Lelieveld, J., Leuenberger, M., Martinsson, B. G., Miemczyk, S., Moret, H. P., Nguyen, H. N., Nyfeler, P., Oram, D., O'Sullivan, D., Penkett, S. A., Platt, U., Pupek, M., Ramonet, M., Randa, B., Reichelt, M., Rhee, T. S., Rohwer, J., Rosenfeld, K., Scharffe, D., Schlager, H., Schumann, U., Slemr, F., Sprung, D., Stock, P., Thaler, R., Valentino, F., van Velthoven, P., Waibel, A., Wandel, A., Waschitschek, K., Wiedensohler, A., Xuref-Remy, I., Zahn, A., Zech, U., and Ziereis, H.: Civil Aircraft for the regular investigation of the atmosphere based on an instrumented container: The new CARIBIC system, Atmos. Chem. Phys., 7, 4953-4976, https://doi.org/10.5194/acp-7-4953-2007, 2007.

Cecil, D. J.: LIS/OTD 2.5 Degree Low Resolution Monthly Climatology Time Series (LRMTS): Data set available online from the NASA Global Hydrology Resource Center DAAC, Huntsville, Alabama, U.S.A. doi: http://dx.doi.org/10.5067/LIS/LIS-OTD/DATA311, access: https://lightning.nsstc.nasa.gov/data/data_lis-otd-climatology.htm, 18. September 2017, 2006.

Cristofanelli, P., Bracci, A., Sprenger, M., Marinoni, A., Bonafè, U., Calzolari, F., Duchi, R., Laj, P., Pichon, J. M., Roccato, F., Venzac, H., Vuillermoz, E., and Bonasoni, P.: Tropospheric ozone variations at the Nepal Climate Observatory-Pyramid (Himalayas, 5079 m a.s.l.) and influence of deep stratospheric intrusion events, Atmospheric Chemistry and Physics, 10, 6537-6549, 10.5194/acp-10-6537-2010, 2010.

Crutzen, P. J., and Schmailzl, U.: Chemical budgets of the stratosphere, Planet. Space Sci., 31, 1009-1032, 1983.

Deckert, R., Jöckel, P., Grewe, V., Gottschaldt, K., and Hoor, P.: A quasi chemistry-transport model mode for EMAC, Geoscientific Model Development, 4, 195-206, 10.5194/gmd-4-195-2011, 2011.

Dee, D. P., Uppala, S. M., Simmons, A. J., Berrisford, P., Poli, P., Kobayashi, S., Andrae, U., Balmaseda, M. A., Balsamo, G., Bauer, P., Bechtold, P., Beljaars, A. C. M., van de Berg, L., Bidlot, J., Bormann, N., Delsol, C., Dragani, R., Fuentes, M.,

Geer, A. J., Haimberger, L., Healy, S. B., Hersbach, H., Hólm, E. V., Isaksen, L., Kållberg, P., Köhler, M., Matricardi, M., McNally, A. P., Monge-Sanz, B. M., Morcrette, J. J., Park, B. K., Peubey, C., de Rosnay, P., Tavolato, C., Thépaut, J. N., and Vitart, F.: The ERA-Interim reanalysis: configuration and performance of the data assimilation system, Quarterly Journal of the Royal Meteorological Society, 137, 553-597, 10.1002/qj.828, 2011.

Dethof, A., O'Neill, A., Slingo, J. M., and Smit, H. G. J.: A mechanism for moistening the lower stratosphere involving the Asian summer monsoon, Quarterly Journal of the Royal Meteorological Society, 125, 1079-1106, 10.1002/qj.1999.49712555602, 1999.

Draxler, R. R., and Hess, G. D.: An overview of the HYSPLIT_4 modelling system for trajectories, dispersion and deposition, Aust. Met. Mag., 47, 295-308, 1998.

Draxler, R. R., and Rolph, G.: HYSPLIT (HYbrid Single-ParticleLagrangian Integrated Trajectory) model: http://www.arl.noaa.gov/ready/hysplit4.html, access: 26 June 2015, 2015.

Dunkerton, T. J.: Evidence of meridional motion in the summer lower stratosphere adjacent to monsoon regions, Journal of Geophysical Research, 100, 16675–16688, 10.1029/95JD01263, 1995.

Ehhalt, D. H., and Rohrer, F.: The impact of commercial aircraft on tropospheric ozone, Proceedings of the 7th BOC Priestley Conference, Lewisburg, Pennsylvania, USA, 1994,

Fischer, H., Wienhold, F. G., Hoor, P., Bujok, O., Schiller, C., Siegmund, P., Ambaum, M., Scheeren, H. A., and Lelieveld, J.: Tracer correlations in the northern high latitude lowermost stratosphere: Influence of cross-tropopause mass exchange, Geophysical Research Letters, 27, 97-100, 10.1029/1999gl010879, 2000.

Flohn, H.: Recent investigation on the mechanism of the "summer monsoon" of southern and eastern Asia, in: Proc. Symp. Monsoon of the World, 1960, 75-88,

Fu, R., Hu, Y., Wright, J. S., Jiang, J. H., Dickinson, R. E., Chen, M., Filipiak, M., Read, W. G., Waters, J. W., and Wu, D. L.: Short circuit of water vapor and polluted air to the global stratosphere by convective transport over the Tibetan Plateau, Proceedings of the National Academy of Sciences of the United States of America, 103, 5664-5669, 10.1073/pnas.0601584103, 2006.

Garny, H., and Randel, W. J.: Dynamic variability of the Asian monsoon anticyclone observed in potential vorticity and correlations with tracer distributions, Journal of Geophysical Research: Atmospheres, 118, 13,421-413,433, 10.1002/2013jd020908, 2013.

Garny, H., and Randel, W. J.: Transport pathways from the Asian Monsoon Anticyclone to the Stratosphere, Draft for ACPD, 2015.

Gettelman, A., Hoor, P., Pan, L. L., Randel, W. J., Hegglin, M. I., and Birner, T.: The Extratropical Upper Troposphere and Lower Stratosphere, Reviews of Geophysics, 49, 10.1029/2011rg000355, 2011.

Goswami, B. N.: South Asian monsoon, in: Intraseasonal Variability in the Atmosphere-Ocean Climate System, 2nd ed., edited by: Lau, W. K. M., and Waliser, D. E., Springer-Verlag, Berlin, Heidelberg, 21–72, 2012.

Gottschaldt, K., Voigt, C., Jöckel, P., Righi, M., Deckert, R., and Dietmüller, S.: Global sensitivity of aviation NOx effects to the HNO3-forming channel of the HO2 + NO reaction, Atmospheric Chemistry and Physics, 13, 3003-3025, 10.5194/acp-13-3003-2013, 2013.

Gottschaldt, K., Schlager, H., Baumann, R., Bozem, H., Eyring, V., Hoor, P., Jöckel, P., Jurkat, T., Voigt, C., Zahn, A., and Ziereis, H.: Trace gas composition in the Asian summer monsoon anticyclone: a case study based on aircraft observations and model simulations, Atmospheric Chemistry and Physics, 17, 6091-6111, 10.5194/acp-17-6091-2017, 2017.

Grewe, V., Brunner, D., Dameris, M., Grenfell, J. L., Hein, R., Shindell, D., and Staehelin, J.: Origin and variability of upper tropospheric nitrogen oxides and ozone at northern mid-latitudes, Atmospheric Environment, 35, 3421-3433, 2001.

Grewe, V.: Impact of Lightning on Air Chemistry and Climate, in: Lightning: Principles, Instruments and Applications, edited by: Betz, H. D., Schumann, U., and Laroche, P., Springer Science+Business Media B. V., 537-549, 2009.

Grewe, V., Tsati, E., Mertens, M., Frömming, C., and Jöckel, P.: Contribution of emissions to concentrations: The TAGGING 1.0 submodel based on the Modular Earth Submodel System (MESSy 2.52), Geoscientific Model Development Discussions, 1-33, 10.5194/gmd-2016-298, 2017.

Grooß, J. U., Brühl, C., and Peter, T.: Impact of aircraft emissions on tropospheric and stratospheric ozone. Part 1: Chemistry and 2-d model results, Atmospheric Environment, 32, 3171-3184, 1998.

Holton, J. R., Haynes, P. H., McIntyre, M. E., Douglass, A. R., Rood, R. B., and Pfister, L.: Stratosphere-troposphere exchange, Reviews of Geophysics, 33, 403-439, 10.1029/95RG02097, 1995.

Hoor, P., Fischer, H., Lange, L., Lelieveld, J., and Brunner, D.: Seasonal variations of a mixing layer in the lowermost stratosphere as identified by the CO-O3correlation from in situ measurements, Journal of Geophysical Research, 107, 10.1029/2000jd000289, 2002.

Hoor, P., Gurk, C., Brunner, D., Hegglin, M. I., Wernli, H., and Fischer, H.: Seasonality and extent of extratropical TST derived from in-situ CO measurements during SPURT, Atmos. Chem. Phys., 4, 1427-1442, 10.5194/acp-4-1427-2004, 2004.

Hsu, C. J., and Plumb, R. A.: Nonaxisymmetric Thermally Driven Circulations and Upper-Tropospheric Monsoon Dynamics, J. Atmos. Sci., 57, 1255-1276, http://dx.doi.org/10.1175/1520-0469(2000)057<1255:NTDCAU>2.0.CO;2 2001.

IPCC: Climate Change 2013: The Physical Science Basis. Contribution of Working Group I to the Fifth Assessment Report of the Intergovernmental Panel on Climate Change, edited by: Stocker, T. F., Qin, D., Plattner, G.-K., Tignor, M., Allen, S. K., Boschung, J., Nauels, A., Xia, Y., Bex, V., and Midgley, P. M., Cambridge University Press, Cambridge, United Kingdom and New York, NY, USA,, 1535 pp., 2013.

Jaeglé, L., Jacob, D. J., Brune, W. H., Tan, D., Faloona, I. C., Weinheimer, A. J., Ridley, B. A., Campos, T. L., and Sachse, G. W.: Sources of HOxand production of ozone in the upper troposphere over the United States, Geophysical Research Letters, 25, 1709-1712, 10.1029/98gl00041, 1998.

Jöckel, P., Tost, H., Pozzer, A., Brühl, C., Buchholz, J., Ganzeveld, L., Hoor, P., Kerkweg, A., Lawrence, M., Sander, R., Steil, B., Stiller, G., Tanarhte, M., Taraborrelli, D., van Aardenne, J., and Lelieveld, J.: The atmospheric chemistry general circulation model ECHAM5/MESSy1: consistent simulation of ozone from the surface to the mesosphere, Atmos. Chem. Phys., 6, 5067-5104, 2006.

Jöckel, P., Kerkweg, A., Pozzer, A., Sander, R., Tost, H., Riede, H., Baumgaertner, A., Gromov, S., and Kern, B.: Development cycle 2 of the Modular Earth Submodel System (MESSy2), Geoscientific Model Development, 3, 717-752, 10.5194/gmd-3-717-2010, 2010.

Jöckel, P., Tost, H., Pozzer, A., Kunze, M., Kirner, O., Brenninkmeijer, C. A. M., Brinkop, S., Cai, D. S., Dyroff, C., Eckstein, J., Frank, F., Garny, H., Gottschaldt, K.-D., Graf, P., Grewe, V., Kerkweg, A., Kern, B., Matthes, S., Mertens, M.,

Meul, S., Neumaier, M., Nützel, M., Oberländer-Hayn, S., Ruhnke, R., Runde, T., Sander, R., Scharffe, D., and Zahn, A.: Earth System Chemistry integrated Modelling (ESCiMo) with the Modular Earth Submodel System (MESSy) version 2.51, Geoscientific Model Development, 9, 1153-1200, 10.5194/gmd-9-1153-2016, 2016.

Jurkat, T., Voigt, C., Kaufmann, S., Zahn, A., Sprenger, M., Hoor, P., Bozem, H., Müller, S., Dörnbrack, A., Schlager, H., Bönisch, H., and Engel, A.: A quantitative analysis of stratospheric HCl, HNO3, and O3in the tropopause region near the subtropical jet, Geophysical Research Letters, 41, 3315-3321, 10.1002/2013gl059159, 2014.

Jurkat, T., Kaufmann, S., Voigt, C., Schäuble, D., Jeßberger, P., and Ziereis, H.: The airborne mass spectrometer AIMS – Part 2: Measurements of trace gases with stratospheric or tropospheric origin in the UTLS, Atmospheric Measurement Techniques, 9, 1907-1923, 10.5194/amt-9-1907-2016, 2016.

Kaiser, J. W., Heil, A., Andreae, M. O., Benedetti, A., Chubarova, N., Jones, L., Morcrette, J. J., Razinger, M., Schultz, M. G., Suttie, M., and van der Werf, G. R.: Biomass burning emissions estimated with a global fire assimilation system based on observed fire radiative power, Biogeosciences, 9, 527-554, 10.5194/bg-9-527-2012, 2012.

Konopka, P., Grooß, J.-U., Günther, G., Ploeger, F., Pommrich, R., Müller, R., and Livesey, N.: Annual cycle of ozone at and above the tropical tropopause: observations versus simulations with the Chemical Lagrangian Model of the Stratosphere (CLaMS), Atmos. Chem. Phys., 10, 121-132, 10.5194/acp-10-121-2010, 2010.

Kunz, A., Sprenger, M., and Wernli, H.: Climatology of potential vorticity streamers and associated isentropic transport pathways across PV gradient barriers, Journal of Geophysical Research: Atmospheres, 120, 3802-3821, 10.1002/2014jd022615, 2015.

Kunze, M., Braesicke, P., Langematz, U., Stiller, G., Bekki, S., Brühl, C., Chipperfield, M., Dameris, M., Garcia, R., and Giorgetta, M.: Influences of the Indian Summer Monsoon on Water Vapor and Ozone Concentrations in the UTLS as Simulated by Chemistry–Climate Models, Journal of Climate, 23, 3525-3544, 10.1175/2010jcli3280.1, 2010.

Lawrence, M. G., and Lelieveld, J.: Atmospheric pollutant outflow from southern Asia: a review, Atmospheric Chemistry and Physics, 10, 11017-11096, 10.5194/acp-10-11017-2010, 2010.

Lelieveld, J., Crutzen, P. J., Ramanathan, V., Andreae, M. O., Brenninkmeijer, C. A. M., Campos, T., Cass, G. R., Dickerson, R. R., Fischer, H., de Gouw, J. A., Hansel, A., Jefferson, A., Kley, D., de Laat, A. T. J., Lal, S., Lawrence, M. G., Lobert, J. M., Mayol-Bracero, O. L., Mitra, A. P., Novakov, T., Oltmans, S. J., Prather, K. A., Reiner, T., Rodhe, H., Scheeren, H. A., Sikka, D., and Williams, J.: The Indian Ocean Experiment: Widespread Air Pollution from South and Southeast Asia, Science, 291, 1031-1036, 10.1126/science.1057103, 2001.

Lelieveld, J., Berresheim, H., Borrmann, S., Crutzen, P. J., Dentener, F. J., Fischer, H., Feichter, J., Flatau, P. J., Heland, J., Holzinger, R., Korrmann, R., Lawrence, M. G., Levin, Z., Markowicz, K. M., Mihalopoulos, N., Minikin, A., Ramanathan, V., de Reus, M., Roelofs, G. J., Scheeren, H. A., Sciare, J., Schlager, H., Schultz, M., Siegmund, P., Steil, B., Stephanou, E. G., Stier, P., Traub, M., Warneke, C., Williams, J., and Ziereis, H.: Global Air Pollution Crossroads over the Mediterranean, Science, 298, 794-799, 10.1126/science.1075457, 2002.

Lelieveld, J., Hoor, P., Jöckel, P., Pozzer, A., Hadjinicolaou, P., Cammas, J.-P., and Beirle, S.: Severe ozone air pollution in the Persian Gulf region, Atmos. Chem. Phys., 9, 1393-1406, 2009.

Li, Q., Jacob, D. J., Logan, J. A., Bey, I., Yantosca, R. M., Liu, H., Martin, R. V., Fiore, A. M., Field, B. D., Duncan, B. N., and Thouret, V.: A Tropospheric Ozone Maximum Over the Middle East, Geophysical Research Letters, 28, 3235-3238, 10.1029/2001gl013134
10.1029/2001GL013134, 2001.

Li, Q., Jiang, J. H., Wu, D. L., Read, W. G., Livesey, N. J., Waters, J. W., Zhang, Y., Wang, B., Filipiak, M. J., Davis, C. P., Turquety, S., Wu, S., Park, R. J., Yantosca, R. M., and Jacob, D. J.: Convective outflow of South Asian pollution: A global CTM simulation compared with EOS MLS observations, Geophysical Research Letters, 32, L14826, 10.1029/2005gl022762, 2005.

Lin, J.-L., Weickman, K. M., Kiladis, G. N., Mapes, B. E., Schubert, S. D., Suarez, M. J., Bacmeister, J. T., and Lee, M.-I.: Subseasonal Variability Associated with Asian Summer Monsoon Simulated by 14 IPCC AR4 Coupled GCMs, Journal of Climate, 21, 4541-4567, 10.1175/2008jcli1816.1, 2008.

Liu, J. J., Jones, D. B. A., Worden, J. R., Noone, D., Parrington, M., and Kar, J.: Analysis of the summertime buildup of tropospheric ozone abundances over the Middle East and North Africa as observed by the Tropospheric Emission Spectrometer instrument, Journal of Geophysical Research, 114, 10.1029/2008jd010993, 2009a.

Liu, J. J., Jones, D. B. A., Zhang, S., and Kar, J.: Influence of interannual variations in transport on summertime abundances of ozone over the Middle East, Journal of Geophysical Research, 116, 10.1029/2011jd016188, 2011.

Liu, Y., Wang, Y., Liu, X., Cai, Z., and Chance, K.: Tibetan middle tropospheric ozone minimum in June discovered from GOME observations, Geophysical Research Letters, 36, 10.1029/2008gl037056, 2009b.

Lopez, P.: A Lightning Parameterization for the ECMWF Integrated Forecasting System, Monthly Weather Review, 144, 3057-3075, 10.1175/mwr-d-16-0026.1, 2016.

Lubis, S. W., and Nakamura, N.: Stratospheric Influence on Summer Monsoon and Associated Planetary Wave Breaking and Mixing in the Subtropical Tropopause Region, AGU Fall Meeting, A51N-05, New Orleans, LA, 15 Dec., 2017.

Marcy, T. P., Fahey, D. W., Gao, R. S., Popp, P. J., Richard, E. C., Thompson, T. L., Rosenlof, K. H., Ray, E. A., Salawitch, R. J., Atherton, C. S., Bergmann, D. J., Ridley, B. A., Weinheimer, A. J., Loewenstein, M., Weinstock, E. M., and Mahoney, M. J.: Quantifying Stratospheric Ozone in the Upper Troposphere with in Situ Measurements of HCl, Science, 304, 261-265, 10.1126/science.1093418, 2004.

Müller, S., Hoor, P., Bozem, H., Gute, E., Vogel, B., Zahn, A., Bönisch, H., Keber, T., Krämer, M., Rolf, C., Riese, M., Schlager, H., and Engel, A.: Impact of the Asian monsoon on the extratropical lower stratosphere: trace gas observations during TACTS over Europe 2012, Atmospheric Chemistry and Physics, 16, 10573-10589, 10.5194/acp-16-10573-2016, 2016.

Nützel, M., Dameris, M., and Garny, H.: Movement, drivers and bimodality of the South Asian High, Atmospheric Chemistry and Physics, 16, 14755-14774, 10.5194/acp-16-14755-2016, 2016.

Pan, L. L., Randel, W. J., Gary, B. L., Mahoney, M. J., and Hintsa, E. J.: Definitions and sharpness of the extratropical tropopause: A trace gas perspective, Journal of Geophysical Research: Atmospheres, 109, n/a-n/a, 10.1029/2004jd004982, 2004.

Pan, L. L., Honomichl, S. B., Kinnison, D., Abalos, M., Randel, W. J., Bergman, J. W., and Bian, J.: Transport of chemical tracers from the boundary layer to stratosphere associated with the dynamics of the Asian summer monsoon, Journal of Geophysical Research: Atmospheres, 121, 1-16, 10.1002/2016JD025616, 2016.

Park, M., Randel, W. J., Emmons, L. K., Bernath, P. F., Walker, K. A., and Boone, C. D.: Chemical isolation in the Asian monsoon anticyclone observed in Atmospheric Chemistry Experiment (ACE-FTS) data, Atmos. Chem. Phys., 8, 757-764, 10.5194/acp-8-757-2008, 2008.

Park, M., Randel, W. J., Emmons, L. K., and Livesey, N. J.: Transport pathways of carbon monoxide in the Asian summer monsoon diagnosed from Model of Ozone and Related Tracers (MOZART), Journal of Geophysical Research, 114, D08303, 10.1029/2008jd010621, 2009.

Ploeger, F., Gottschling, C., Griessbach, S., Grooß, J. U., Guenther, G., Konopka, P., Müller, R., Riese, M., Stroh, F., Tao, M., Ungermann, J., Vogel, B., and von Hobe, M.: A potential vorticity-based determination of the transport barrier in the Asian summer monsoon anticyclone, Atmospheric Chemistry and Physics, 15, 13145-13159, 10.5194/acp-15-13145-2015, 2015.

Pokhrel, S., Chaudhari, H. S., Saha, S. K., Dhakate, A., Yadav, R. K., Salunke, K., Mahapatra, S., and Rao, S. A.: ENSO, IOD and Indian Summer Monsoon in NCEP climate forecast system, Climate Dynamics, 39, 2143-2165, 10.1007/s00382-012-1349-5, 2012.

Popovic, J. M., and Plumb, R. A.: Eddy Shedding from the Upper-Tropospheric Asian Monsoon Anticyclone, Journal of the Atmospheric Sciences, 58, 93-104, 10.1175/1520-0469(2001)058<0093:ESFTUT>2.0.CO;2, 2001.

Randel, W. J., and Park, M.: Deep convective influence on the Asian summer monsoon anticyclone and associated tracer variability observed with Atmospheric Infrared Sounder (AIRS), Journal of Geophysical Research, 111, D12314, 10.1029/2005jd006490, 2006.

Randel, W. J., Pan, L. L., and Bian, J.: Workshop on dynamics, transport and chemistry of the UTLS Asian Monsoon, Advances in Atmospheric Sciences, 33, 1096-1098, 10.1007/s00376-016-6169-9, 2016.

Rauthe-Schöch, A., Baker, A. K., Schuck, T. J., Brenninkmeijer, C. A. M., Zahn, A., Hermann, M., Stratmann, G., Ziereis, H., van Velthoven, P. F. J., and Lelieveld, J.: Trapping, chemistry, and export of trace gases in the South Asian summer monsoon observed during CARIBIC flights in 2008, Atmospheric Chemistry and Physics, 16, 3609-3629, 10.5194/acp-16-3609-2016, 2016.

Ren, R., Wu, G., Cai, M., Sun, S., Liu, X., and Li, W.: Progress in Research of Stratosphere-Troposphere Interactions: Application of Isentropic Potential Vorticity Dynamics and the Effects of the Tibetan Plateau, J. Meteor. Res., 28, 714-731, 10.1007 /s13351-014-4026-2, 2014.

Richards, N. A. D., Arnold, S. R., Chipperfield, M. P., Miles, G., Rap, A., Siddans, R., Monks, S. A., and Hollaway, M. J.: The Mediterranean summertime ozone maximum: global emission sensitivities and radiative impacts, Atmospheric Chemistry and Physics, 13, 2331-2345, 10.5194/acp-13-2331-2013, 2013.

Rodwell, M. J., and Hoskins, B. A.: Monsoons and the dynamics of deserts, Q. J. R. Meteorol. Soc., 122, 1385-1404, 10.1002/qj.49712253408, 1996.

Rogers, H., Teyssedre, H., Pitari, G., Grewe, V., van Velthoven, P., and Sundet, J.: Model intercomparison of the transport of aircraft-like emissions from sub- and supersonic aircraft, Meteorologische Zeitschrift, 11, 151-159, 10.1127/0941-2948/2002/0011-0151, 2002.

Safieddine, S., Boynard, A., Hao, N., Huang, F., Wang, L., Ji, D., Barret, B., Ghude, S. D., Coheur, P.-F., Hurtmans, D., and Clerbaux, C.: Tropospheric ozone variability during the East Asian summer monsoon as observed by satellite (IASI), aircraft (MOZAIC) and ground stations, Atmospheric Chemistry and Physics, 16, 10489-10500, 10.5194/acp-16-10489-2016, 2016.

Santee, M. L., Manney, G. L., Livesey, N. J., Schwartz, M. J., Neu, J. L., and Read, W. G.: A comprehensive overview of the climatological composition of the Asian summer monsoon anticyclone based on 10 years of Aura Microwave Limb Sounder measurements, Journal of Geophysical Research: Atmospheres, 122, 5491-5514, 10.1002/2016jd026408, 2017.

Scheeren, H. A., Lelieveld, J., Roelofs, G. J., Williams, J., Fischer, H., de Reus, M., de Gouw, J. A., Warneke, C., Holzinger, R., Schlager, H., Klüpfel, T., Bolder, M., van der Veen, C., and Lawrence, M.: The impact of monsoon outflow from India and Southeast Asia in the upper troposphere over the eastern Mediterranean, Atmos. Chem. Phys., 3, 1589-1608, 2003.

Schiller, C. L., Bozem, H., Gurk, C., Parchatka, U., Königstedt, R., Harris, G. W., Lelieveld, J., and Fischer, H.: Applications of quantum cascade lasers for sensitive trace gas measurements of CO, CH4, N2O and HCHO, Applied Physics B, 92, 419-430, 10.1007/s00340-008-3125-0, 2008.

Schuck, T. J., Brenninkmeijer, C. A. M., Baker, A. K., Slemr, F., von Velthoven, P. F. J., and Zahn, A.: Greenhouse gas relationships in the Indian summer monsoon plume measured by the CARIBIC passenger aircraft, Atmos. Chem. Phys., 10, 3965-3984, 2010.

Schumann, U., and Huntrieser, H.: The global lightning-induced nitrogen oxides source, Atmos. Chem. Phys., 7, 3823-3907, 2007.

Seinfeld, J. H., and Pandis, S. N.: Relative roles of VOC and NOx in ozone formation, in: Atmospheric Chemistry and Physics, John Wiley & Sons, New York, 209-303, 1998.

Sprung, D., and Zahn, A.: Acetone in the upper troposphere/lowermost stratosphere measured by the CARIBIC passenger aircraft: Distribution, seasonal cycle, and variability, Journal of Geophysical Research, 115, 10.1029/2009jd012099, 2010.

Stratmann, G., Ziereis, H., Stock, P., Brenninkmeijer, C. A. M., Zahn, A., Rauthe-Schöch, A., Velthoven, P. V., Schlager, H., and Volz-Thomas, A.: NO and NOy in the upper troposphere: Nine years of CARIBIC measurements onboard a passenger aircraft, Atmospheric Environment, 133, 93-111, 10.1016/j.atmosenv.2016.02.035, 2016.

Tiedtke, M.: A comprehensive mass flux scheme for cumulus parameterization in large-scale models, Mon. Weather. Rev., 117, 1179-1800, 1989.

Tost, H.: Global Modelling of Cloud, Convection and Precipitation Influences on Trace Gases and Aerosols, PhD, University Bonn, Bonn, 2006.

Tost, H., Jöckel, P., and Lelieveld, J.: Lightning and convection parameterisations – uncertainties in global modelling, Atmos. Chem. Phys., 7, 4553-4568, 2007.

Tyrlis, E., Škerlak, B., Sprenger, M., Wernli, H., Zittis, G., and Lelieveld, J.: On the linkage between the Asian summer monsoon and tropopause fold activity over the eastern Mediterranean and the Middle East, Journal of Geophysical Research: Atmospheres, 119, 3202-3221, 10.1002/2013jd021113, 2014.

Vogel, B., Günther, G., Müller, R., Grooß, J. U., Hoor, P., Krämer, M., Müller, S., Zahn, A., and Riese, M.: Fast transport from Southeast Asia boundary layer sources to northern Europe: rapid uplift in typhoons and eastward eddy shedding of the Asian monsoon anticyclone, Atmospheric Chemistry and Physics, 14, 12745-12762, 10.5194/acp-14-12745-2014, 2014.

Voigt, C., Jessberger, P., Jurkat, T., Kaufmann, S., Baumann, R., Schlager, H., Bobrowski, N., Giuffrida, G., and Salerno, G.: Evolution of CO2, SO2, HCl, and HNO3 in the volcanic plumes from Etna, Geophysical Research Letters, 41, 2196–2203, 10.1002/2013GL058974, 2014.

Yan, R.-C., Bian, J.-C., and Fan, Q.-J.: The Impact of the South Asia High Bimodality on the Chemical Composition of the Upper Troposphere and Lower Stratosphere, Atmospheric and Oceanic Science Letters, 4, 229-234, 2011.

Zahn, A., Weppner, J., Widmann, H., Schlote-Holubek, K., Burger, B., Kühner, T., and Franke, H.: A fast and precise chemiluminescence ozone detector for eddy flux and airborne application, Atmospheric Measurement Techniques, 5, 363-375, 10.5194/amt-5-363-2012, 2012.

Ziereis, H., Schlager, H., and Schulte, P.: Distributions of NO, NOx, and NOy in the upper troposphere and lower stratosphere between 28° and 61°N during POLINAT 2, Journal of Geophysical Research, 105, 3653-3664, 10.1029/1999JD900870, 2000.

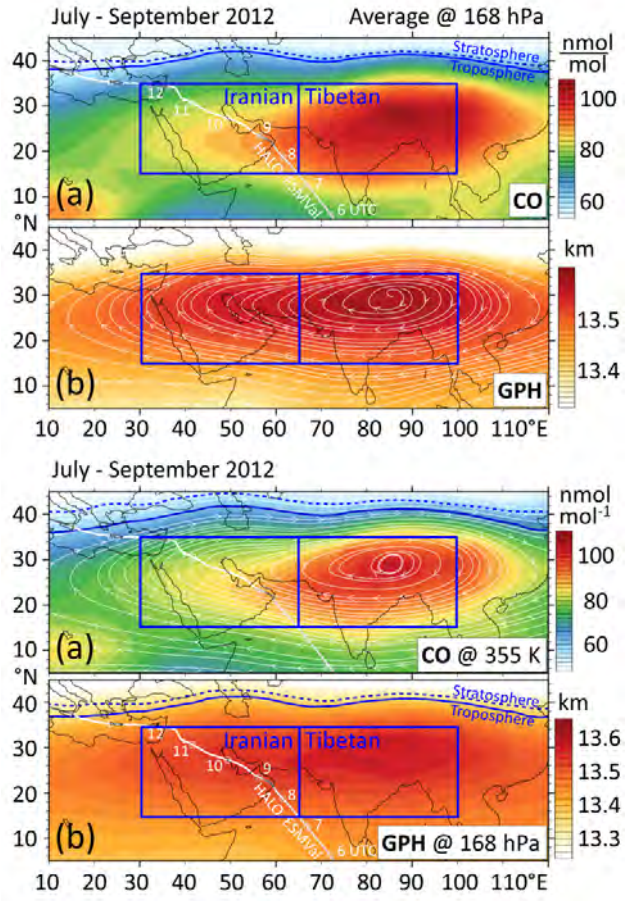

Figure 1. CO mixing ratios and geopotential height (GPH) as simulated by EMAC ~~at 168 hPa , averaged~~ for the monsoon months of 2012. Enhanced CO is considered to be a chemical characteristic of the ASMA ~~(Pan et al., 2016)~~, and increased GPH is a dynamical proxy to delimit the ASMA ~~(Barret et al., 2016)~~. The Iranian and Tibetan domains are used throughout the paper to discuss differences between the convectively driven eastern part and the western part that is mainly controlled by UT transport. ~~correspond to the regions used for lateral averaging throughout the paper (e.g. Figs. 2 – 5, S4 – S10).~~ The Iranian region was traversed by the HALO ESMVal campaign during a flight from Male (Maldives) to Larnaca (Cyprus) on 18 September 2012. ~~HALO was flying in the upper troposphere where the flight track is coloured white and dived to the lower troposphere where it is grey.~~ Beads show the HALO positions at full UTC hours, and the chosen isentropic (a) or pressure (b) levels roughly correspond to UT flight sections.

Formatted: Font: 9 pt

Formatted: Font color: Red

Formatted: Font color: Red

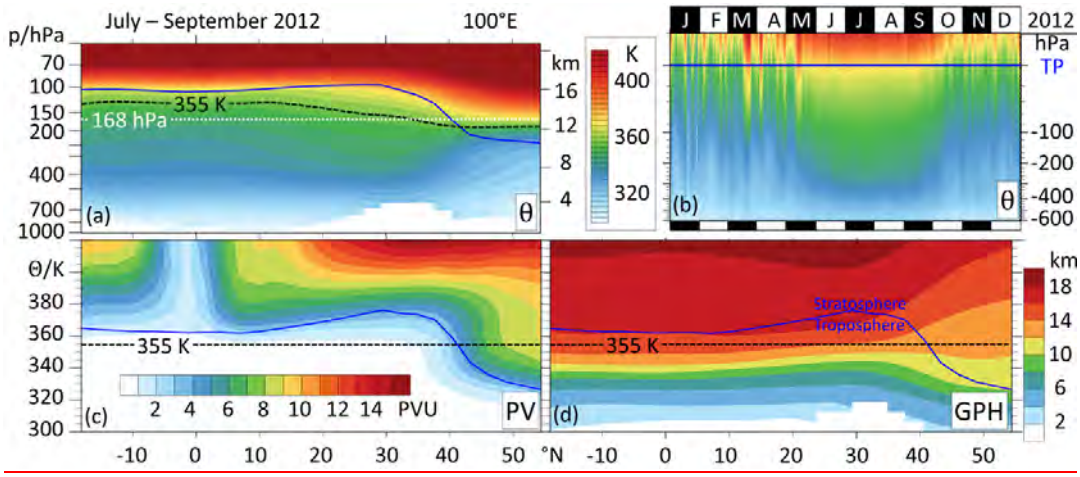

Figure 2. EMAC simulated relations between different parameters of the stratification of the atmosphere in the Tibetan region. Potential temperature (θ), potential vorticity (PV) and geopotential height (GPH) in curtains at 100°E. The levels of θ = 355 K and p = 168 hPa are chosen for horizontal slices in the paper. Panels (a), (c), (d) show time averages for the monsoon months of 2012. Panel (b) shows the evolution of θ profiles (grid-cell dry air mass weighted averages from 15 - 35°N, 65 – 100°E) throughout 2012 in pressure coordinates relative to tropopause (TP). Note the steeply inclining TP over the Tibetan plateau, which marks the transition from the extratropics (dominated by baroclinic wave activity and downward stratospheric circulation) to the tropics (dominated by radiative-convective balance and upward stratospheric circulation). Heating of the Tibetan plateau in summer brings UT isentropes closer to the surface (panel b), leading to intersections between the inclined TP and a range of isentropes (panel a).

~~**. Panel a additionally shows the intersection between the tropopause and the 168 hPa pressure level, panel b additionally shows streamlines.**~~

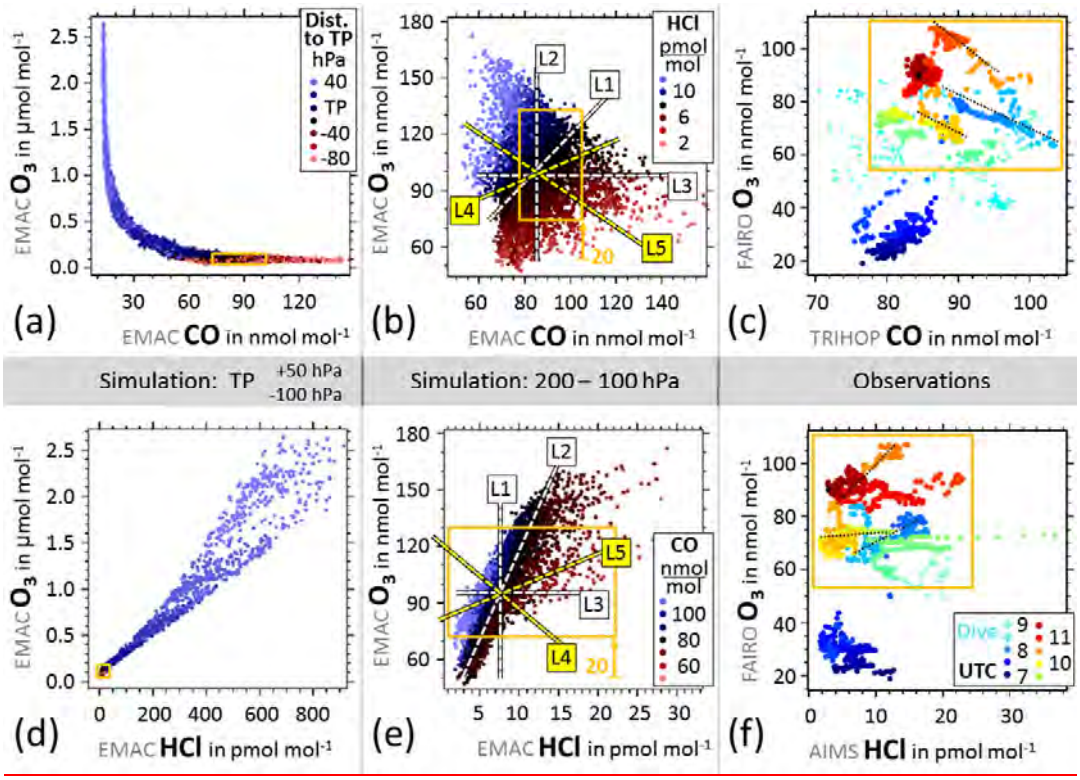

Figure 3. Tracer-tracer relations as simulated by EMAC for the entire September 2012 in the ASMA region, and as observed by HALO during the HALO ESMVal campaign on 18 September 2012. (a, d) Simulated samples from the region 15°N – 35°N, 30°E - 100°E. Colour coding corresponds to the pressure distance to the tropopause, from 100 hPa below to 50 hPa above. (b) Simulated tracer mixing ratios from the same region, but limited to tropospheric cells in the pressure altitude range 200 – 100 hPa. Colour coding indicates corresponding mixing ratios of HCl. See text for details of hypothetic lines L1 - L5. (c) Observed tracer mixing ratios of the HALO flight from Male to Larnaca (without initial and final stages). Colours correspond to the UTC time of measurement, also indicating spatial proximity. The orange boxes show the ranges covered by the measurements from within the ASMA.

Formatted: Normal

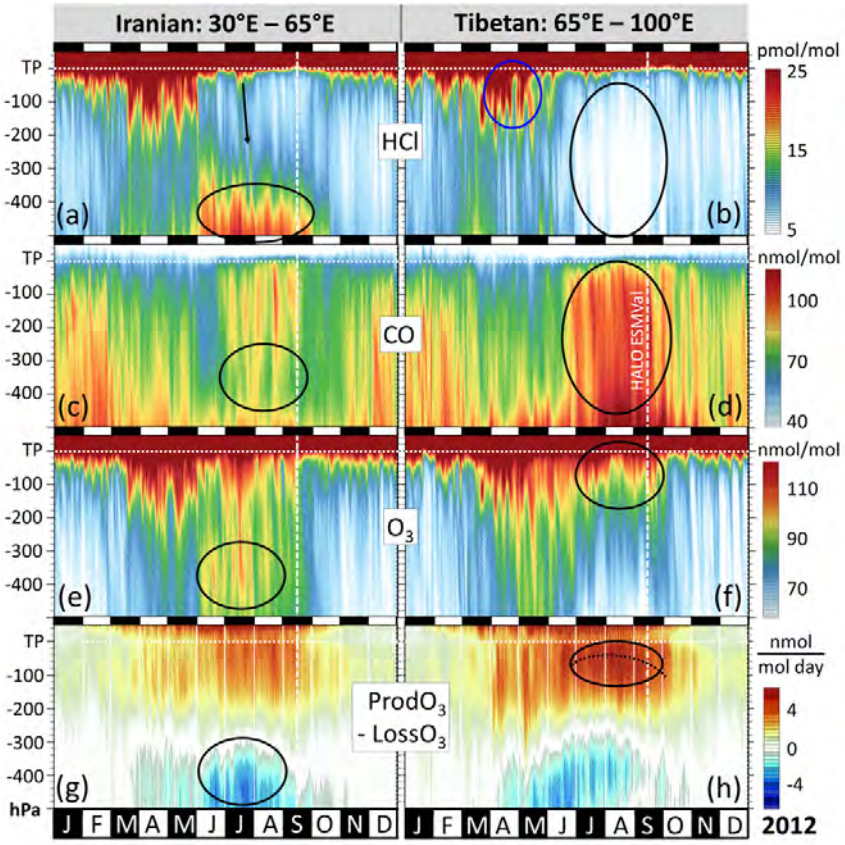
Iranian: 30°E – 65°E
Tibetan: 65°E – 100°E
TP
-100
-200
-300
-400
hPa
(a)
(b)
(c)
(d)
(e)
(f)
(g)
(h)
HCl
CO
O_3
$ProdO_3$
- $LossO_3$
HALO ESMVal
pmol/mol
25
15
5
nmol/mol
100
70
40
nmol/mol
110
90
70
nmol
mol day
4
0
-4
J F M A M J J A S O N D
2012

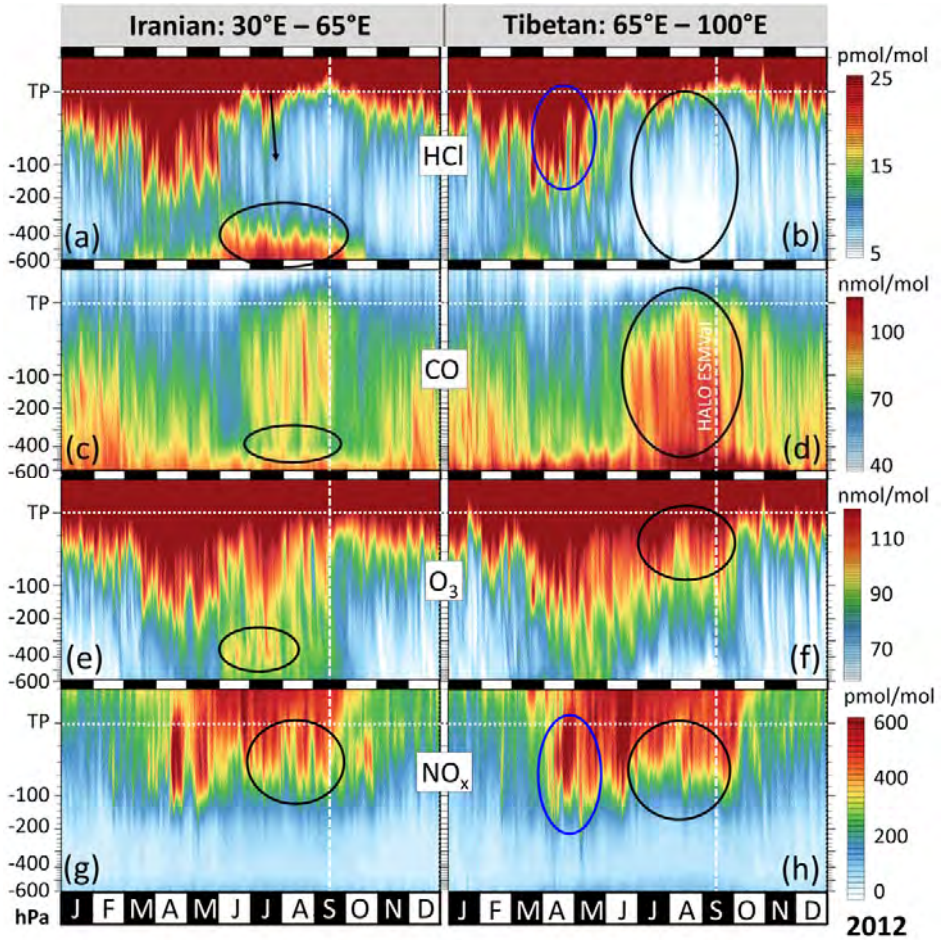

Figure #2.+4 Evolution of simulated trace gas profiles ~~and related diagnostics~~ in the western and eastern ASMA regions throughout 2012 ~~in the UTLS and middle troposphere of the ASMA region~~. The time of the HALO ESMVal measurements is indicated by a dashed line. ~~Vertical coordinates~~ Vertical coordinates are given as pressure distance to the tropopause ("TP"), whose altitude depends on time and location~~are , given as pressure distance to the tropopause ("TP"), whose altitude depends on time and location.~~ All values are grid-cell dry air mass weighted averages from 15°N to 35°N ~~, respectively for the western (30° - 65°E) and eastern (65° - 100°E) parts of the ASMA~~ (see Fig. 1).~~.~~ Marked features are discussed in the text. ~~See text for details of the calculation of O_3 net photochemical production, and for the discussion of features marked by circles and arrows.~~

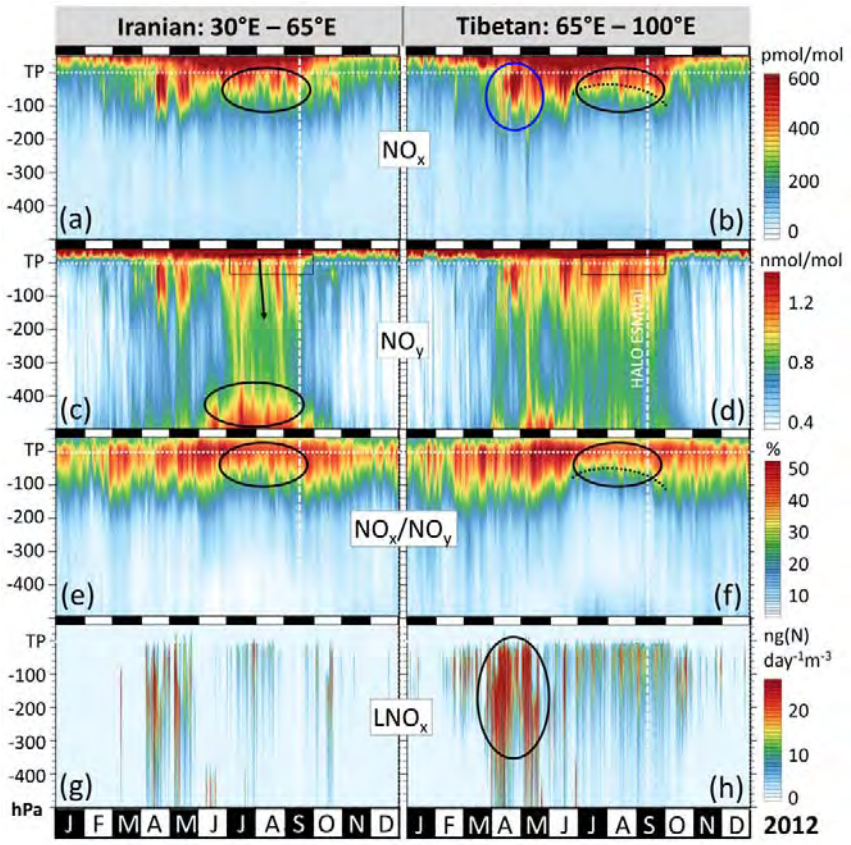
Iranian: 30°E – 65°E
Tibetan: 65°E – 100°E
TP
-100
-200
-300
-400
hPa
(a)
(b)
(c)
(d)
(e)
(f)
(g)
(h)
NOx
NOy
NOx/NOy
LNOx
HALO ESM (v1)
pmol/mol
600
400
200
0
nmol/mol
1.2
0.8
0.4
%
50
40
30
20
10
ng(N) day-1m-3
20
10
0
J F M A M J J A S O N D
2012

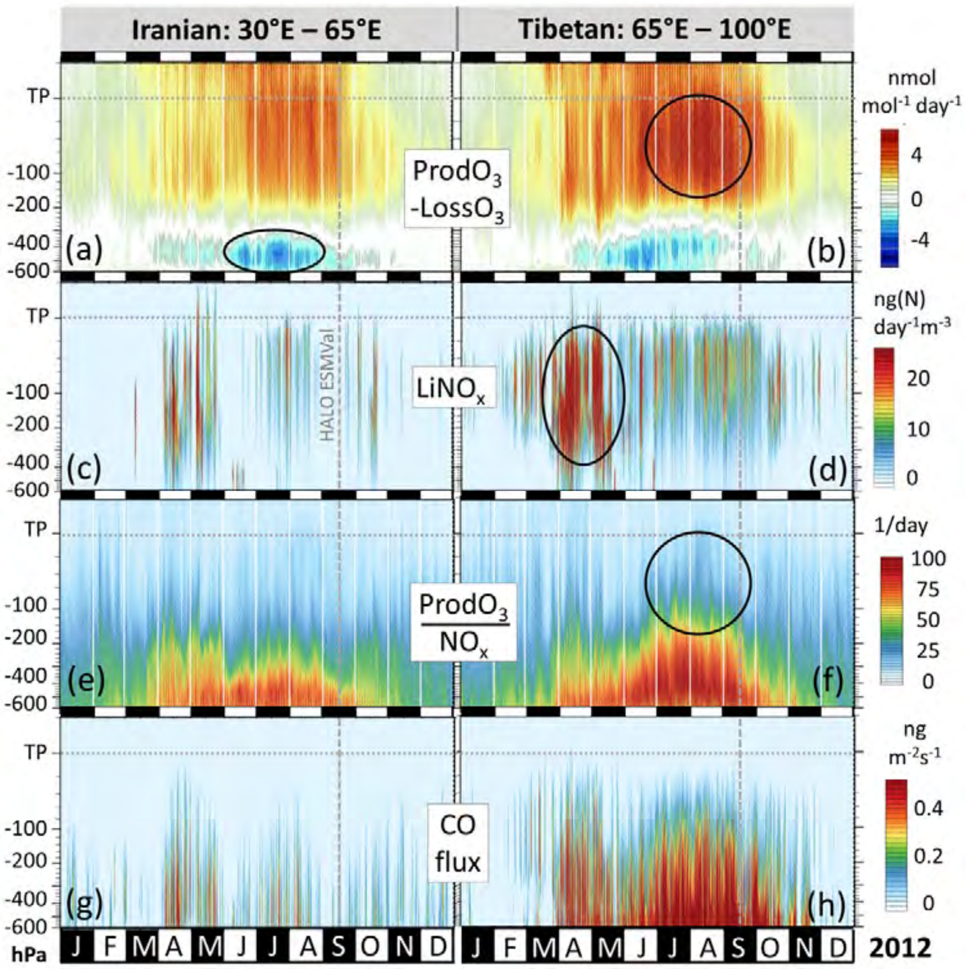

Figure 53. As Fig. 42, but for different parameters related to net photochemical O_3 production ($ProdO_3$-$LossO_3$)~~aspects of reactive nitrogen~~. -Lightning NO_x ($LiNO_x$) emissions in the model are determined by parameterizations for convection, lightning and NO_x emissions per flash. "CO flux" reflects the tempo-spatial concurrence of deep convective mass flux and CO mixing ratio, but as simple product of both does not account for entrainment and detrainment of convection. Panels (e) and (f) highlight the non-linear dependence of O_3 production on NO_x mixing ratios. Strong gradients indicate the transition between NO_x-limited and NO_x-saturated photochemical regimes, but are superimposed by the effects of other O_3 precursors. Individual profiles from panels (a)

Formatted: Font: 9 pt
Formatted: Font: 9 pt
Formatted: Font: 9 pt
Formatted: Font: 9 pt, Subscript
Formatted: Font: 9 pt
Formatted: Font: 9 pt, Subscript
Formatted: Font: 9 pt
Formatted: Font: 9 pt, Subscript
Formatted: Font: 9 pt
Formatted: Font: 9 pt, Subscript
Formatted: Font: 9 pt
Formatted: Font: 9 pt, Subscript
Formatted: Font: 9 pt
Formatted: Font: 9 pt, Subscript
Formatted: Font: 9 pt
Formatted: Font: 9 pt, Subscript
Formatted: Font: 9 pt
Formatted: Font: 9 pt, Subscript
Formatted: Font: 9 pt
Formatted: Font: 9 pt, Subscript
Formatted: Font: 9 pt
Formatted: Font: 9 pt, Subscript
Formatted: Font: 9 pt
Formatted: Font color: Red
Formatted: Font: 9 pt, Font color: Red
Formatted: Font: 9 pt
Formatted: Font: 9 pt, Subscript
Formatted: Font: 9 pt

and (b) are shown in the supplement (Fig. S8).~~See Appendix A for details concerning lightning NO_x (LNO_x), and the supplementary material for a zoom into the regions indicated by black rectangles in panels c and d.~~

Formatted: Normal

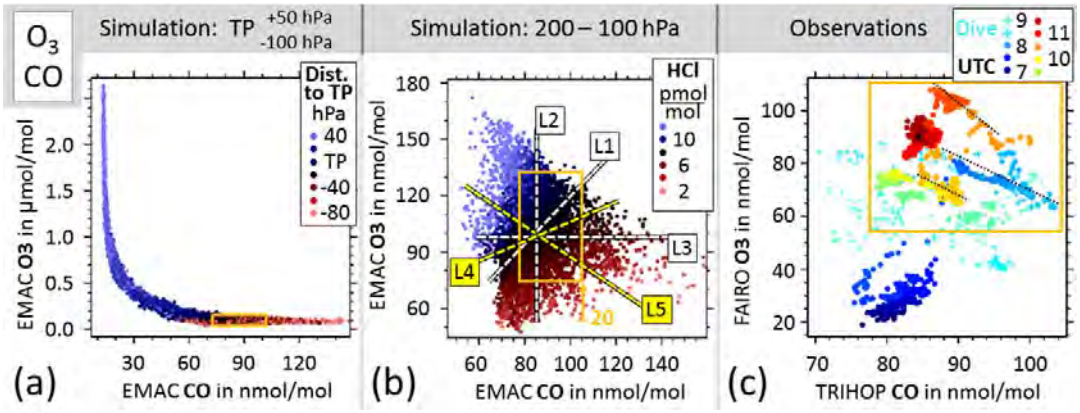

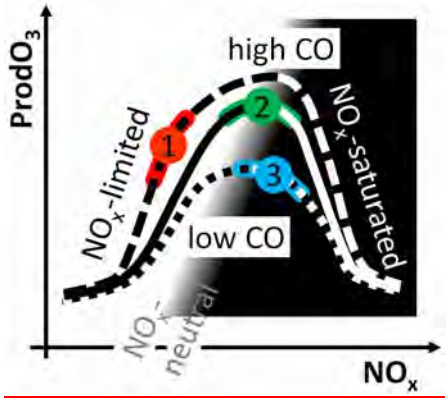

Figure 6. Schematic of the dependence of photochemical O_3 production ($ProdO_3$) on NO_x and CO mixing ratios (after Grooß et al. (1998). Red, green and blue highlight photochemical conditions that are discussed in the text. Approximate numbers (Ehhalt and Rohrer, 1994; Jaeglé et al., 1998; Grooß et al., 1998): For UT conditions at northern mid latitudes the point of maximum O_3 production may vary between 200 and 700 nmol/mol NO_x. The maximum net O_3 production varies by a factor of about 4, depending on ambient conditions.

~~Figure 4. Tracer-tracer relations (CO vs. O_3) as simulated by EMAC for the entire September 2012 in the ASMA region, and as observed by HALO during the HALO ESMVal campaign on 18 September 2012. (a) Simulated samples from the region 15°N – 35°N, 30°E - 100°E. Colour coding corresponds to the pressure distance to the tropopause, from 100 hPa below to 50 hPa above.~~

Formatted: Font: 9 pt
Formatted: Font: 9 pt, Subscript
Formatted: Font: 9 pt
Formatted: Font: 9 pt
Formatted: Font: 9 pt
Formatted: Font: 9 pt
Formatted: Font: 9 pt

~~(b) Simulated tracer mixing ratios from the same region, but limited to tropospheric cells in the pressure altitude range 200 – 100 hPa. Colour coding indicates corresponding mixing ratios of HCl. See text for details of hypothetic lines L1 – L5. (c) Observed tracer mixing ratios of the HALO flight from Male to Larnaca (POI2 to POI6). Colours correspond to the UTC time of measurement, also indicating spatial proximity. The orange boxes show the ranges covered by the measurements from within the ASMA.~~

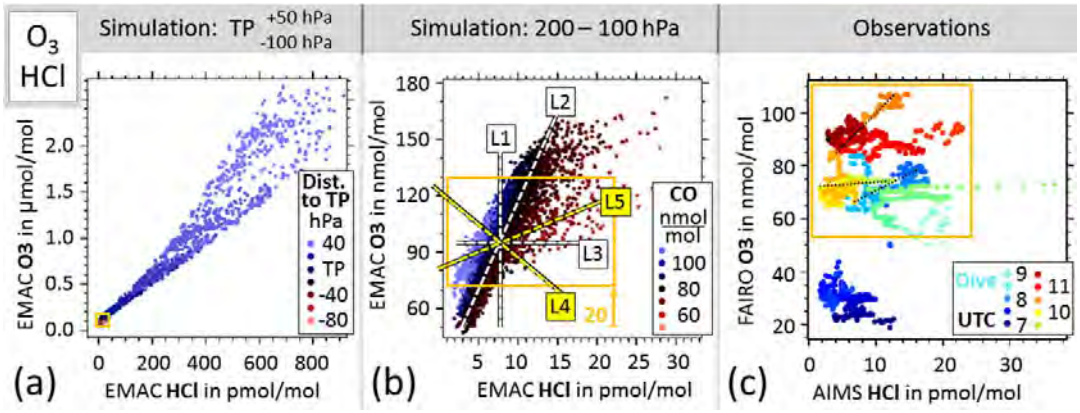

~~Figure 5. As Fig. 4, but for HCl vs. O_3.~~

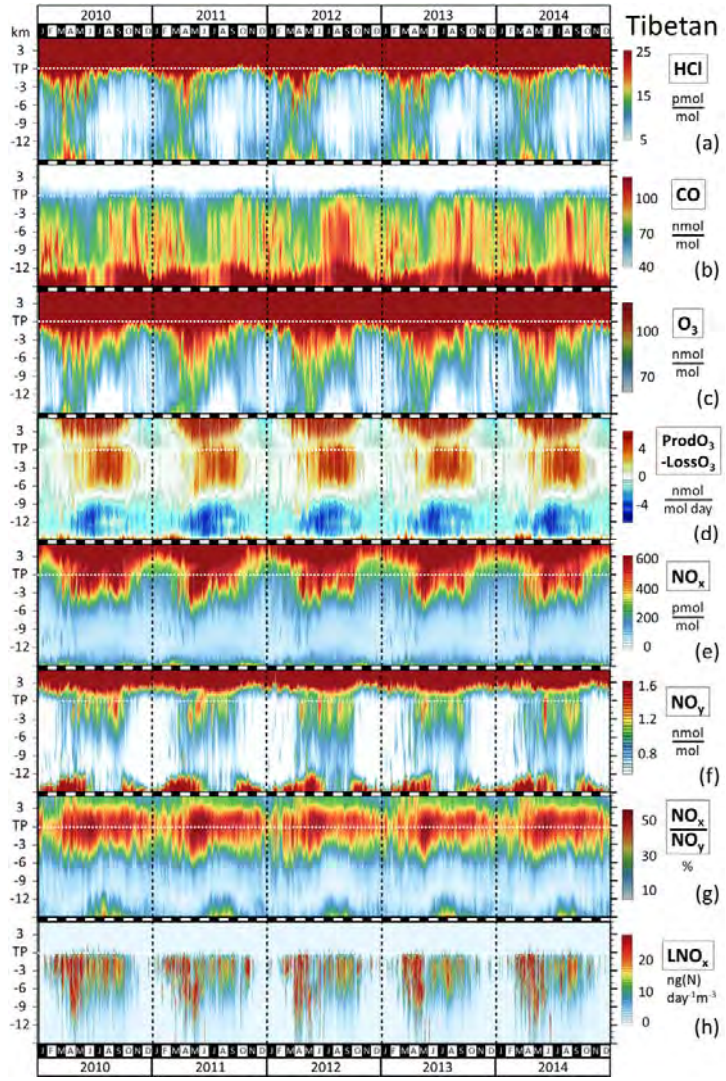

~~Figure 6. Evolution of simulated trace gas profiles and related diagnostics for the years 2010 - 2014 in the Tibetan ASMA region (65° - 100°E, see Fig. 1). Vertical coordinates are given as distance to the tropopause ("TP"), whose altitude depends on time and location. All values are grid-cell dry air mass weighted averages from 15°N to 35°N. The column for the year 2012 is identical to the corresponding panels in Figs. S4, S5. The corresponding figure for the Iranian region is shown in the supplementary material (Fig. S18).~~

Formatted: Font color: Background 1

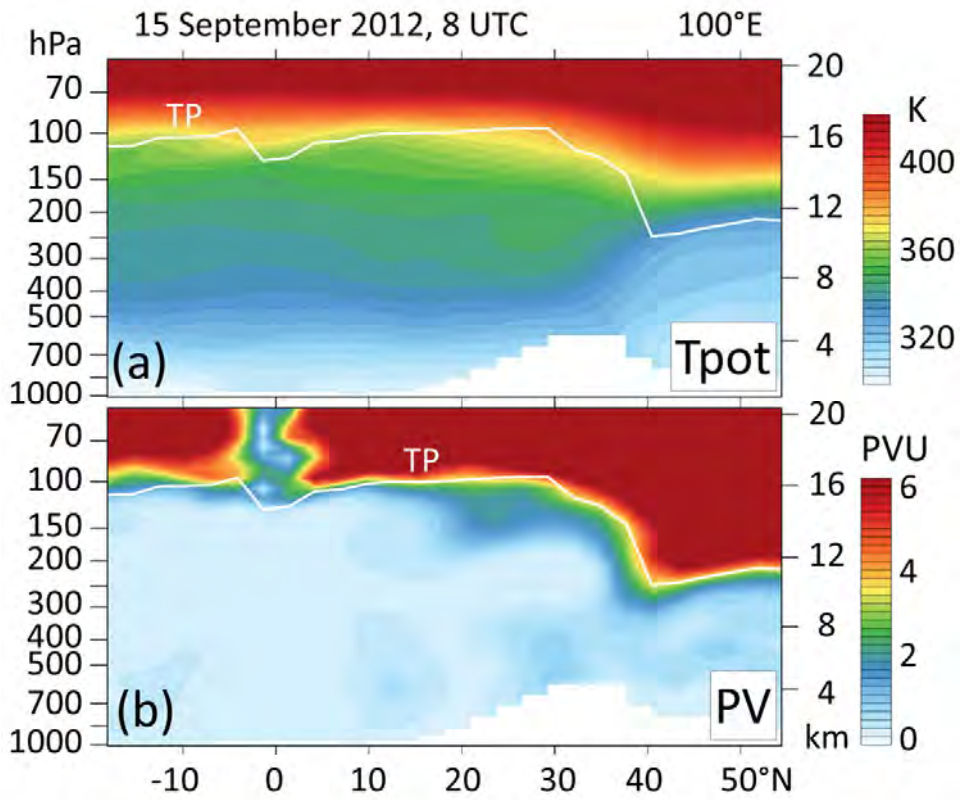

~~Figure 7. EMAC simulated potential temperature and potential vorticity in curtains at 100°E, at the time when the air corresponding to POI3 was passing there at about 165 hPa. Note the steeply inclining TP over the Tibetan plateau, which marks the transition from the extratropics (dominated by baroclinic wave activity and downward stratospheric circulation) to the tropics (dominated by radiative-convective balance and upward stratospheric circulation). North of 30°N the EMAC TP is defined by the 3.5 PVU isocontour. Isentropes intersect the inclining TP, thereby allowing cross-TP transport without leaving a tell-tale signature of increased Tpot in the corresponding air masses in the tropics. This includes the 350 – 370 K isentropes that were encountered during the HALO ESMVal campaign in the tropics (see also Figs. S11, S12).~~

Formatted: Font color: Background 1

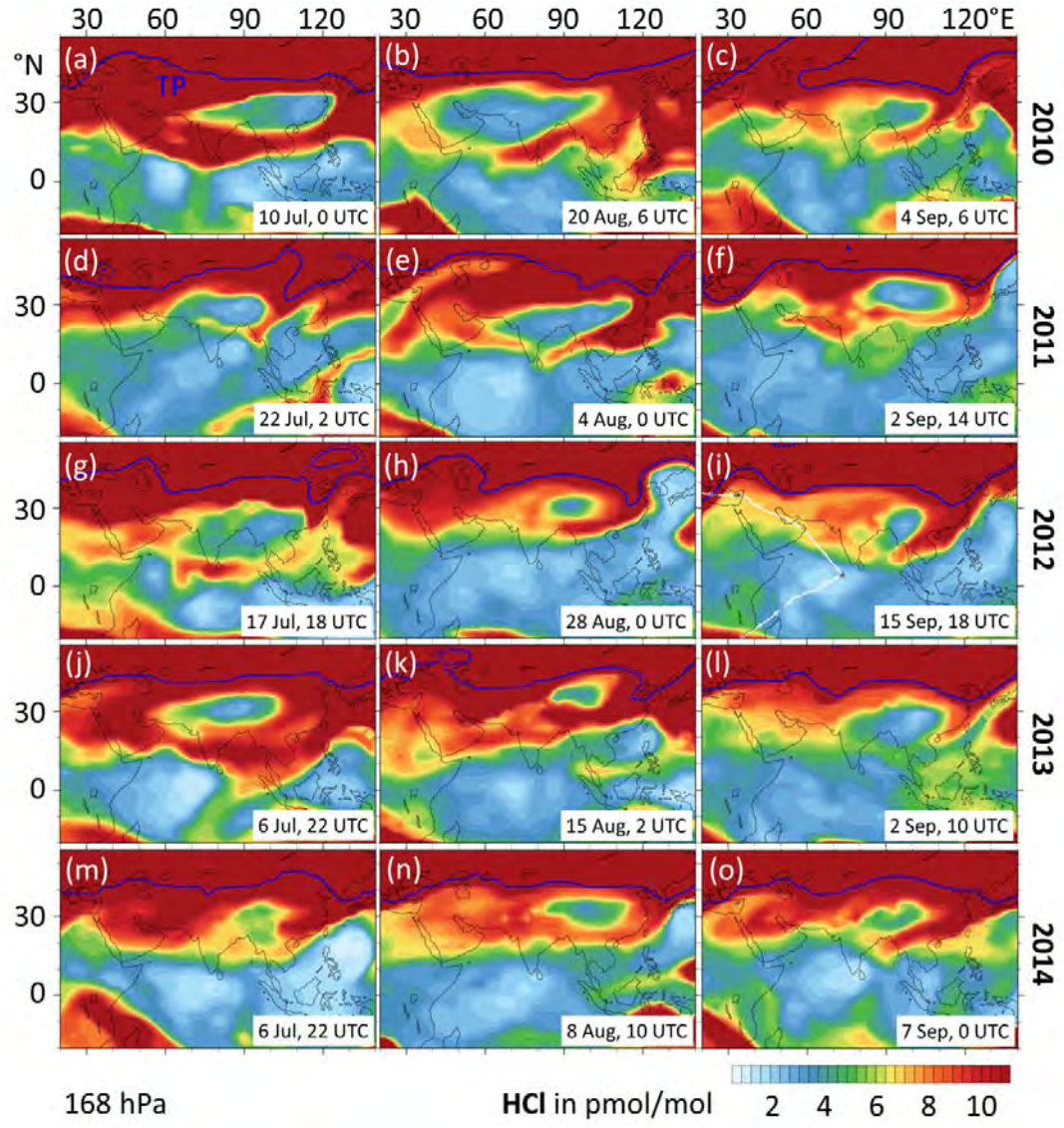

~~Figure 8. EMAC simulated HCl mixing ratios at 168 hPa in the ASMA region, complementing Fig. 10. The snapshots were selected to represent independent situations, where the southern ASMA fringe is marked by a filament of enhanced HCl. The filaments are often associated with a TP trough at the eastern ASMA flank. Enhanced HCl serves as a proxy for TL or stratospheric air.~~

Formatted: Font color: Background 1

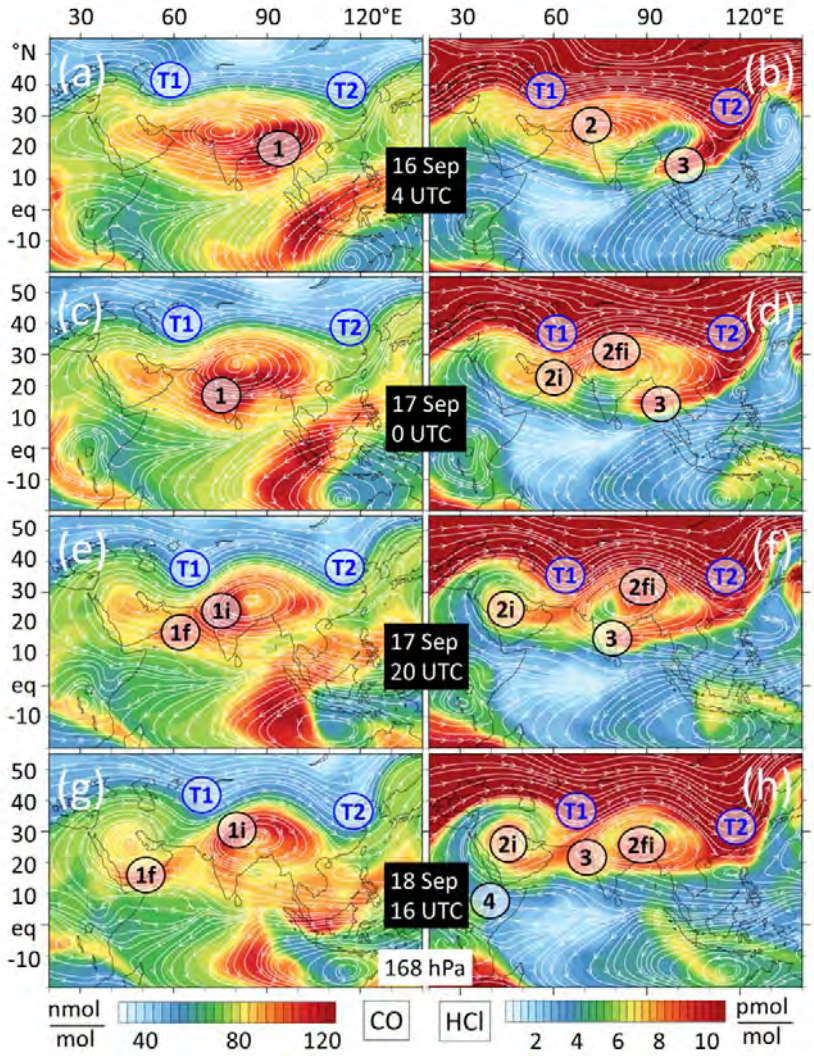

~~Figure 9. Sequence simulated tracer fields at 168 hPa, illustrating the stirring associated with the splitting up event of the ASMA that occurred during the HALO ESMVal campaign in September 2012. It starts with a single large anticyclone, and ends with a Tibetan and an Iranian part, shortly after the HALO flight from Male to Larnaca had passed through. Streamlines represent instantaneous wind fields. Circled annotations mark some features discussed in the text.~~

Formatted: Normal

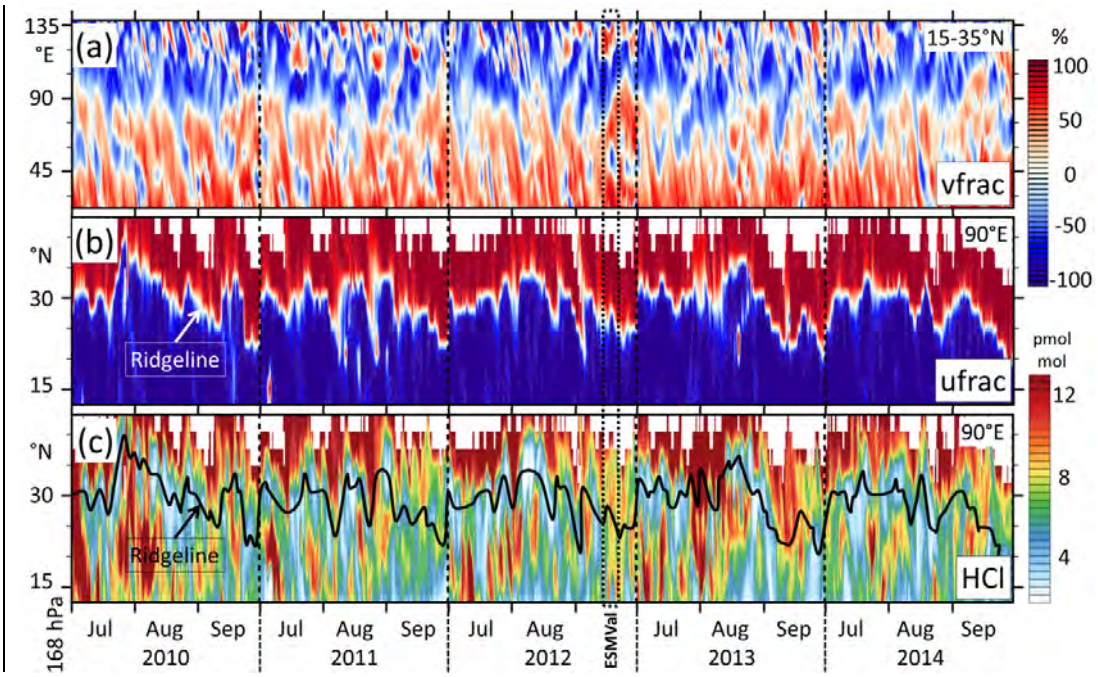
(a)
15-35°N
vfrac
%
100
50
0
-50
-100
135
°E
90
45
(b)
90°E
ufrac
Ridgeline
°N
30
15
(c)
90°E
HCl
Ridgeline
pmol
mol
12
8
4
168 hPa
Jul
Aug
Sep
2010
2011
2012
2013
2014
ESMVal

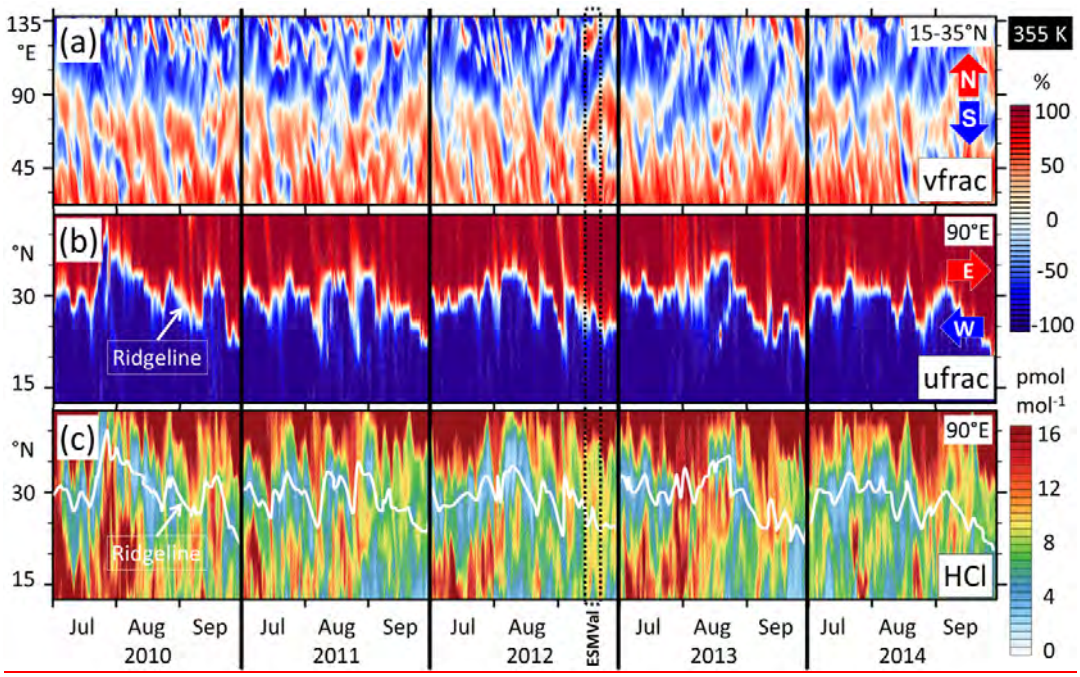

Figure 7~~10~~. Exploratory analyses of the frequency of occurrence of (i) dynamical instabilities ~~of two aspects discussed for the HALO ESMVal campaign case, which are relevant for the (re-)distribution of trace gases in the ASMA region: (1) Splitting, eddy shedding/remerging~~ of the ASMA and (ii) t~~; (2) T~~ransport of TL air in the free troposphere along the southern ASMA fringe. All panels show 10-hourly EMAC simulation results at the 355 K isentropic level~~168 hPa~~, for the summer monsoon months in the ASMA region. ~~The analyses are based on 10 h output steps. Grid cells not entirely within the troposphere are ignored.~~ (a) Meridional wind fraction (calculated as $v/\sqrt{u^2+v^2}$, with meridional velocity v, and zonal velocity u) along a wide zonal transect, averaged with dry grid cell mass weighting at each longitude from 15°N to 35°N. Blue shades indicate southward and red shades northward winds. Each red-blue pair (from west to east) at a given time marks an anticyclone or a smaller eddy. (b) As panel (a), but for zonal wind fraction ($u/\sqrt{u^2+v^2}$) along a meridional transect at 90°E. Blue shades indicate west~~east~~ward and red east~~west~~ward winds. (c) Time evolution of HCl mixing ratios. At any given time, locally increased HCl south of the ridgeline is a proxy for air from the TL or the stratosphere.

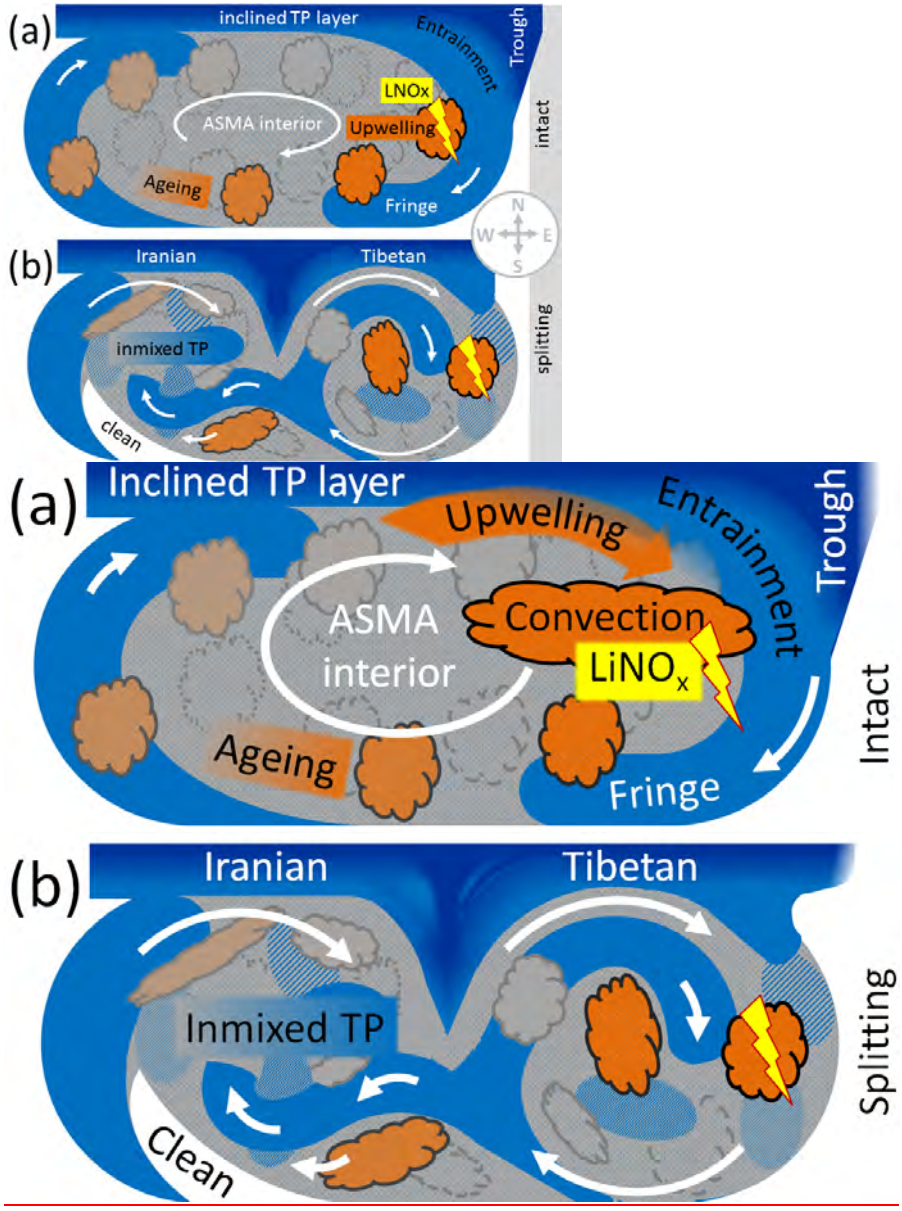
(a)
inclined TP layer
Entrainment
Trough
LNOx
ASMA interior
Upwelling
intact
Ageing
Fringe
N
W
E
S
(b)
Iranian
Tibetan
inmixed TP
splitting
clean
(a)
Inclined TP layer
Upwelling
Entrainment
Trough
ASMA
interior
Convection
LiNOx
Intact
Ageing
Fringe
(b)
Iranian
Tibetan
Inmixed TP
Splitting
Clean

Figure 8~~11~~. Schematics of processes determining trace gas distributions in the ASMA at an UT ~~pressure~~ level: (a) One undisturbed anticyclone, encompassing the Tibetan and Iranian regions; (b) Splitting into an Iranian and a Tibetan part. See text for details.

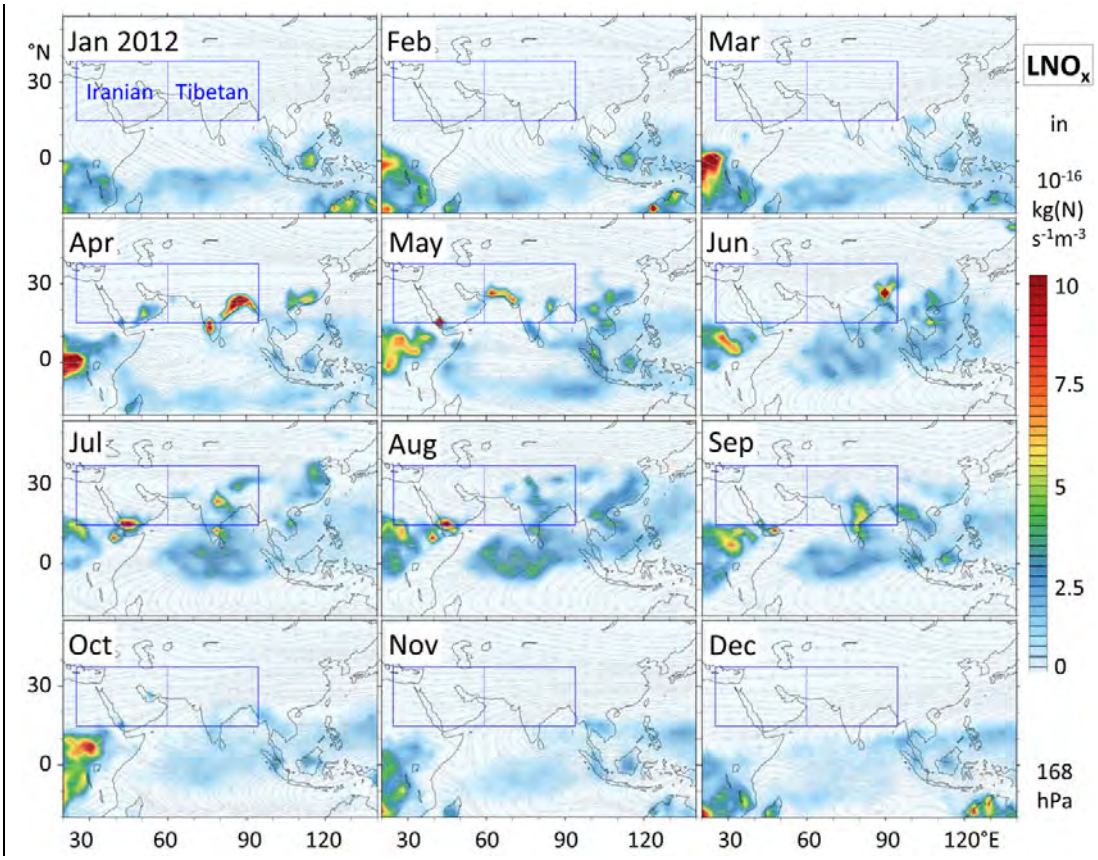
Jan 2012
Feb
Mar
Apr
May
Jun
Jul
Aug
Sep
Oct
Nov
Dec
Iranian
Tibetan
°N
30
0
30
60
90
120
120°E
LNO$_x$
in
10^{-16}
kg(N)
$s^{-1}m^{-3}$
10
7.5
5
2.5
0
168
hPa

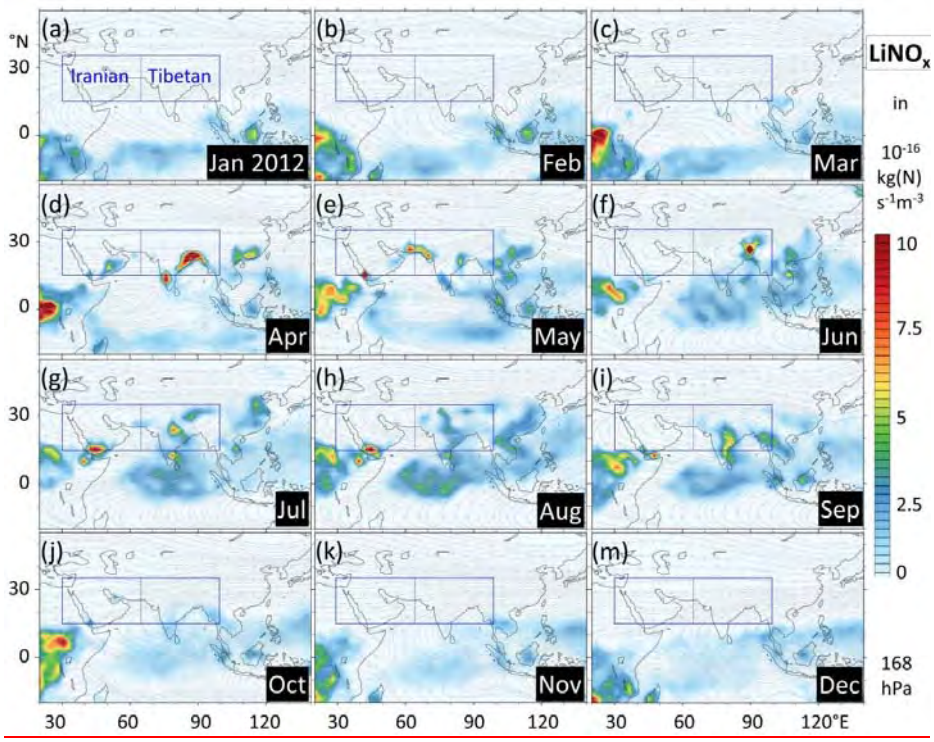

Figure A1. Monthly mean lightning NO_x emissions in 2012 at 168 hPa, based an EMAC simulation RC1SD-base-10a. Blue rectangles indicate the region(s) on that lateral averaging in Figs. 53 and A43 is based on. The ASMA circulation prints through in the monthly mean wind fields from June to September, as shown by streamlines (grey).

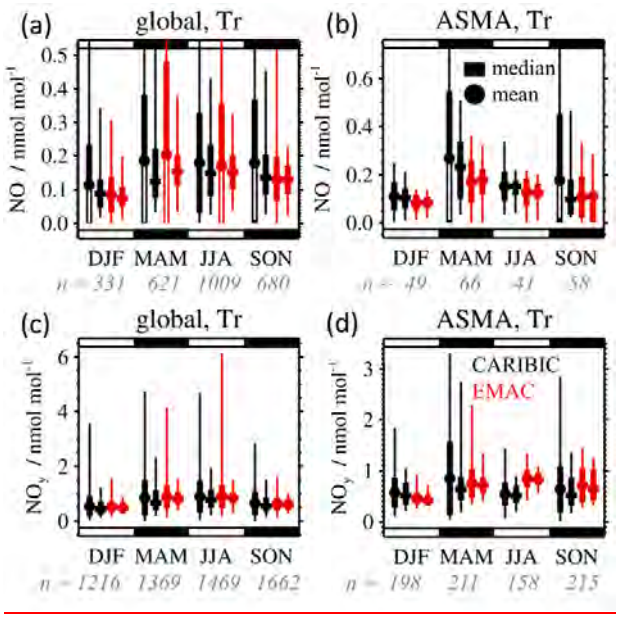

Figure A2. Comparison of IAGOS-CARIBIC (black) measurements in the altitude range between 300 hPa and the TP ("Tr") with corresponding results of the EMAC RC1SD-base-10a simulation (red) for (a) NO globally, (b) NO in the ASMA region (15-35°N, 30-100°E), (c) NO_y globally, (d) NO_y in the ASMA region. All data stem from the period May 2005 to April 2014. The simulation was sampled along the IAGOS-CARIBIC flight tracks with a resolution of 12 min, and IAGOS-CARIBIC observations were subsequently interpolated (interval mean) to a resolution of 12 min. Numbers n below the plots show the number of the remaining data pairs (after interpolation and filtering) available for the respective seasons. Dots represent mean values, whiskers indicate standard deviation, min & max values. Rectangles represent the median, and whiskers the percentiles 5, 25, 75, 95.

Formatted: Line spacing: 1,5 lines

Formatted: Font: 9 pt

Formatted: Font: 9 pt

Formatted: Font: 9 pt

Formatted: Font: 9 pt

Formatted: Subscript

Formatted: Subscript

Formatted: Font: 9 pt

Formatted: Font: 9 pt

Formatted: Font: 9 pt

Formatted: Font: 9 pt

Formatted: Font: 9 pt

Formatted: Font: 9 pt

Formatted: Font: 9 pt

Formatted: Font: 9 pt

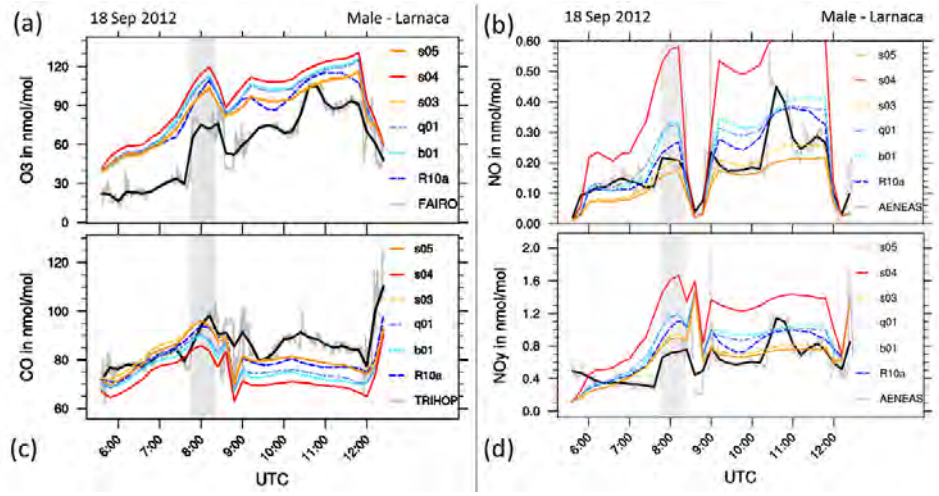

Figure A32. Mixing ratios of O_3, CO, NO and NO_y along the HALO flight track from Male to Larnaca, on 18 September 2012. Grey shading marks the first flight section in ASMA air ~~POI1~~. Grey line: in situ measurements in 10 s resolution, black: in situ averaged to 12 min simulation time steps, R10a: EMAC simulation RC1SD-base-10a. Sensitivity simulations are based on the almost identical RC1SD-base-10 simulation of (Jöckel et al., 2016), feature daily instead of monthly biomass burning emissions, and were performed in quasi chemistry transport model mode (Deckert et al., 2011) to facilitate isolating the effects of modified emissions.

b01: as R10a, but with different traffic and different biomass burning emissions;

q01: as b01, but QCTM;

s03: as q01, but halved ~~LNO~~$_x$LiNO$_x$ emissions; Formatted: Subscript

s04: as q01, but doubled ~~LNO~~$_x$LiNO$_x$ emissions; Formatted: Subscript

s05: as s03, but with a different vertical emission profile of ~~LNO~~$_x$LiNO$_x$ (emission factors not decreased in the mid-troposphere, i.e. no C-shape) Formatted: Subscript

Formatted: Caption

Formatted: Font: 9 pt, Bold

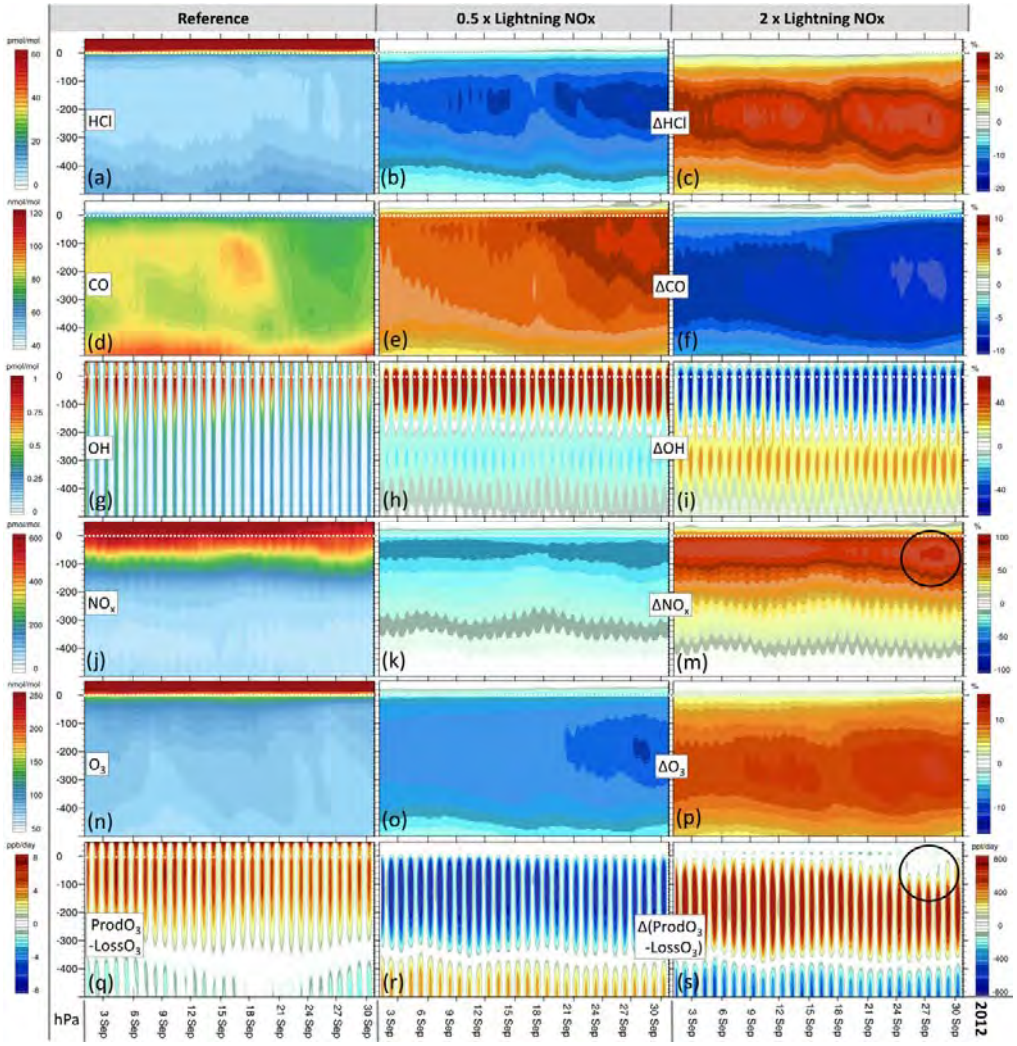

Figure A43. Evolution of simulated trace gas profiles and related diagnostics during September 2012 in the ASMA region (15° N – 35° N, 30° E – 100° E), and their sensitivity to ~~LNO$_x$~~LiNO$_x$ emissions. The vertical axes cover the UTLS and middle troposphere, and their coordinates are given as pressure distance to the tropopause. Left column: QCTM reference simulation (q01). Middle column: s03 – q01, relative deviation of sensitivity simulation s03 wrt. q01 for trace gases, absolute deviation for net O_3 production. Right column: s04 – q01.

Formatted: Subscript

Formatted: Normal

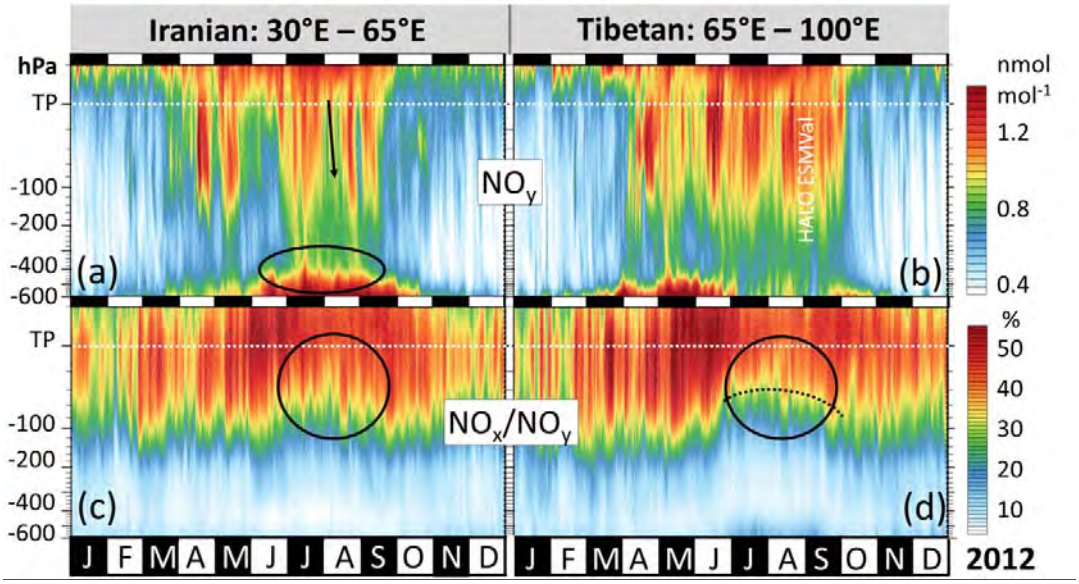

Figure B1. As Fig. 4, but focussing on reactive nitrogen.

Formatted: Font: 9 pt, Bold

Formatted: Font: 9 pt, Bold

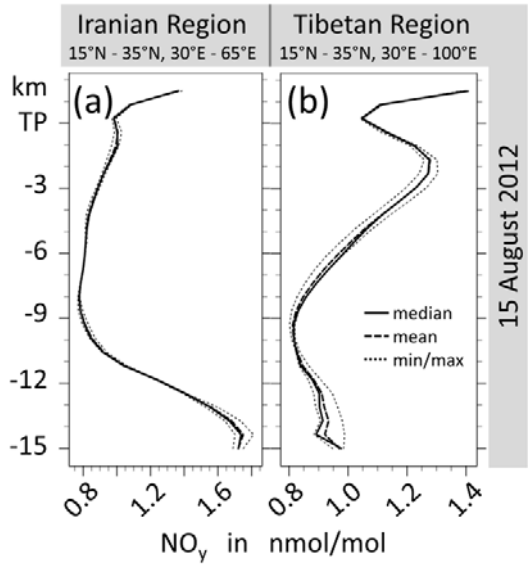

Figure B2. Simulated profiles of NO_y as simulated for 15 August 2012. These are examples of a C-shaped profile in the Iranian region (a) and an E-shaped profile in the Tibetan region (b).

Formatted: Left, Line spacing: single

Formatted: Subscript

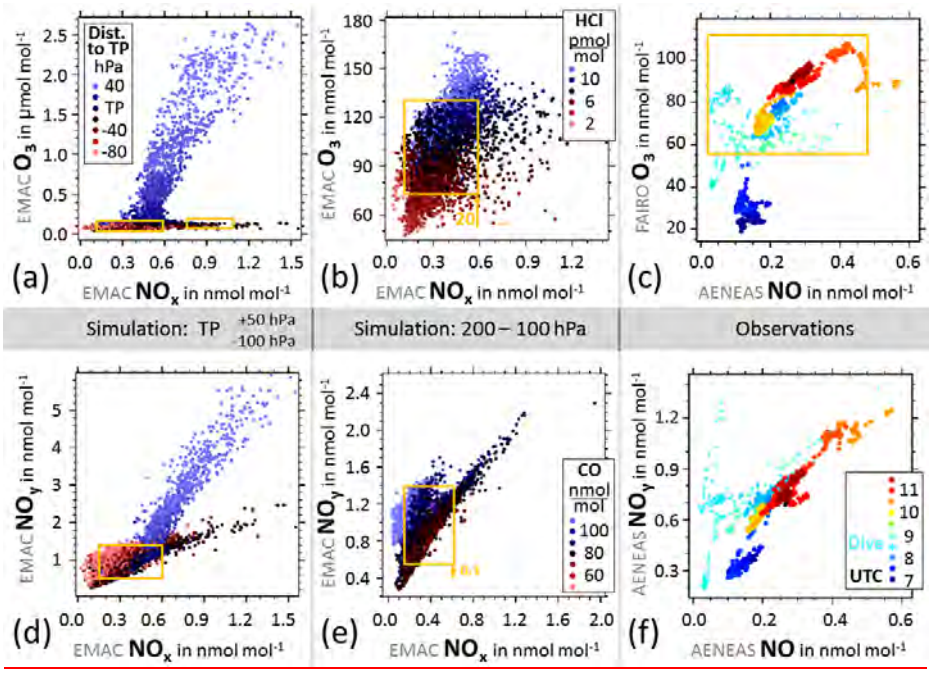

Figure B3. As Fig. 3, but focusing on reactive nitrogen. Panels (c) and (f) show NO instead of NO_y, because only NO was measured. At daytime, i.e. at the time of the measurements, NO is good proxy for NO_x.

Formatted: Font: 12 pt, Not Bold

Formatted: Normal

Page 21: [1] Formatted	Gottschaldt, Klaus-Dirk	21/12/2017 11:01:00

Not Highlight

Page 21: [1] Formatted	Gottschaldt, Klaus-Dirk	21/12/2017 11:01:00

Not Highlight

Page 21: [1] Formatted	Gottschaldt, Klaus-Dirk	21/12/2017 11:01:00

Not Highlight

Page 21: [1] Formatted	Gottschaldt, Klaus-Dirk	21/12/2017 11:01:00

Not Highlight

Page 21: [1] Formatted	Gottschaldt, Klaus-Dirk	21/12/2017 11:01:00

Not Highlight

Page 21: [1] Formatted	Gottschaldt, Klaus-Dirk	21/12/2017 11:01:00

Not Highlight

Page 21: [1] Formatted	Gottschaldt, Klaus-Dirk	21/12/2017 11:01:00

Not Highlight

Page 21: [1] Formatted	Gottschaldt, Klaus-Dirk	21/12/2017 11:01:00

Not Highlight

Page 21: [1] Formatted	Gottschaldt, Klaus-Dirk	21/12/2017 11:01:00

Not Highlight

Page 21: [1] Formatted	Gottschaldt, Klaus-Dirk	21/12/2017 11:01:00

Not Highlight

Page 21: [1] Formatted	Gottschaldt, Klaus-Dirk	21/12/2017 11:01:00

Not Highlight

Page 21: [2] Formatted	Gottschaldt, Klaus-Dirk	21/12/2017 11:01:00

Font color: Auto

Page 21: [2] Formatted	Gottschaldt, Klaus-Dirk	21/12/2017 11:01:00

Font color: Auto

Page 21: [2] Formatted	Gottschaldt, Klaus-Dirk	21/12/2017 11:01:00

Font color: Auto

Page 21: [2] Formatted	Gottschaldt, Klaus-Dirk	21/12/2017 11:01:00

Font color: Auto

Page 21: [2] Formatted	Gottschaldt, Klaus-Dirk	21/12/2017 11:01:00

Font color: Auto

Page 21: [3] Formatted	Gottschaldt, Klaus-Dirk	21/12/2017 11:01:00

Font color: Auto

Page 21: [3] Formatted	Gottschaldt, Klaus-Dirk	21/12/2017 11:01:00

Font color: Auto

Page 21: [3] Formatted	Gottschaldt, Klaus-Dirk	21/12/2017 11:01:00

Font color: Auto

Page 21: [3] Formatted **Gottschaldt, Klaus-Dirk** **21/12/2017 11:01:00**

Font color: Auto

Page 21: [3] Formatted **Gottschaldt, Klaus-Dirk** **21/12/2017 11:01:00**

Font color: Auto

Page 21: [3] Formatted **Gottschaldt, Klaus-Dirk** **21/12/2017 11:01:00**

Font color: Auto

Page 21: [3] Formatted **Gottschaldt, Klaus-Dirk** **21/12/2017 11:01:00**

Font color: Auto

Page 21: [3] Formatted **Gottschaldt, Klaus-Dirk** **21/12/2017 11:01:00**

Font color: Auto

Page 21: [4] Formatted **Gottschaldt, Klaus-Dirk** **21/12/2017 11:01:00**

Font color: Auto

Page 21: [4] Formatted **Gottschaldt, Klaus-Dirk** **21/12/2017 11:01:00**

Font color: Auto

Page 21: [4] Formatted **Gottschaldt, Klaus-Dirk** **21/12/2017 11:01:00**

Font color: Auto

Page 21: [4] Formatted **Gottschaldt, Klaus-Dirk** **21/12/2017 11:01:00**

Font color: Auto

Page 21: [4] Formatted **Gottschaldt, Klaus-Dirk** **21/12/2017 11:01:00**

Font color: Auto

Page 21: [4] Formatted **Gottschaldt, Klaus-Dirk** **21/12/2017 11:01:00**

Font color: Auto

Page 21: [4] Formatted **Gottschaldt, Klaus-Dirk** **21/12/2017 11:01:00**

Font color: Auto

Page 21: [4] Formatted **Gottschaldt, Klaus-Dirk** **21/12/2017 11:01:00**

Font color: Auto

Page 21: [4] Formatted **Gottschaldt, Klaus-Dirk** **21/12/2017 11:01:00**

Font color: Auto

Page 21: [4] Formatted **Gottschaldt, Klaus-Dirk** **21/12/2017 11:01:00**

Font color: Auto

Page 21: [4] Formatted **Gottschaldt, Klaus-Dirk** **21/12/2017 11:01:00**

Font color: Auto

Page 21: [4] Formatted **Gottschaldt, Klaus-Dirk** **21/12/2017 11:01:00**

Font color: Auto

Page 21: [4] Formatted **Gottschaldt, Klaus-Dirk** **21/12/2017 11:01:00**

Font color: Auto

Page 21: [4] Formatted **Gottschaldt, Klaus-Dirk** **21/12/2017 11:01:00**

Font color: Auto

Page 21: [4] Formatted **Gottschaldt, Klaus-Dirk** **21/12/2017 11:01:00**

Font color: Auto

Page 21: [4] Formatted **Gottschaldt, Klaus-Dirk** **21/12/2017 11:01:00**

Font color: Auto

Page 21: [4] Formatted **Gottschaldt, Klaus-Dirk** **21/12/2017 11:01:00**

Font color: Auto

Page 21: [4] Formatted **Gottschaldt, Klaus-Dirk** **21/12/2017 11:01:00**

Font color: Auto

Page 21: [4] Formatted **Gottschaldt, Klaus-Dirk** **21/12/2017 11:01:00**

Font color: Auto

Page 21: [4] Formatted **Gottschaldt, Klaus-Dirk** **21/12/2017 11:01:00**

Font color: Auto

Page 21: [4] Formatted **Gottschaldt, Klaus-Dirk** **21/12/2017 11:01:00**

Font color: Auto

Page 21: [5] Formatted **Gottschaldt, Klaus-Dirk** **01/12/2017 16:23:00**

Font color: Auto

Page 21: [5] Formatted **Gottschaldt, Klaus-Dirk** **01/12/2017 16:23:00**

Font color: Auto

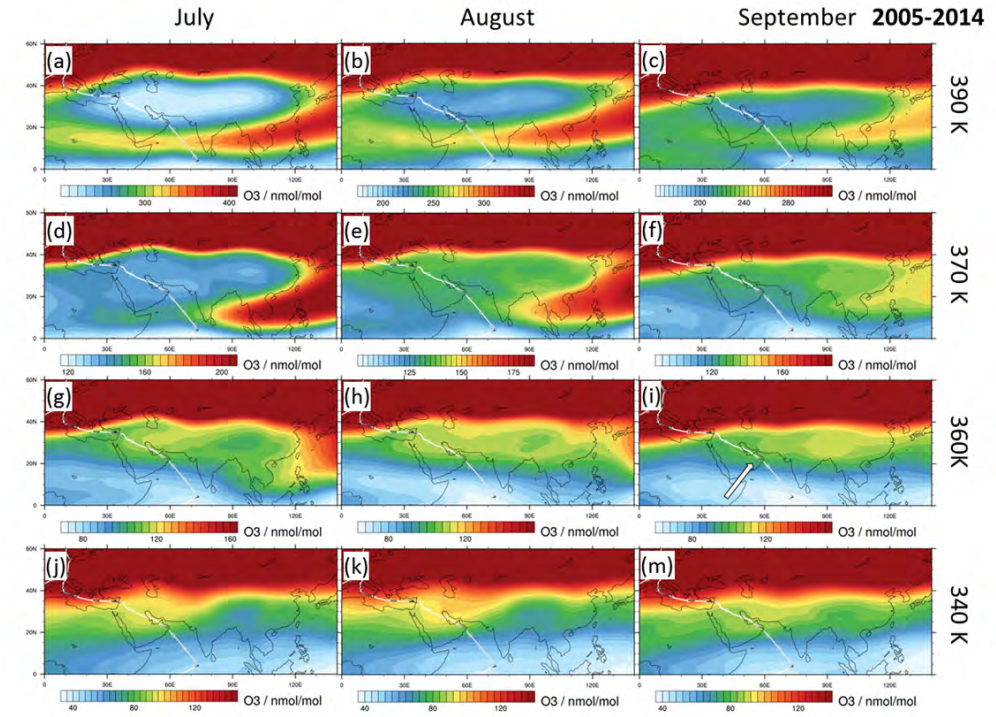

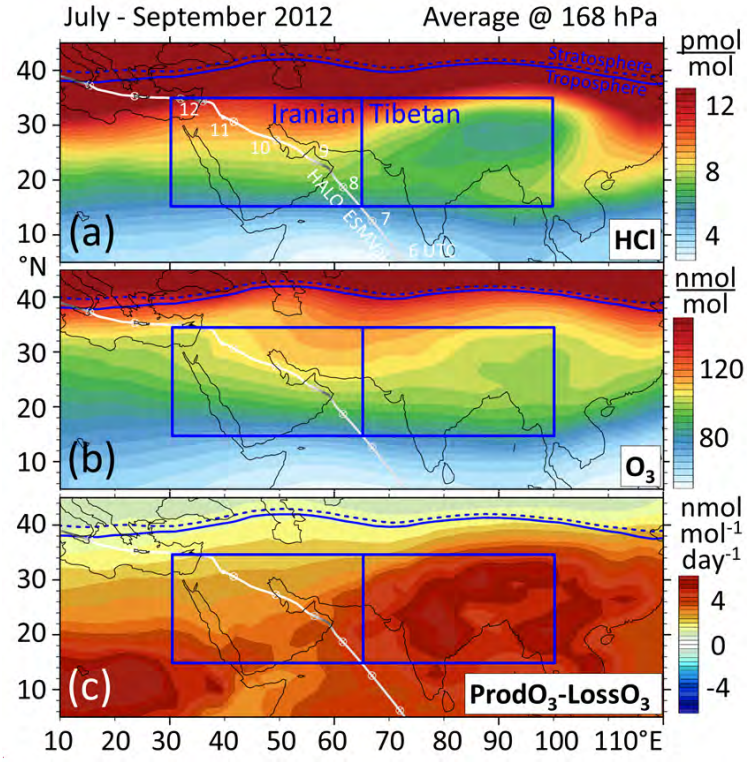

Formatted: Line spacing: 1,5 lines

Figure #+S1. Enhanced O_3 was found in the ASMA during HALO ESMVal and reproduced by EMAC, while Santee et al. (2017) report decreased O_3. Here we show EMAC simulated O_3 at different isentropic surfaces. Monthly averages are calculated for the same period as in Santee et al. (2017) and agree well with their figures (370 K, 390 K). However, at the level corresponding to the HALO flight altitude (360 K), O_3 is enhanced in the ASMA in September (Panel i) and the observed sudden increase at the southern ASMA edge over Oman is also reproduced (arrow). ~~{Livesey, 2013 #149}Trace gas mixing ratios and net O_3 production as simulated by EMAC at 168 hPa for the monsoon months of 2012. The Iranian and Tibetan domains correspond to the regions used for lateral averaging throughout the paper (e.g. Figs. 2 - 5, S4 – S10). The Iranian region was traversed by the HALO ESMVal campaign during a flight from Male (Maledives) to Larnaca (Cyprus) on 18 September 2012. HALO was flying in the upper troposphere where the flight track is colored white and dived to the lower troposphere where it is grey. Beads show the HALO positions at full UTC hours.~~

Formatted: Font: Times New Roman, 9 pt

Formatted: Font: Times New Roman, 9 pt, Subscript

Formatted: Font: Times New Roman, 9 pt

Formatted: Font: Times New Roman, 9 pt

Formatted: Font: Times New Roman, 9 pt

Formatted: Font: Times New Roman, 9 pt, Subscript

Formatted: Font: Times New Roman, 9 pt

Formatted: Font: Times New Roman, 9 pt, Subscript

Formatted: Font: Times New Roman, 9 pt

Formatted: Font: Times New Roman, 9 pt

Formatted: Font: Times New Roman, 9 pt

Formatted: Font: Times New Roman, 9 pt, Subscript

Formatted: Font: Times New Roman, 9 pt

Formatted: Line spacing: 1,5 lines

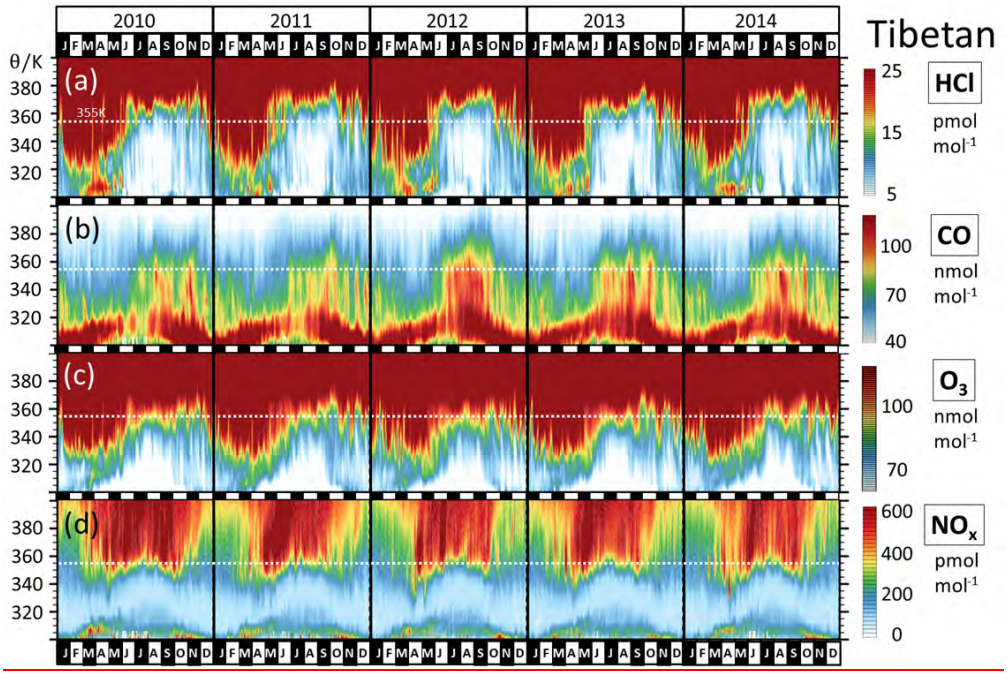
Tibetan
2010
2011
2012
2013
2014
θ/K
(a)
(b)
(c)
(d)
355K
HCl
pmol mol-1
CO
nmol mol-1
O3
nmol mol-1
NOx
pmol mol-1

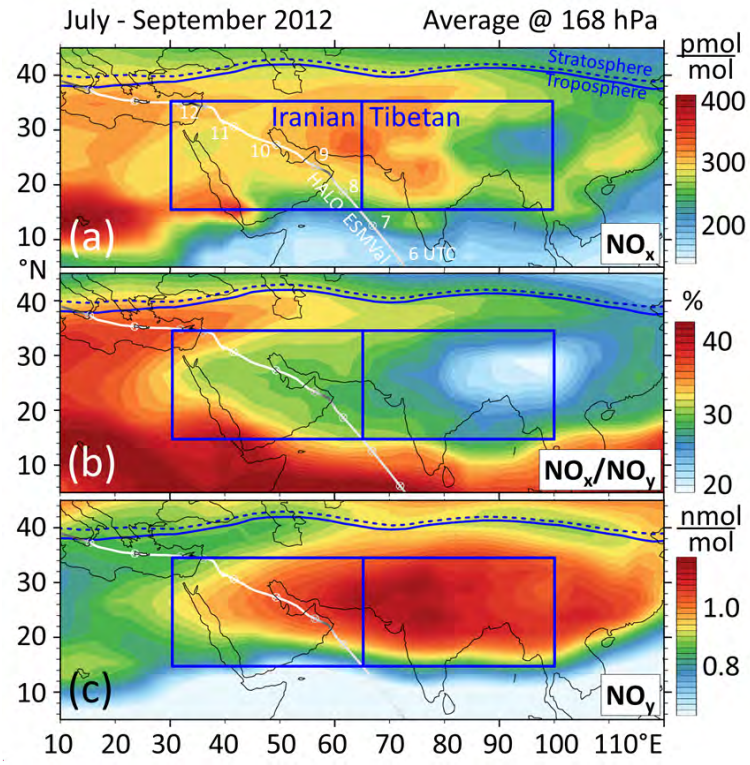
July - September 2012
Average @ 168 hPa
Stratosphere
Troposphere
Iranian
Tibetan
HALO
ESMVal
6 UTC
(a)
NOx
(b)
NOx/NOy
(c)
NOy
pmol mol
nmol mol
%
°N
10 20 30 40 50 60 70 80 90 100 110°E

Figure S2. Evolution of simulated trace gas profiles and related diagnostics for the years 2010 - 2014 in the Tibetan ASMA region (15°N to 35°N , 65° - 100°E). Vertical coordinates are given as distance to the tropopause ("TP"), whose altitude depends on time and location. All values are grid-cell dry air mass weighted averages. The column for 2012 corresponds to Fig. #+3, showing that the trace gas evolution in 2012 was largely similar to other years.

~~As Fig. S1, but for different tracers.~~

Formatted: Line spacing: 1,5 lines

Formatted: Font color: Auto

Formatted: Font: Times New Roman, 9 pt

Formatted: Line spacing: 1,5 lines

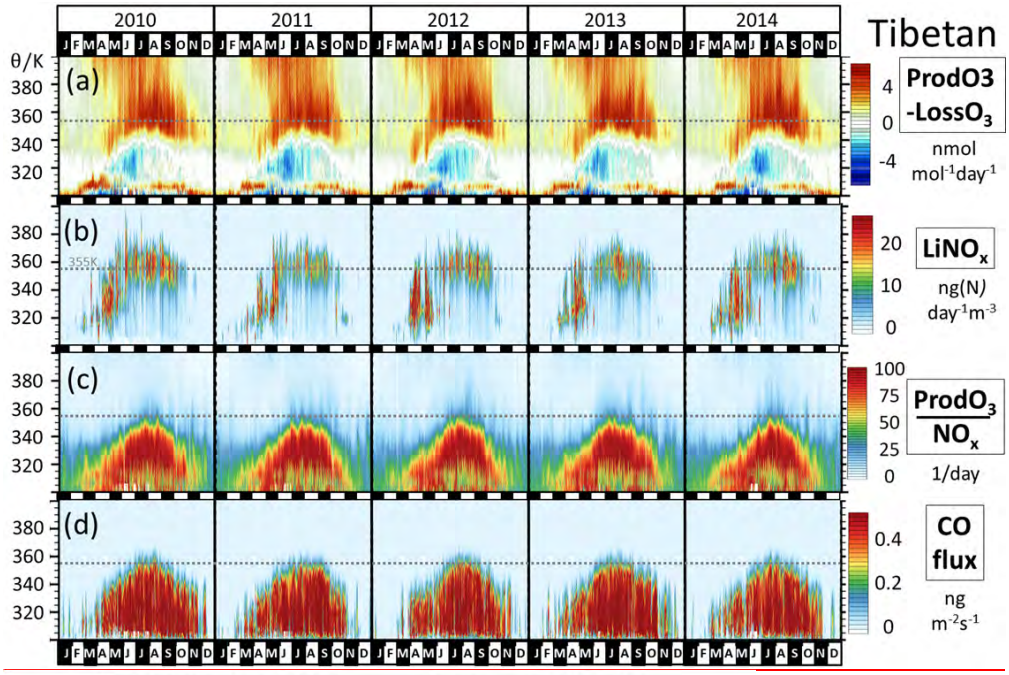

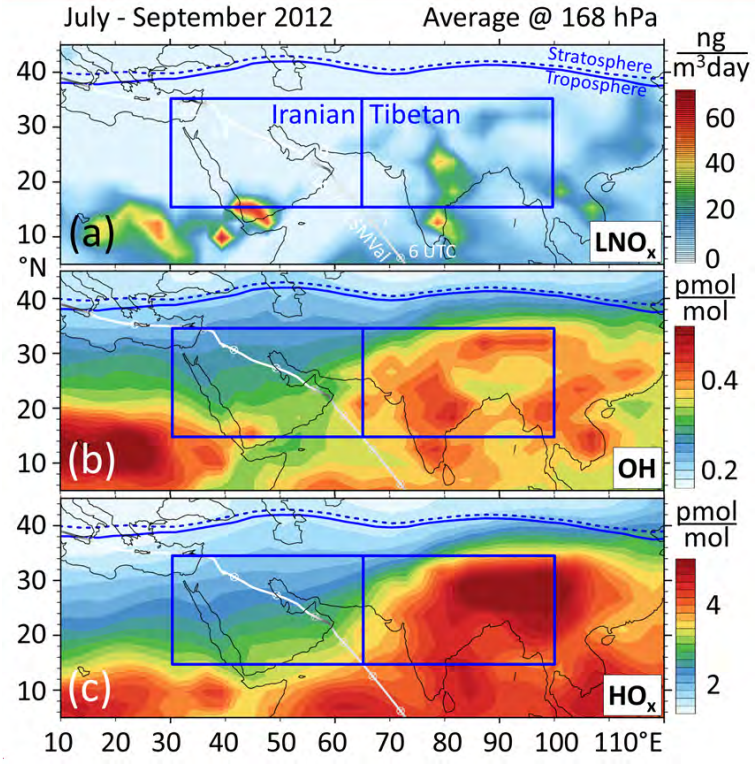

Figure #+S3. As Fig. #+S2, but putting Fig. #+4 in a multi-annual perspective. Regarding the shown parameters, 2012 was a normal year.

Formatted: Font: Times New Roman, 9 pt

Formatted: Font: Times New Roman, 9 pt

31 |

~~As Fig. S1, but for different tracers.~~

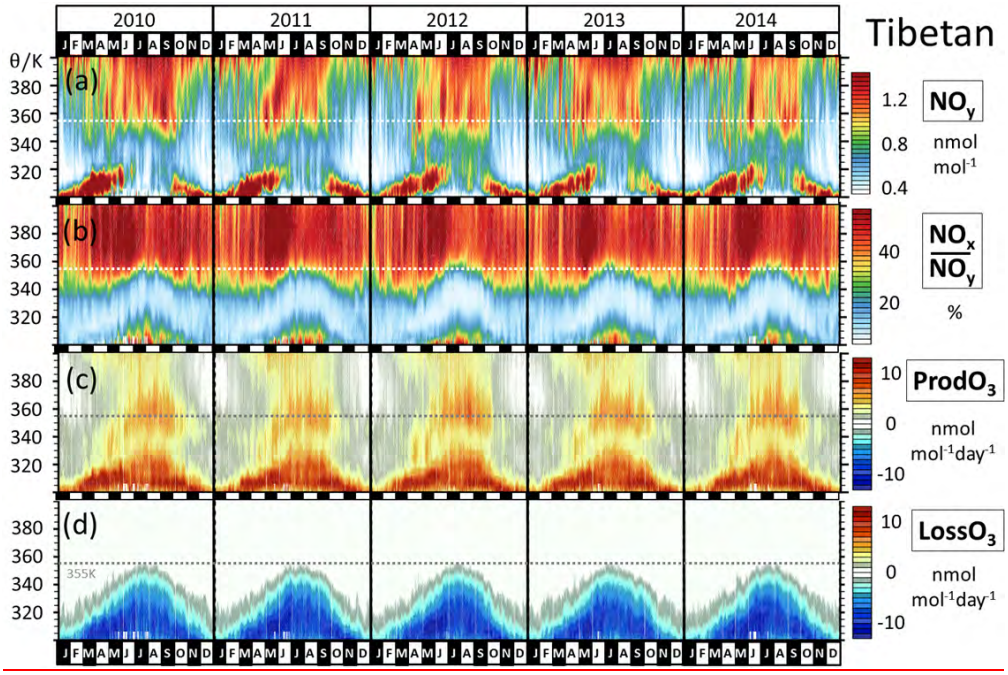
Tibetan
2010
2011
2012
2013
2014
θ/K
(a)
(b)
(c)
(d)
355K
NOy
nmol mol-1
NOx/NOy
%
ProdO3
LossO3
nmol mol-1day-1

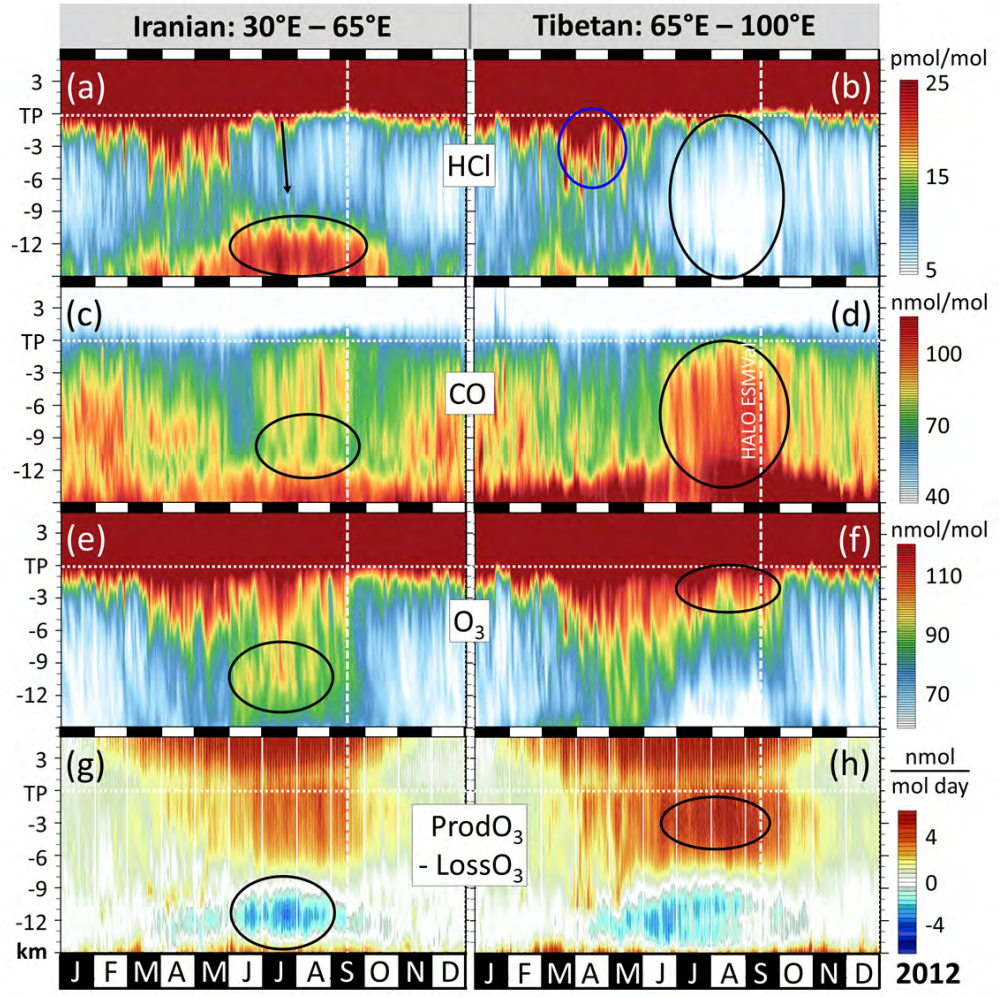

Figure #+S4. ~~Evolution of simulated trace gas profiles and related diagnostics throughout 2012 in the ASMA region. Figure S4 is identical to Fig. 3, except that vertical coordinates are given as distance to the tropopause ("TP") here. Compared to the pressure-based vertical axis' used in Fig. 3, the tropopause region is resolved better here – at the expense of the middle troposphere. All values are grid-cell dry air mass weighted averages from 15°N to 35°N, respectively for the western (30° - 65°E) and eastern (65° - 100°E) parts of the ASMA (see Figs. 1, S1, S2, S3). The features marked by circles and arrows are the same as in Fig. 2 and discussed in the text.~~ As Fig. #+S2, but putting Fig. #+A5 in a multi-annual perspective (Panels a and b). There is no noteworthy anomaly for 2012. Panels (c) and (d) show simulated photochemical O_3 production and destruction separately. $LossO_3$ is negligible at and above 355 K, thus the photochemical regime (NO_x-limited or NO_x-saturated) is determined mainly by $ProdO_3$.

Formatted: Font: Times New Roman, 9 pt
Formatted: Font: Times New Roman, 9 pt
Formatted: Font: Times New Roman, 9 pt, Subscript
Formatted: Font: Times New Roman, 9 pt
Formatted: Font: Times New Roman, 9 pt, Subscript
Formatted: Font: Times New Roman, 9 pt
Formatted: Font: Times New Roman, 9 pt, Subscript
Formatted: Font: Times New Roman, 9 pt
Formatted: Font: Times New Roman, 9 pt, Subscript
Formatted: Font: Times New Roman, 9 pt
Formatted: Font: Times New Roman, 9 pt, Subscript
Formatted: Font: Times New Roman, 9 pt

45

Formatted: Font: 9 pt, Bold

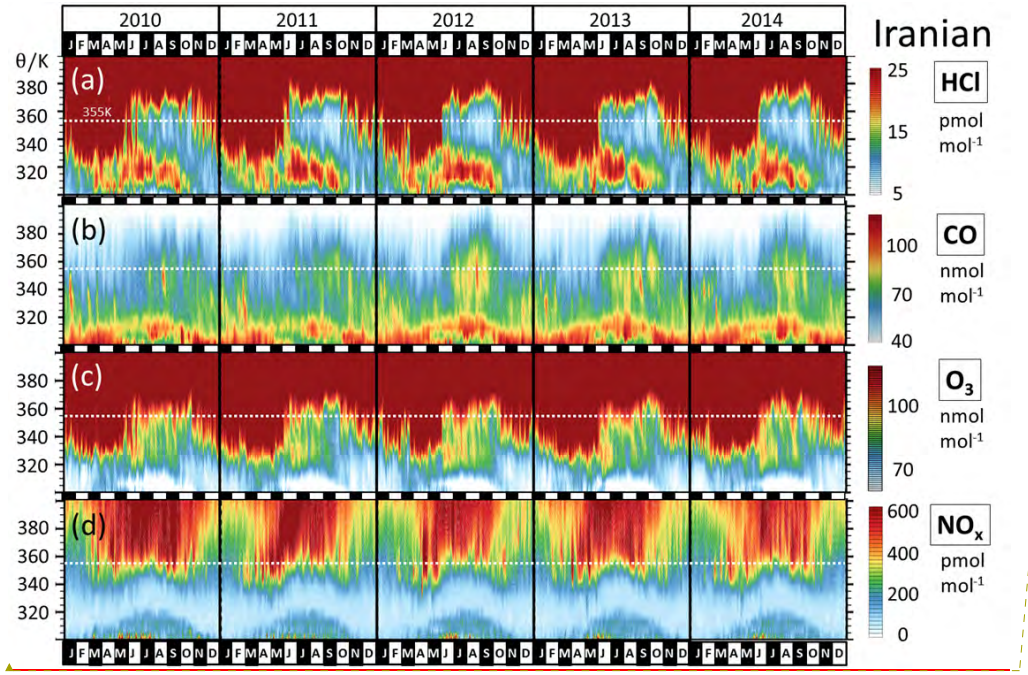

Formatted: Font: 9 pt, Bold

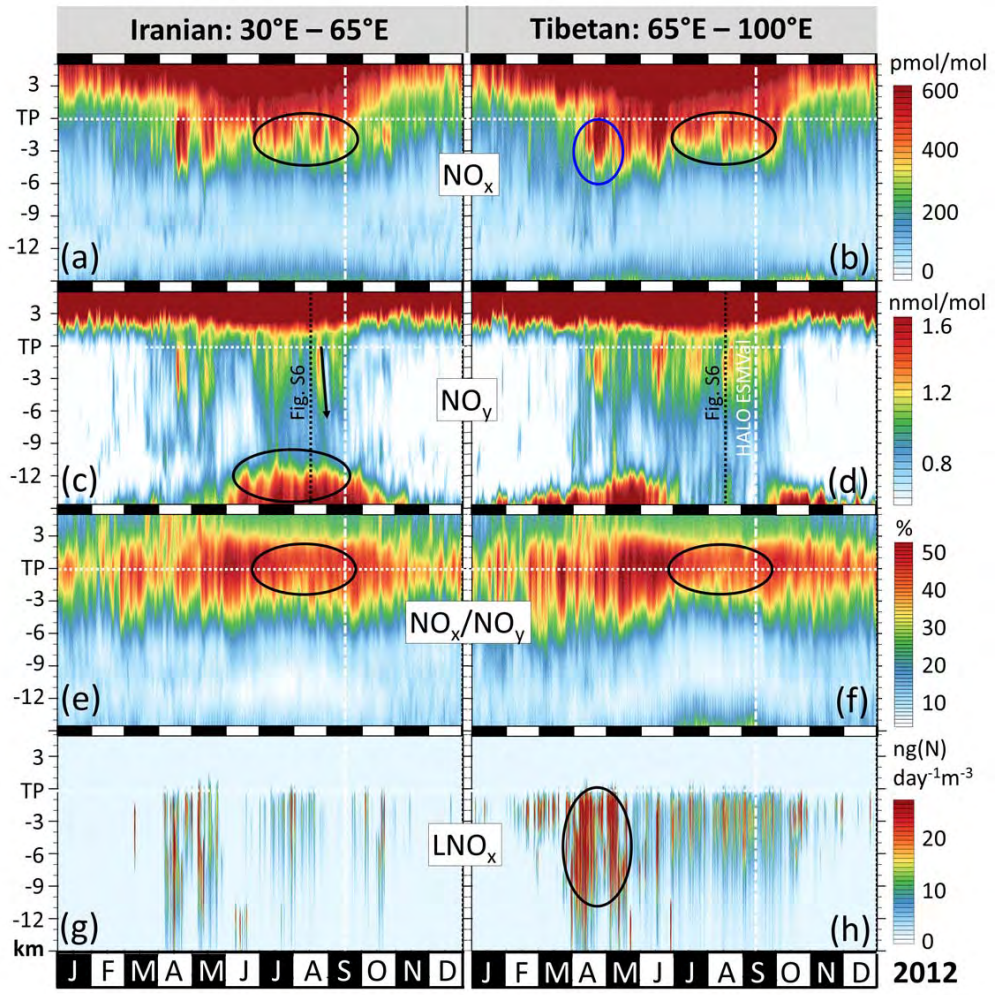

Figure #+S5. As Fig. #+S2, but for the Iranian ASMA region. Of the parameters shown, CO is the most variable one in the UTLS.

Formatted: Font: 9 pt, Bold

Formatted: Font: Times New Roman, 9 pt

Formatted: Font: Times New Roman, 9 pt

~~As Fig. S4, but for different tracers. The individual NO_y profiles shown in Fig. S7 are indicated in panels c and d.~~

Formatted: Line spacing: 1,5 lines

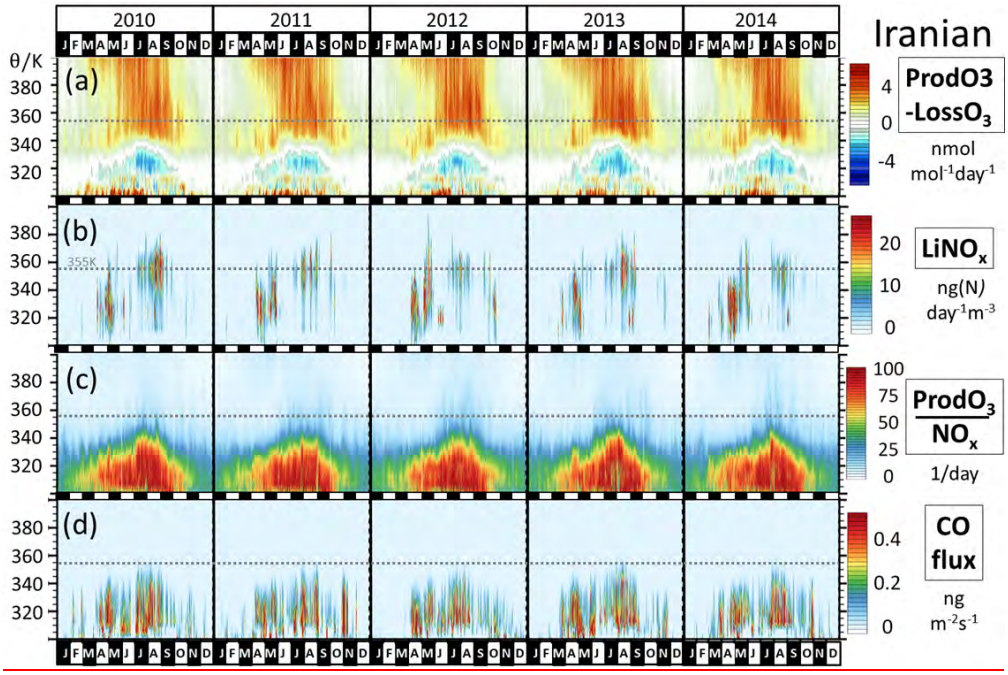
Iranian
2010
2011
2012
2013
2014
θ/K
(a)
(b)
(c)
(d)
355K
ProdO3 -LossO3
nmol mol-1day-1
LiNOx
ng(N) day-1m-3
ProdO3 / NOx
1/day
CO flux
ng m-2s-1

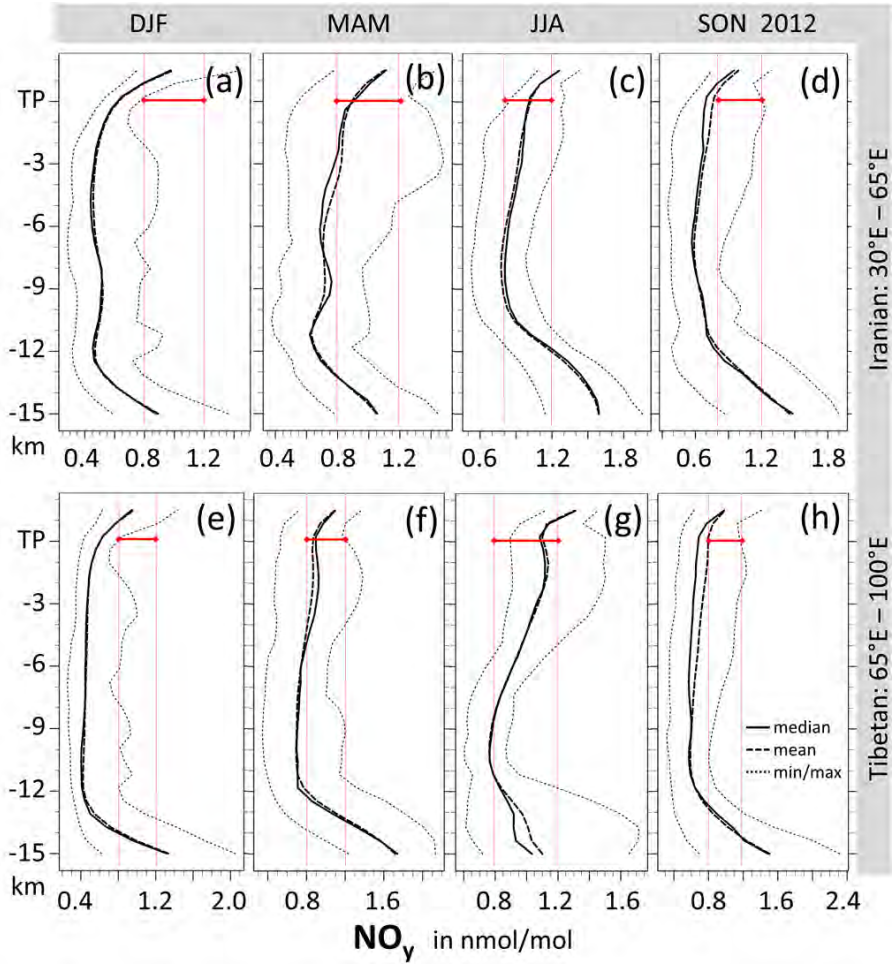

Figure #+S6. As Fig. #+S3, but for the Iranian region. ~~EMAC simulated three-monthly mean NOy profiles in the Iranian and Tibetan regions, respectively. Note that the panels cover different ranges of NOy mixing ratios. Auxiliary red lines always mark the interval 0.8 to 1.2 nmol/mol, as well as the tropopause in that interval.~~

Formatted: Font: Times New Roman, 9 pt

Formatted: Font: Times New Roman, 9 pt

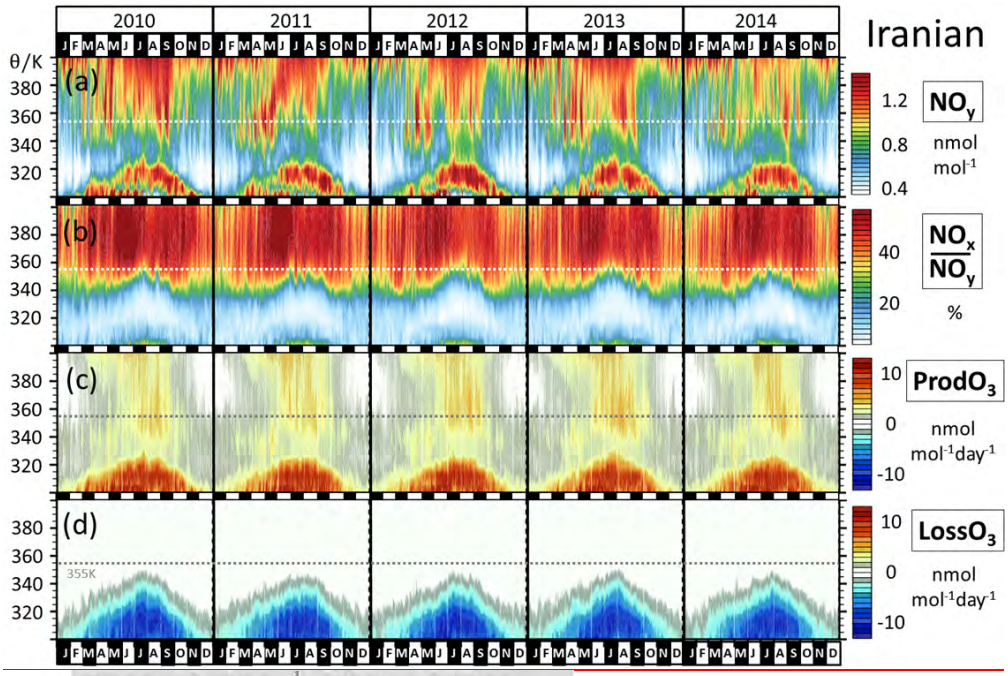

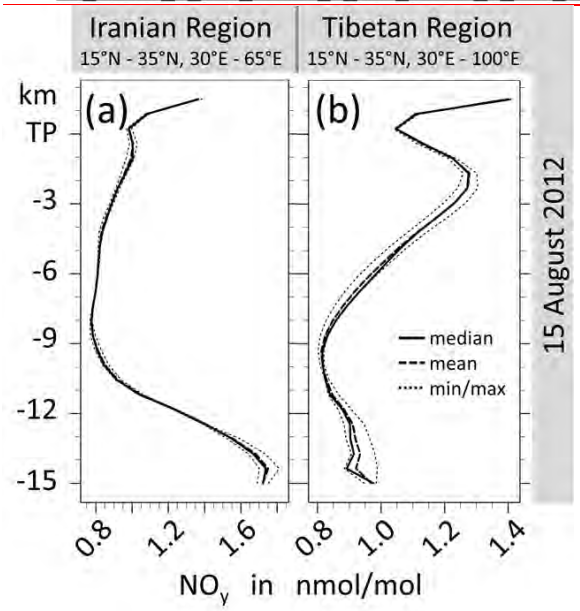

Figure #+S7. As Fig. #+S4, but for the Iranian region.

Formatted: Font: Times New Roman, 9 pt

Formatted: Font: Times New Roman, 9 pt

~~Simulated profiles of NOy as simulated for 15 August 2012. These are examples of a C-shaped profile in the Iranian region (a) and an E-shaped profile in the Tibetan region (b).~~

Formatted: Line spacing: 1,5 lines

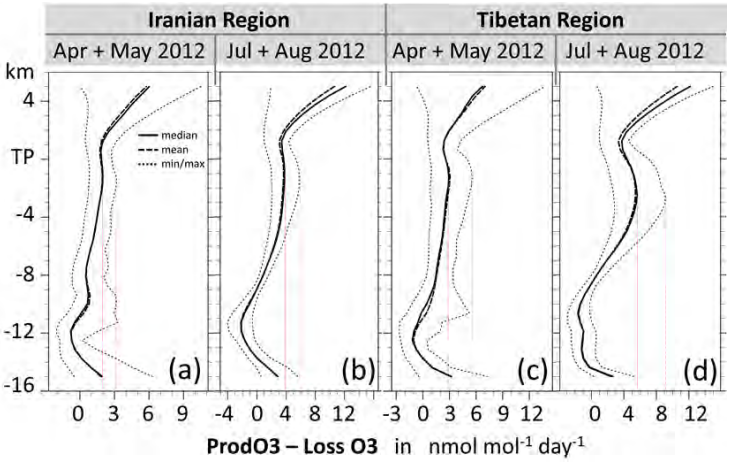

Figure #+S8. Simulated profiles of net O_3 production in the Tibetan region. Auxiliary red lines indicate the mean and maximum net O_3 production in the UT, which are both higher in summer than in spring.

~~See also Fig. S4h for the evolution of these profiles throughout 2012.~~

Comment [KG1]: revise referencing

Formatted: Line spacing: 1,5 lines

Formatted: Font: Bold

Formatted: Font: 9 pt

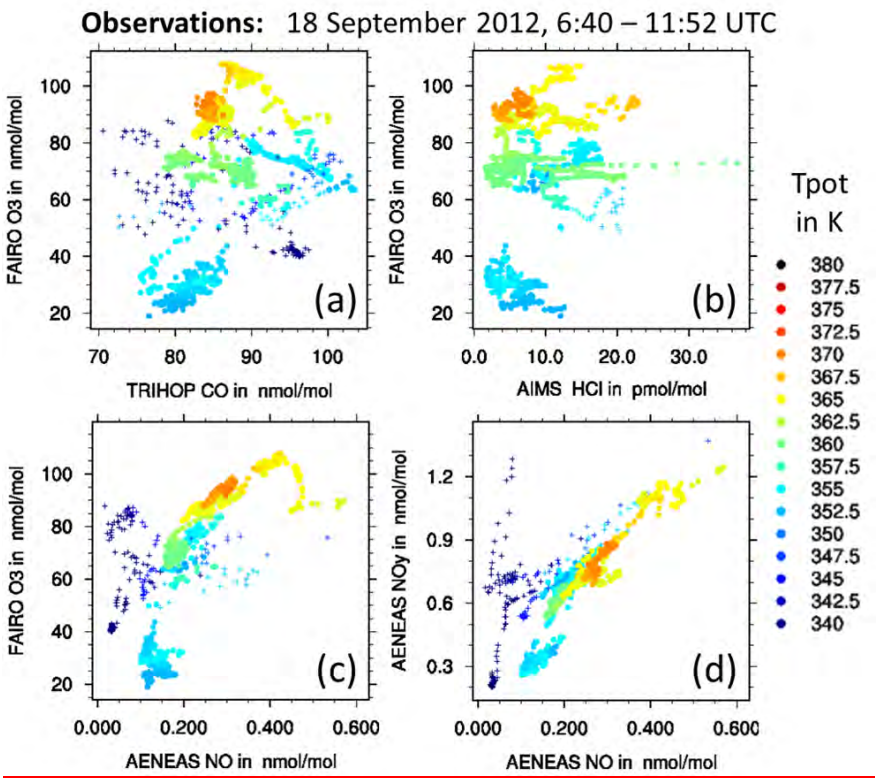

71
72
73 **Figure #+S9. Measured data from the HALO ESMVal flight from Male to Larnaca. In contrast to Figs. #+6cf, #+A7cf**
74 **the samples here are color coded by their potential temperatures. During the dive (HALO descended from the upper**
75 **to the lower troposphere and back to obtain profiles; indicated by crosses) potential temperatures were lower than**
76 **shown, but the color scale is cut off at 340 K.**

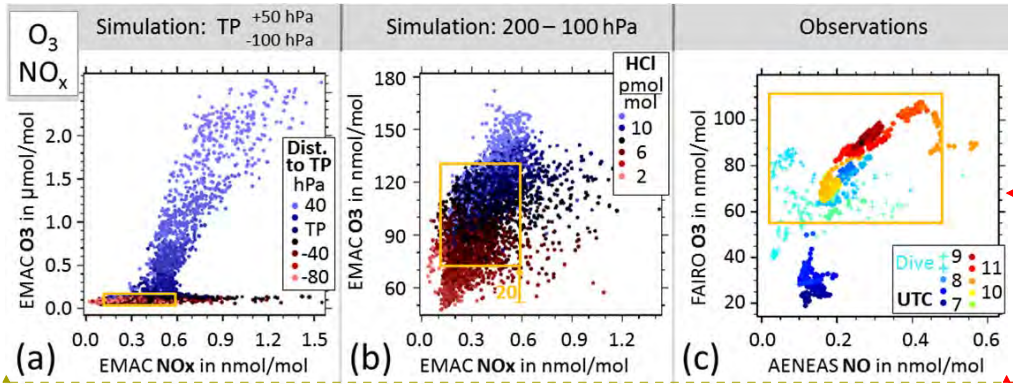

77
78 ~~**Figure S9. As Fig. 3, but for NO_x vs O_3. Panel (c) shows NO instead of NO_x, because only NO was measured. At**~~
79 ~~**daytime, i.e. at the time of the measurements, NO is good proxy for NO_x. Simulated O_3 and NO_x increase in the**~~
80 ~~**stratosphere with a higher O_3/NO_x ratio than in the troposphere (Fig. S9a). At NO_x mixing ratios of more than 0.7**~~
81 ~~**nmol/mol the corresponding O_3 mixing ratios would allow distinguishing stratospheric influence from tropospheric in**~~
82 ~~**situ production, but the range covered by the HALO ESMVal measurements is just at the intersection of stratospheric**~~

Formatted: Font: Times New Roman, 9 pt
Formatted: Font: Times New Roman, 9 pt
Formatted: Font: Times New Roman, 9 pt
Formatted: Font: Times New Roman, 9 pt
Formatted: Font: 9 pt
Formatted: Line spacing: 1,5 lines
Formatted: Font: 9 pt

~~and tropospheric branch (orange box in Fig. S9a). Similar HCl mixing ratios are simulated throughout the ranges of measured NO_x and O_3 (orange box in Fig. S9b). Measurements of increased NO_x in combination with increased O_3 (upper right corner of the orange boxes in Fig. S9) are compatible with both, increased in situ O_3 production and influence from the stratospheric branch. Consequently almost all measurements in the ASMA filament are well correlated on the scale of all our ASMA measurements (Fig. S9c). As discussed in the accompanying paper, the positive correlation between NO and O_3 is attributed to enhanced O_3 production due to increased NO, if NO also positively correlates with NO_y.~~

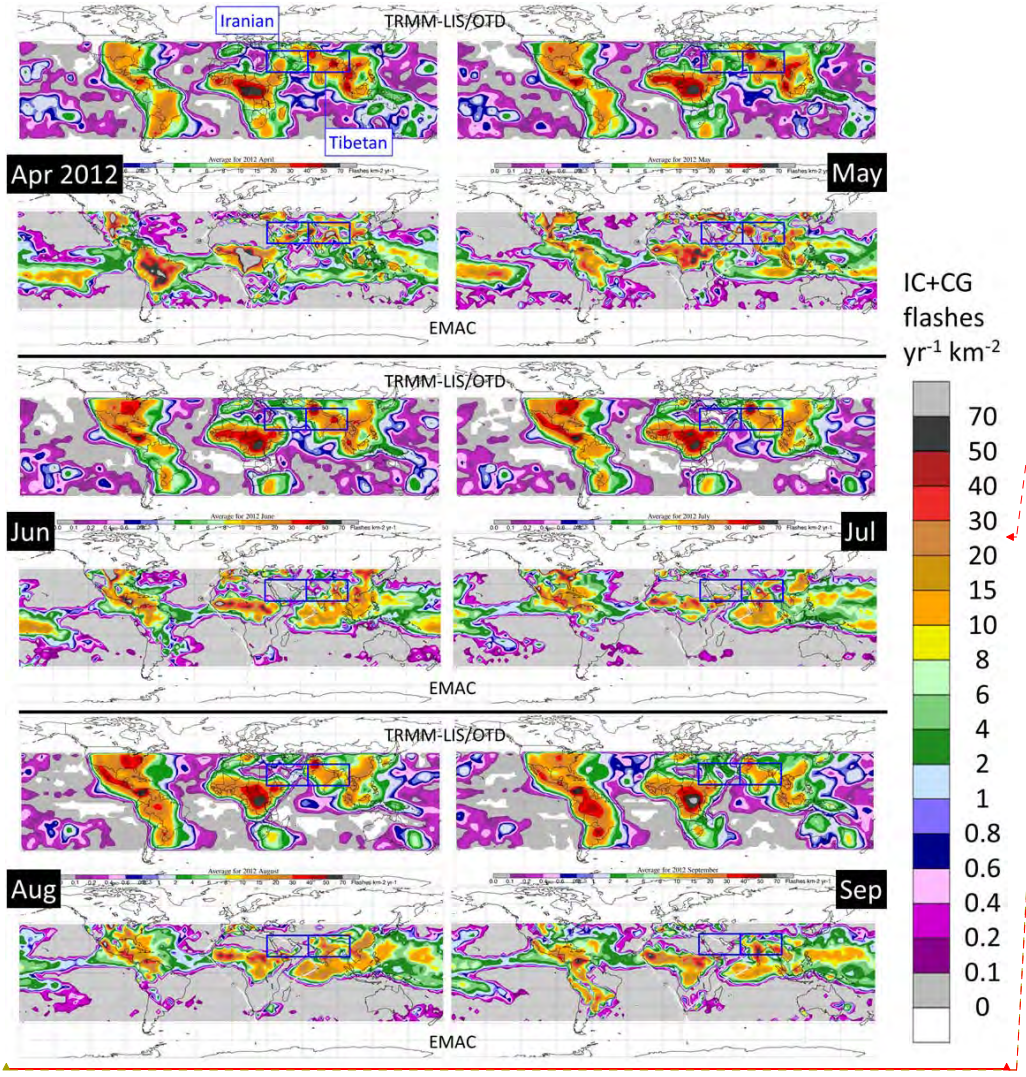

Formatted: Font: 9 pt

Formatted: Font: 9 pt

Formatted: Font: 9 pt

Formatted: Line spacing: 1,5 lines

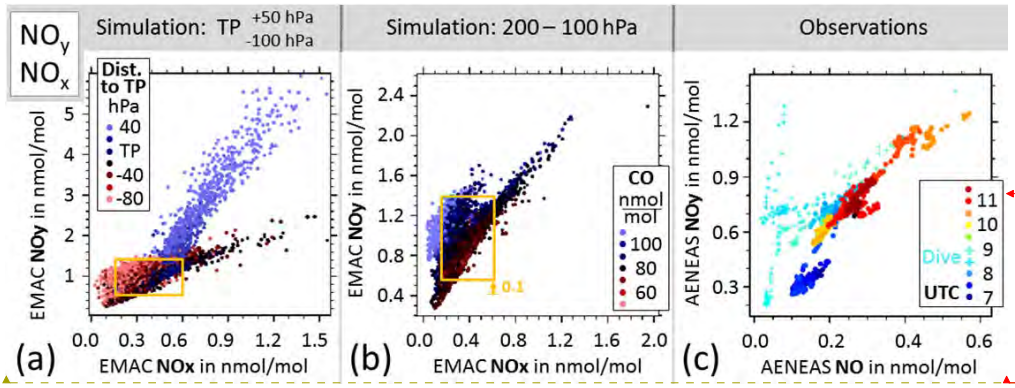

Figure #+S10. EMAC-simulated monthly mean lightning activity (intra-cloud + cloud-to-ground flash frequency) compared to the corresponding TRMM-LIS/OTD observations (Cecil, 2006)~~(Cecil, 2006)~~. Data coverage and color scale are determined by the observations. Simulated lightning appears to be more localized, and thus exceeds the scale more often.

Convection is not explicitly resolved in the simulation, and the parameterizations for convection and lightning both introduce uncertainties to the simulation results for lightning. Uncertainties in the observations are due to a space- and time-dependent detection limit of 69% to 88%, and the application of a 3 month smoothing. Considering those uncertainties, the match between simulated and observed global distribution and frequency of lightning activity is reasonable.

Formatted: Font: 9 pt
Formatted: Line spacing: 1,5 lines
Formatted: Font: 9 pt
Formatted: Font: Times New Roman, 9 pt
Formatted: Font: 9 pt
Formatted: Font: Times New Roman, 9 pt
Formatted: Font: 9 pt
Field Code Changed
Field Code Changed
Formatted: Font: Times New Roman, 9 pt
Formatted: Font: 9 pt
Formatted: Font: Times New Roman, 9 pt
Formatted: Font: Times New Roman, 9 pt

Formatted: Line spacing: 1,5 lines

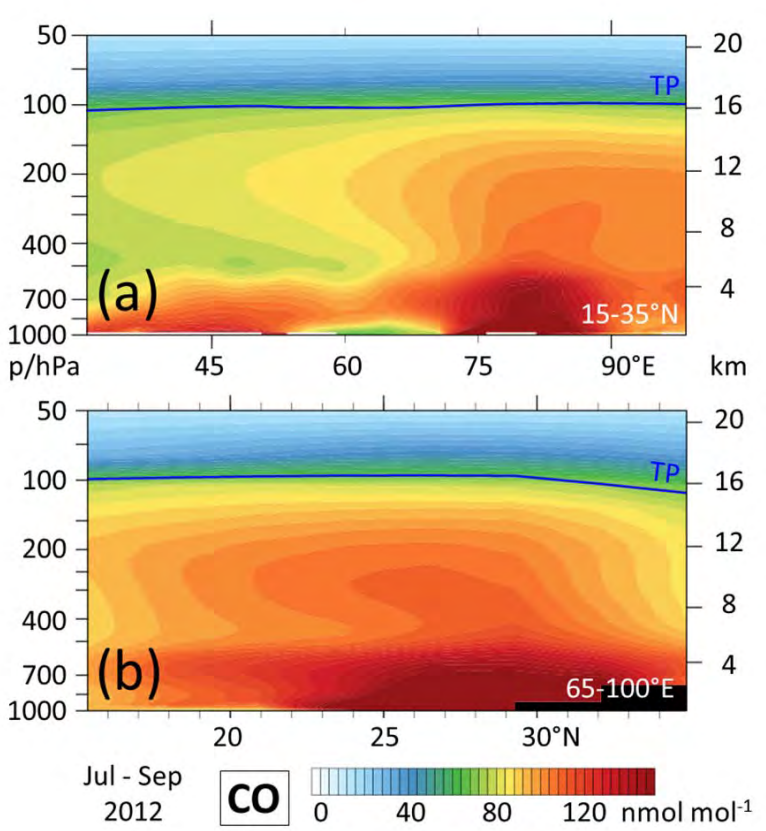

Figure #+S11. EMAC-simulated three-month mean curtains of CO mixing ratios: (a) Covering Iranian and Tibetan parts, meridional mean; (b) Tibetan part, zonal mean. On average, the hotspot of ascending CO in our simulation is located at about 29°N, 80°E, corresponding to the south-western flank of the Himalayas.

~~As Fig. S9, but for NO_x vs NO_y. There are three distinct regions in Fig. S10a: a blueish stratospheric branch, a dark TL branch, and a reddish UT region. As a consequence of the local NO_y minimum directly above the tropopause (Figs. 2d, S5, S7), the most decreased NO_y mixing ratios in Fig. S10a also show up in samples taken from near the tropopause. Measured NO and NO_y values in the ASMA filament are well correlated (Fig. S10c), consistent with almost constant NOx/NOy ratios in the UT (Figs 2ef). Furthermore, the simulation shows much more scatter in NO_x- vs O_3 space than the observations. The narrow, linear distribution of the ASMA measurements in Figs. S9c and S10c indicates that all parts of the transected filament had similar sources of reactive nitrogen. This is consistent with Appendix A, where lightning is found to be the dominating source of reactive nitrogen in the ASMA. In the accompanying study is also shown that the filament had seen convection at the eastern ASMA flank three to five days before the measurements. Thus the gradients of NO and NO_y in Fig. S9c and Fig. S10c can be explained by different amounts of lightning NO_x of approximately the same age.~~

Formatted: Line spacing: 1,5 lines

Formatted: Font: Bold

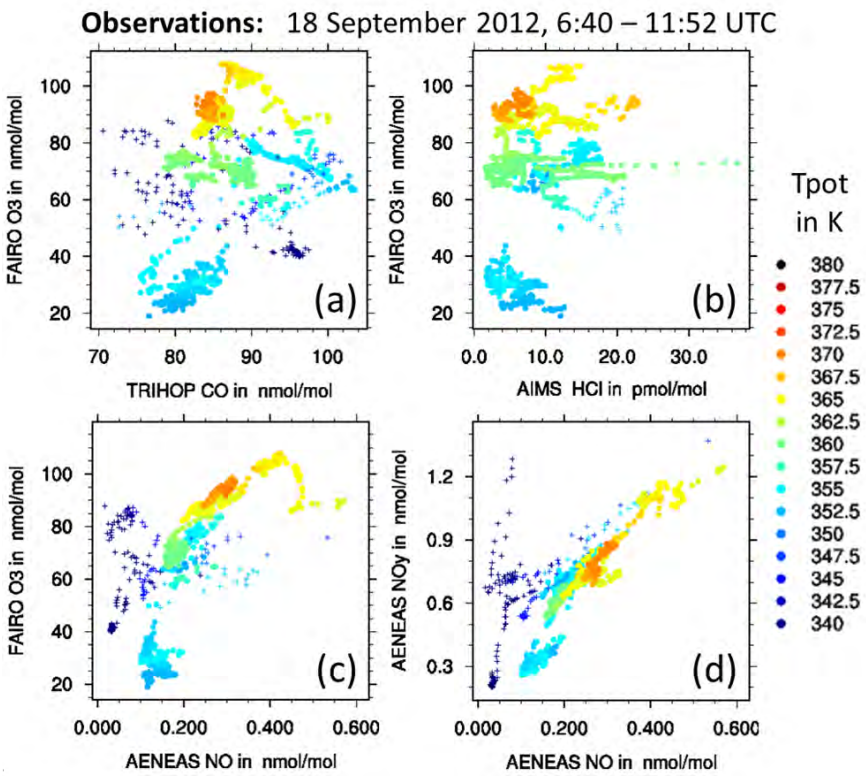

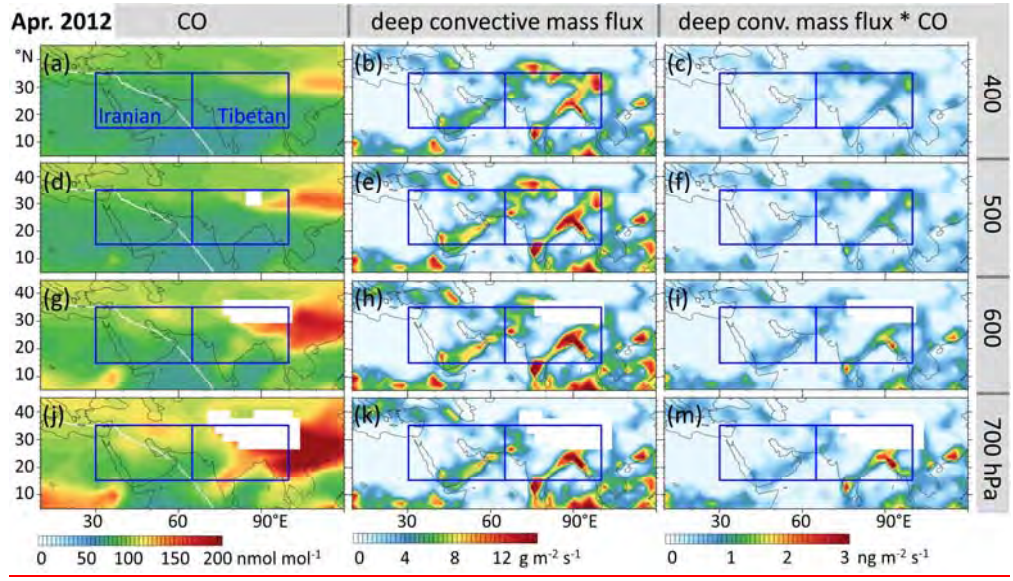

Figure ~~S11#+S12~~. EMAC-simulated monthly mean distributions of CO (left) and deep convective mass flux (middle) in different pressure altitudes during spring (April 2012). The right column shows the deep convective mass flux of CO based on individual output steps. Blue rectangles mark the outline of the regions used to produce Figs. #+3 and

Formatted: Font: 9 pt, Bold

Formatted: Font: Times New Roman, 9 pt

Formatted: Font: Times New Roman, 9 pt

Formatted: Font: Times New Roman, 9 pt

~~#+4. Panels a, b, c, d show measured data from the HALO ESMVal flight from Male to Larnaca as Figs. 4c, 5c, S9c, S10c, respectively. The only difference is that the samples here are color coded by their potential temperatures. During the dive (POI4: crosses) potential temperatures were lower than shown, but the color scale is cut off at 340 K. See also Figs. S12 and S13 for simulated potential temperatures in the ASMA region.~~

Formatted: Line spacing: 1,5 lines

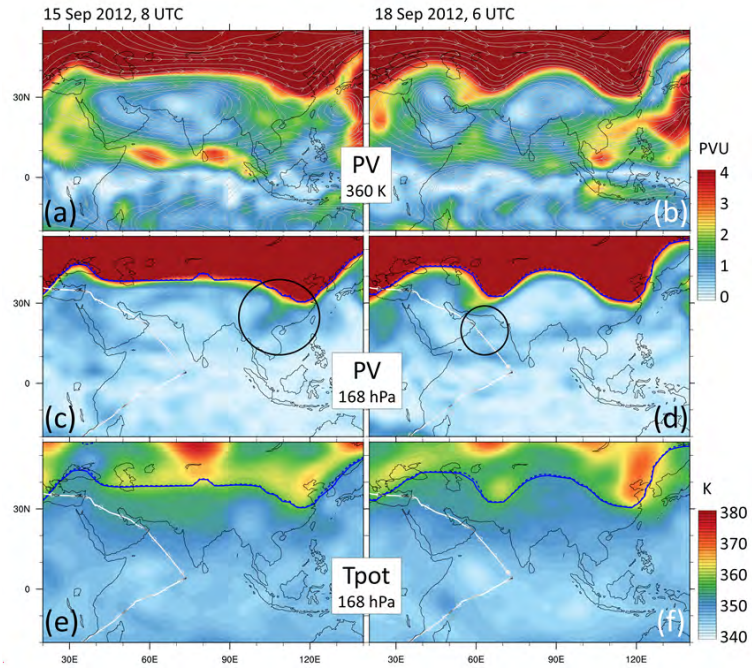

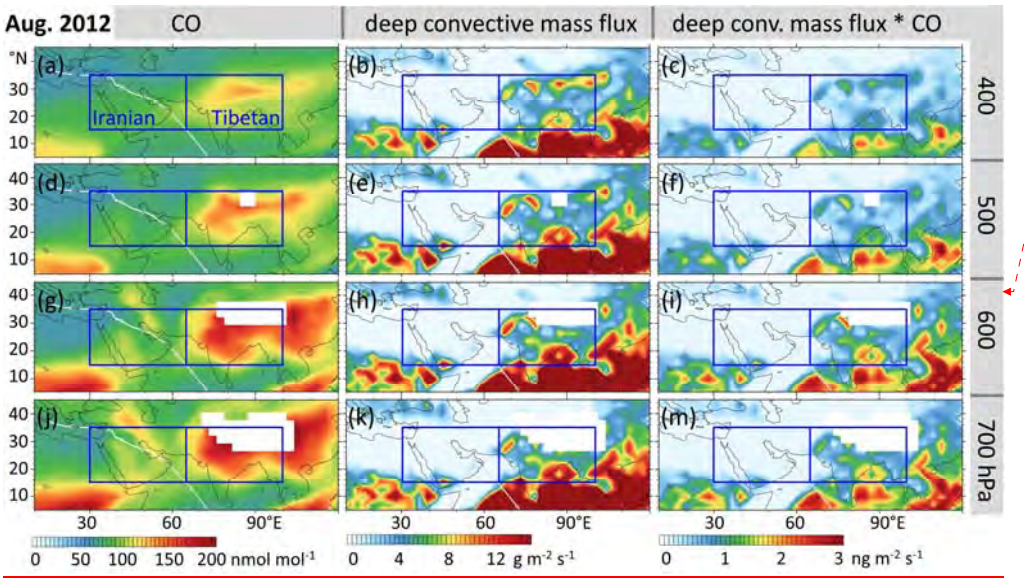

Figure ~~S12#+S13~~. As Fig. #+S12, but for August 2012, i.e. during the monsoon season.

~~EMAC simulated potential vorticity at the 360 K isentropic level (panels a, b) and the 168 hPa pressure level (panels c, d). The black circle in panel c shows the entrainment of TL air, which occurred when the air mass corresponding to POI3 was passing the eastern ASMA flank. Panels b, d, f show simulated snapshots 2 hours before POI3, with the region of POI3 marked in panel d. The corresponding potential temperatures are shown in panels e and f. Note that TL layer entrainments are visible in PV, but are hardly detected by Tpot.~~

Formatted: Line spacing: 1,5 lines

Formatted: Font: Times New Roman, 9 pt

Formatted: Font: Times New Roman, 9 pt

Formatted: Line spacing: 1,5 lines

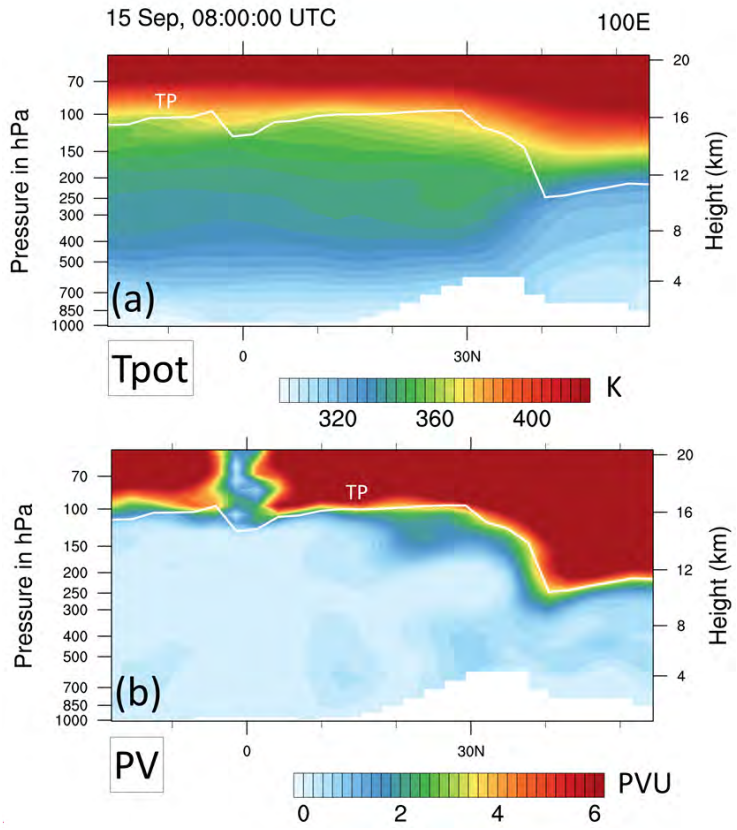

Figure S13. EMAC simulated potential temperature and potential vorticity in curtains at 100°E, at the time when the air corresponding to POI3 was passing there at about 165 hPa. Note the steeply inclining TP over the Tibetan plateau, which marks the transition from the extratropics (dominated by baroclinic wave activity and downward stratospheric circulation) to the tropics (dominated by radiative-convective balance and upward stratospheric circulation). North of 30°N the EMAC TP is defined by the 3.5 PVU isocontour. Isentropes intersect the inclining TP, thereby allowing cross-TP transport without leaving a tell-tale signature of increased Tpot in the corresponding air masses in the tropics. This includes the 350 – 370 K isentropes, that were encountered during the HALO ESMVal campaign in the tropics (see also Figs. S11, S12).

Formatted: Line spacing: 1,5 lines

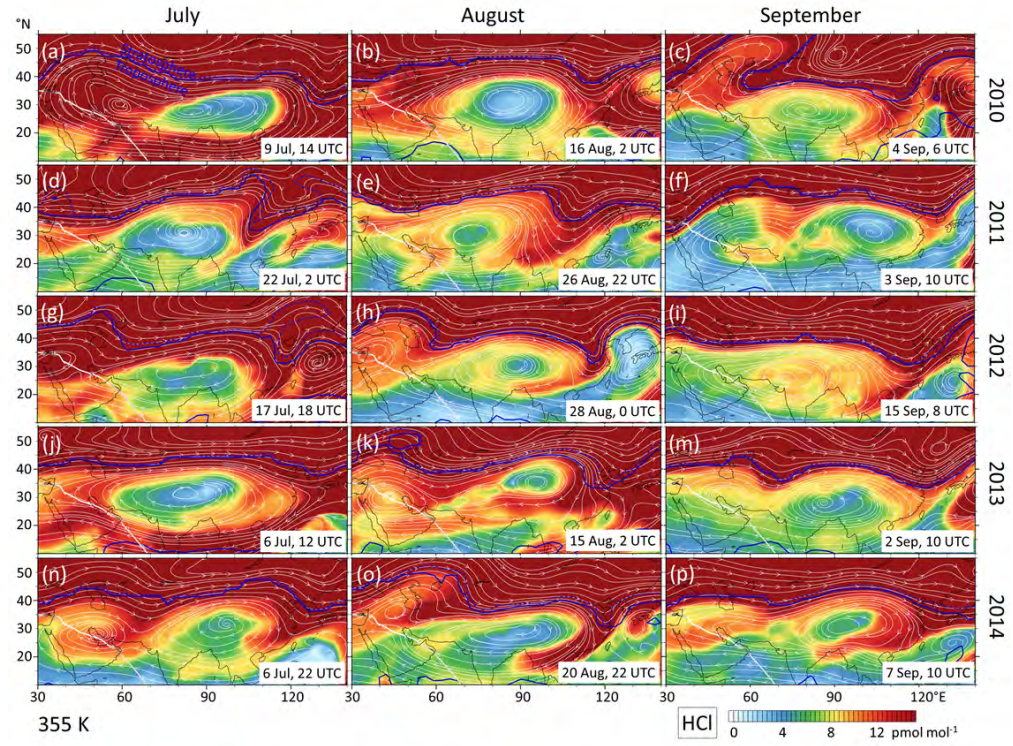

154

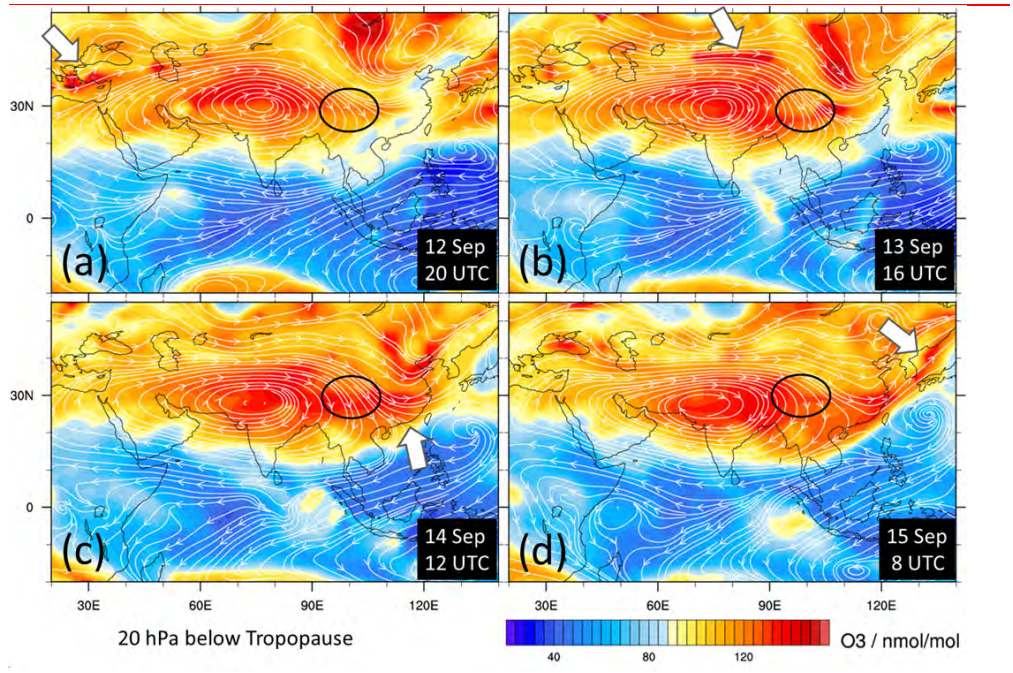

155

156 **Figure S1#+S144. EMAC simulated HCl mixing ratios at 168 hPa in the ASMA region, complementing Fig. #+7. The**

157 **snapshots were selected to represent independent situations, where the southern ASMA fringe is marked by a**

Formatted: Line spacing: 1,5 lines

Formatted: Font color: Auto

filament of enhanced HCl. The filaments are often associated with a TP trough at the eastern ASMA flank. Enhanced HCl serves as a proxy for TL or stratospheric air.

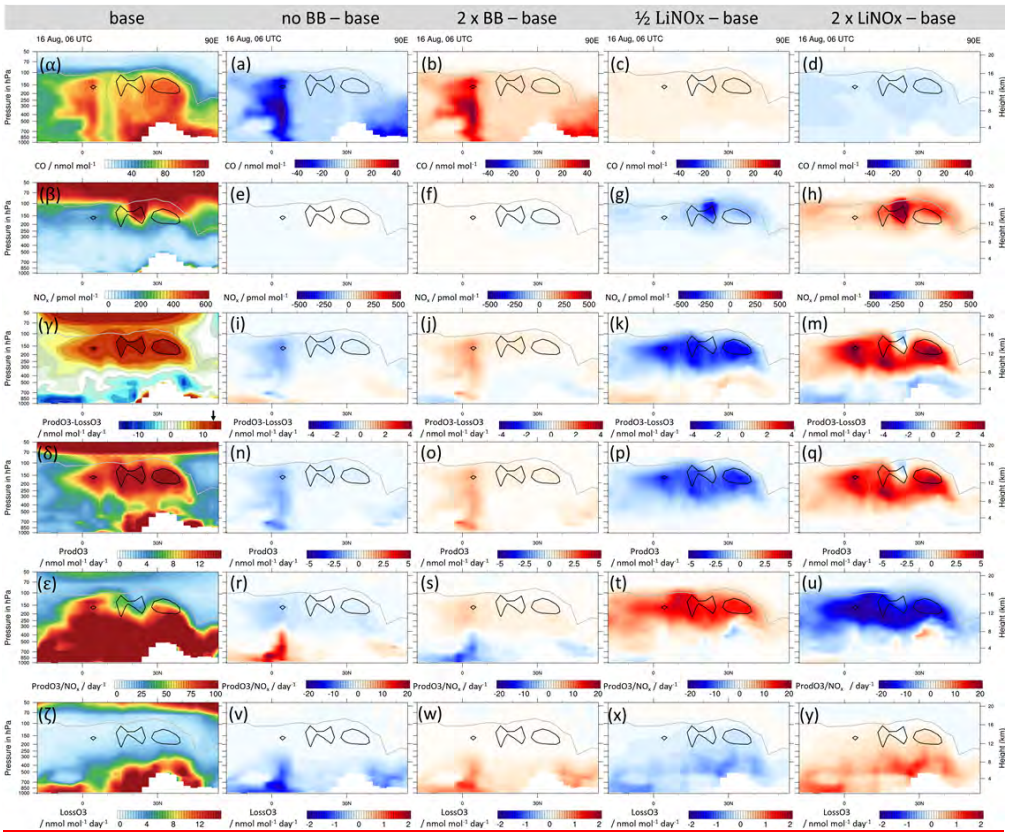

~~Sequence of O_3 mixing ratios in the ASMA region and streamlines as simulated by EMAC for a layer 20 hPa below the tropopause. This layer was chosen to illustrate O_3 variations and transport just below the TP. EMAC tropopause height varies spatially and temporally, as it is diagnosed each time step, according to the WMO definition between 30°S and 30°N, and by PV = 3.5 PVU otherwise. Note that the layer may not, or may only partially show altitudes that contributed to the HALO measurements. The streamlines are based on instantaneous wind fields and thus not identical to backward trajectories. Grey arrows indicate a pocket of increased O_3, which originated in the tropopause folding region over the Eastern Mediterranean. It is picked up by the ASMA circulation and transported along the northern ASMA flank. The pocket passes the eastern ASMA flank before the time (last panel), when the air mass to be encountered by HALO arrived there (region indicated by black circles). However, a part of the increased O_3 patch might have been entrained in the divergent flow there, diverted away from the TP and carried along the southern ASMA flank back east.~~

Formatted: Font: 9 pt, Bold

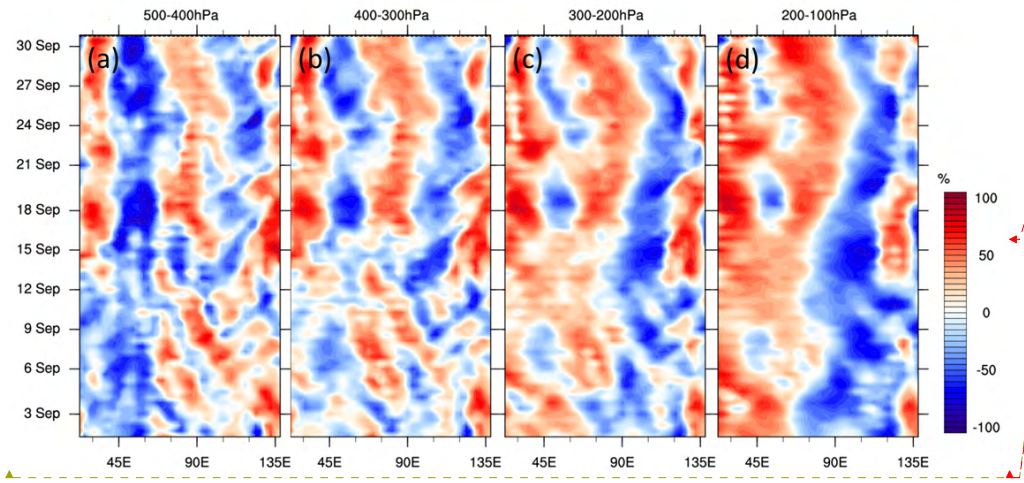

Figure #+S15. Selection of parameters related to photochemical O_3 production in a meridional curtain through the Tibetan part of the ASMA in a snapshot taken mid August 2012. The left column shows the results of the EMAC QCTM simulation that has been introduced in appendix A. The other columns show the difference of that reference to sensitivity simulations, which feature identical dynamics but differ in biomass burning (BB) and lightning NO_x (LiNOx) emissions. The black lines represent the 13 nmol mol^{-1} day^{-1} isocontour of net O_3 production (taken from panel γ), the grey line denotes the tropopause.

Formatted: Font: 9 pt, Bold

Formatted: Line spacing: 1,5 lines

Formatted: Font: 9 pt, Bold

Formatted: Font: Times New Roman, 9 pt

Comment [KG2]: JP3: I thought the QCTM reference was also with daily BB emissions??? But maybe I do not remember correctly.

KG: This refers to the difference between the QCTM reference simulation ("base") and the corresponding QCTM sensitivity simulations (here: no BB, 2 x BB). No ESCiMo simulation was analyzed for this figure.

Formatted: Font: Times New Roman, 9 pt

Formatted: Font: Times New Roman, 9 pt

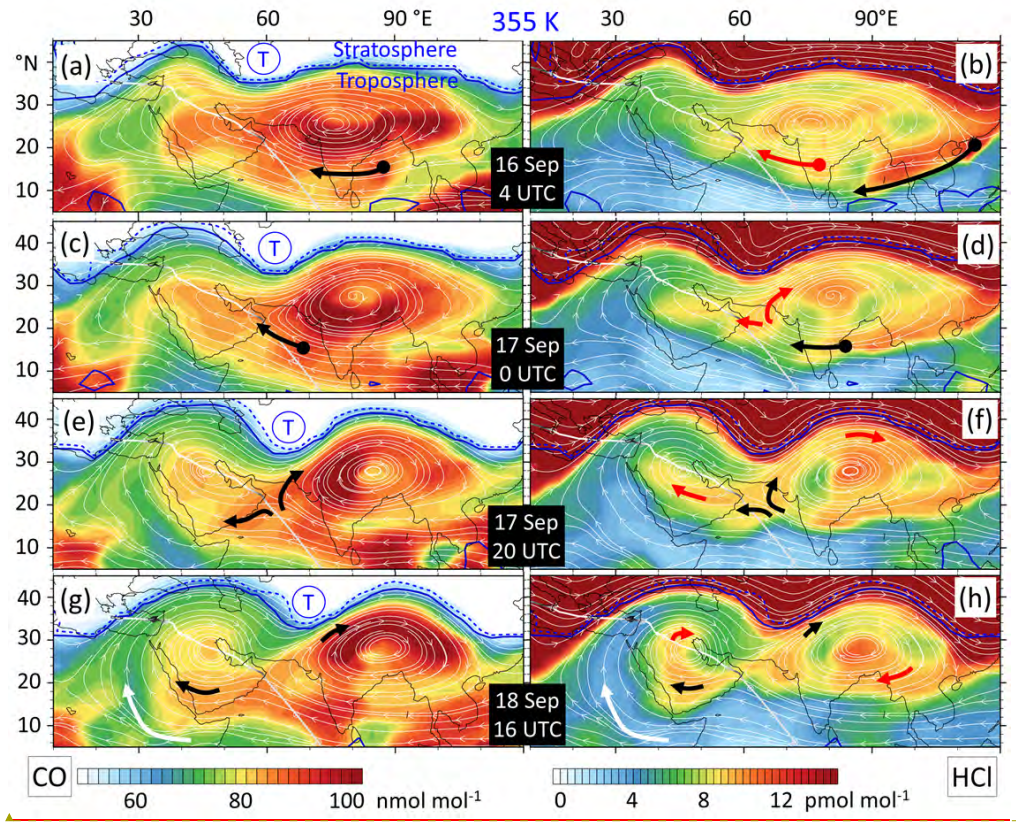

Figure #+S16. Sequence simulated tracer fields at 355 K, illustrating the stirring associated with the splitting-up event of the ASMA that occurred during the HALO ESMVal campaign in September 2012. Streamlines represent instantaneous wind fields, and arrows highlight the redistribution of selected air masses. CO mainly originates in the ASMA interior and HCl serves as a proxy to track the ASMA fringe.

The sequence starts with an elongated anticyclone on 16 September 2012. Then a tropopause trough (T) evolves from the west along the northern ASMA flank. The anticyclone succumbs to the perturbation and splits up into a Tibetan and an Iranian part, shortly after the HALO flight from Male to Larnaca had passed through. A part of the increased CO interior region is entrained by the outer streamlines of the Iranian part, while the rest of the patch is diverted into the interior of the Tibetan anticyclone (black arrows in the left panels). The evolution of freshly entrained HCl (black arrows) and an older patch (red arrows) are shown in the right panels. We also note entrainment of tropospheric air by southerly winds at the western flank (white arrows).

~~**Figure S15. Evolution of meridional wind fraction, as averaged over 10°N – 40°N and the respective altitude range. The results are based on 10-hourly output of EMAC simulation RC1SD-base-10a for September 2012 in the ASMA region. Weighting considers the dry air mass in the cell, and completely or partly stratospheric cells are ignored. At a given time, each red-blue pair (from left to right) represents an anticyclone, because positive values indicate overall northward meridional wind fractions. Blue shades represent mainly southward wind fractions.**~~

Formatted: Font: Times New Roman, 9 pt

Formatted: Line spacing: 1,5 lines

Formatted: Font: Times New Roman, 9 pt

Formatted: Font: Times New Roman, 9 pt

Formatted: Font: Times New Roman, 9 pt, Font color: Auto

Formatted: Font: Times New Roman, 9 pt

Formatted: Font: 9 pt, Bold

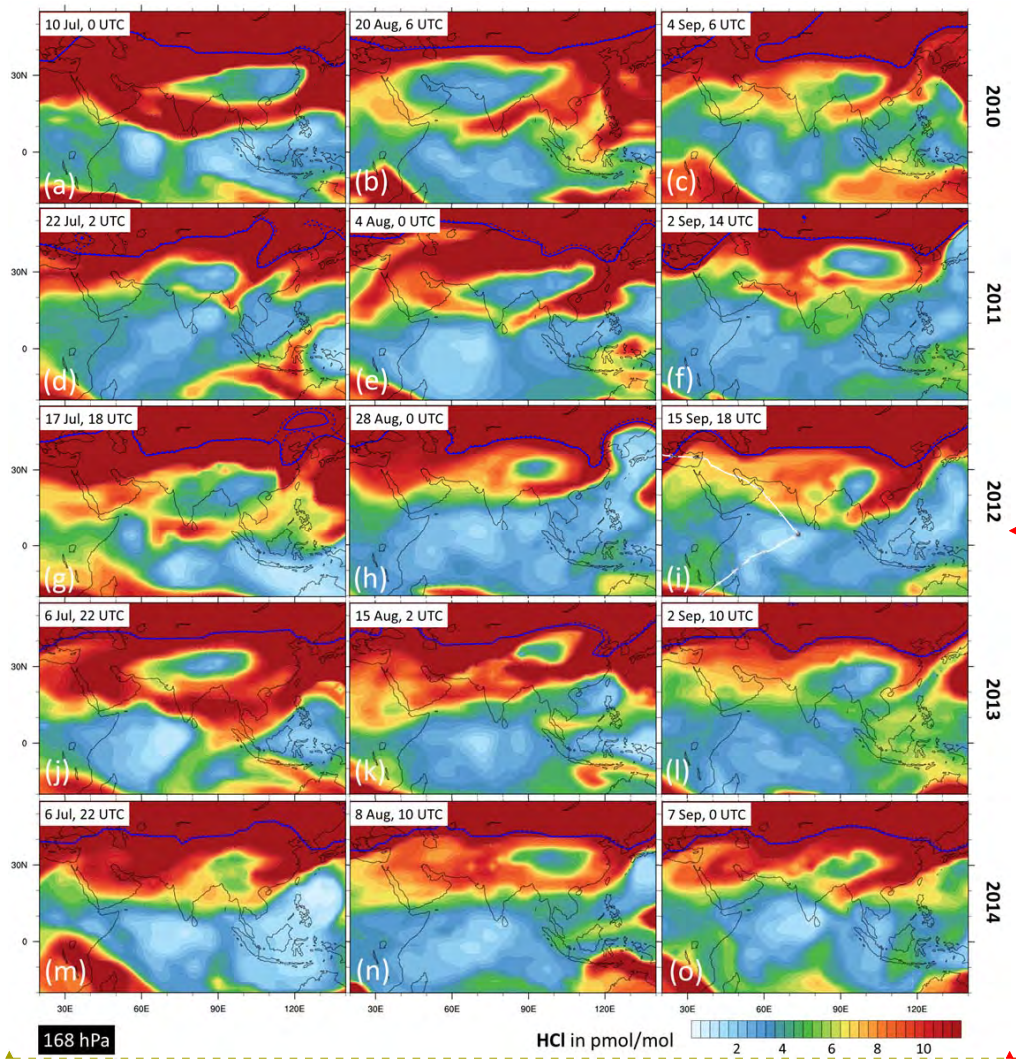

Figure S16. EMAC simulated HCl mixing ratios at 168 hPa in the ASMA region, complementing Fig. 6. The snapshots were selected to represent independent situations, where the southern ASMA fringe is marked by a filament of enhanced HCl. The filaments are often associated with a TP trough at the eastern ASMA flank. Enhanced HCl serves as a proxy for TL or stratospheric air.

Formatted: Font: 9 pt, Bold

Formatted: Line spacing: 1,5 lines

Formatted: Font: 9 pt, Bold

Formatted: Font: 9 pt, Bold

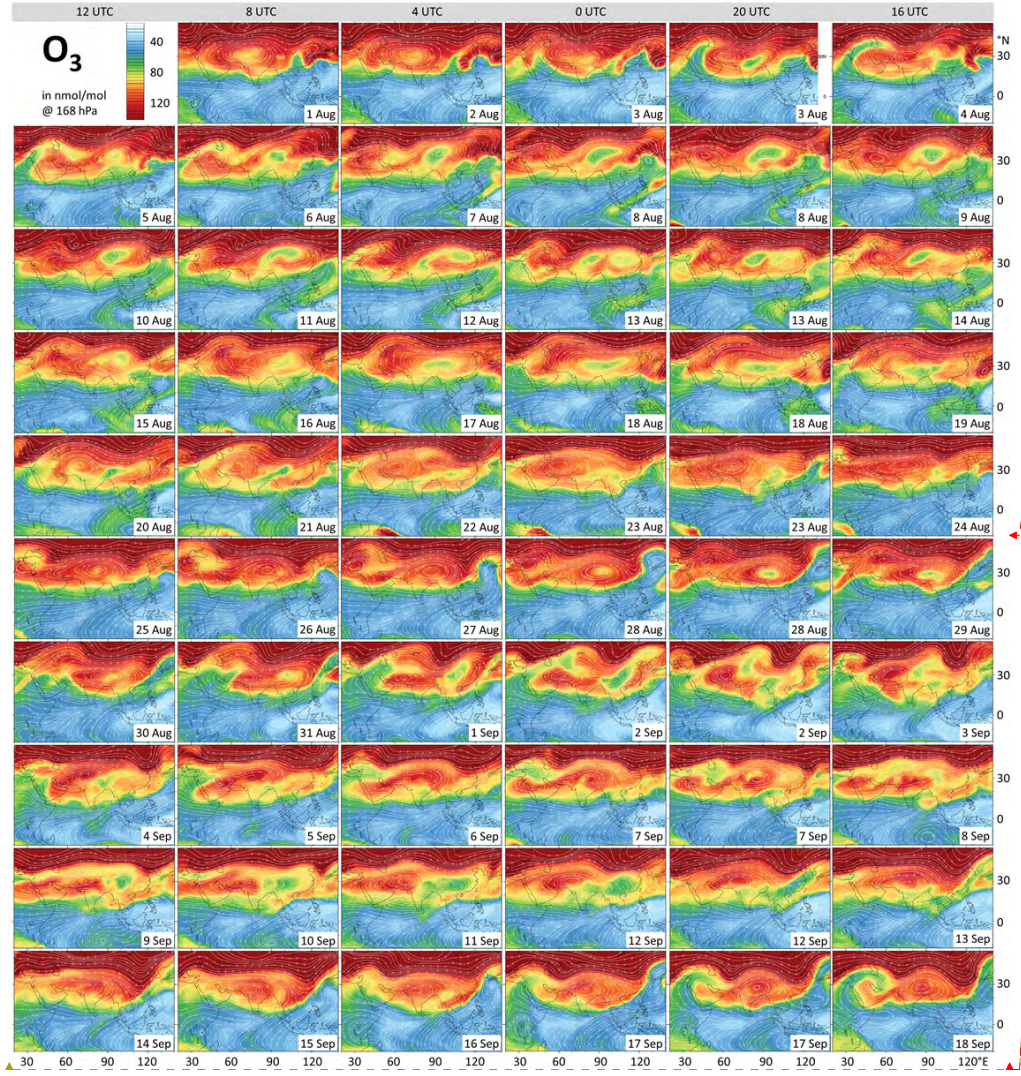

Figure S1#+S17. EMAC simulated O_3 mixing ratios and streamlines at 168 hPa in the ASMA region. The snapshots are 20 hours apart and cover the period from 1 August to 18 September 2012.

Larger fractions of the O_3-rich fringe were entrained during splitting up events. The sequence of snapshots (Fig. #+S17) covers almost half a monsoon season and episodic O_3-poor upwellings over the Tibetan plateau are smaller and shorter lived than O_3-rich regions at 168 hPa. This is consistent to the long-term average at a corresponding isentropic level (Fig. #+S1i).

Formatted: Font: 9 pt, Bold

Formatted: Line spacing: 1,5 lines

Formatted: Font: 9 pt, Bold

Formatted: Font: Times New Roman, 9 pt

Formatted: Font: Times New Roman, 9 pt

Formatted: Line spacing: 1,5 lines

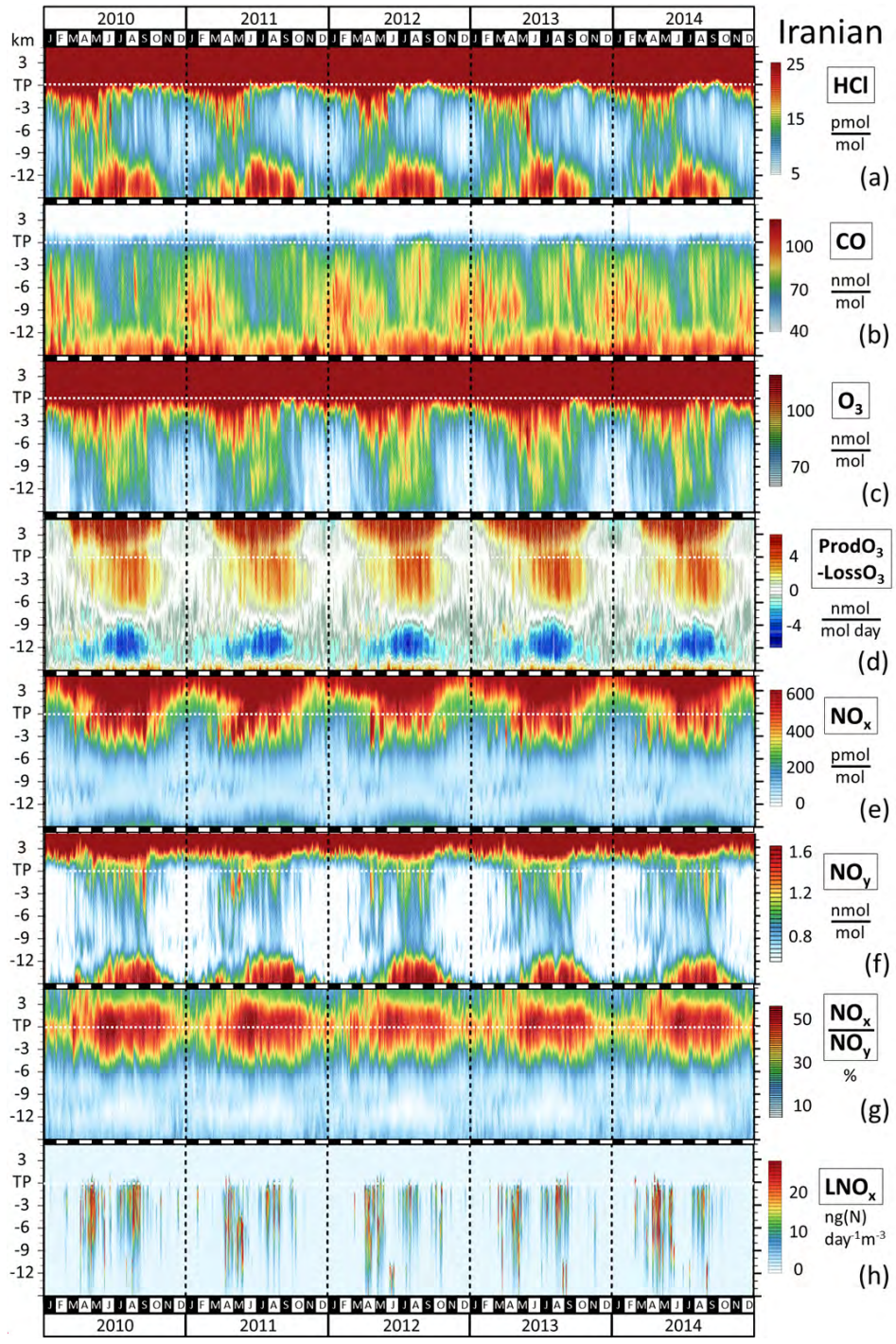

Figure S18. Evolution of simulated trace gas profiles and related diagnostics for the years 2010 - 2014 in the Iranian ASMA region. The column for the year 2012 is identical to the corresponding panels in Figs. S4, S5.

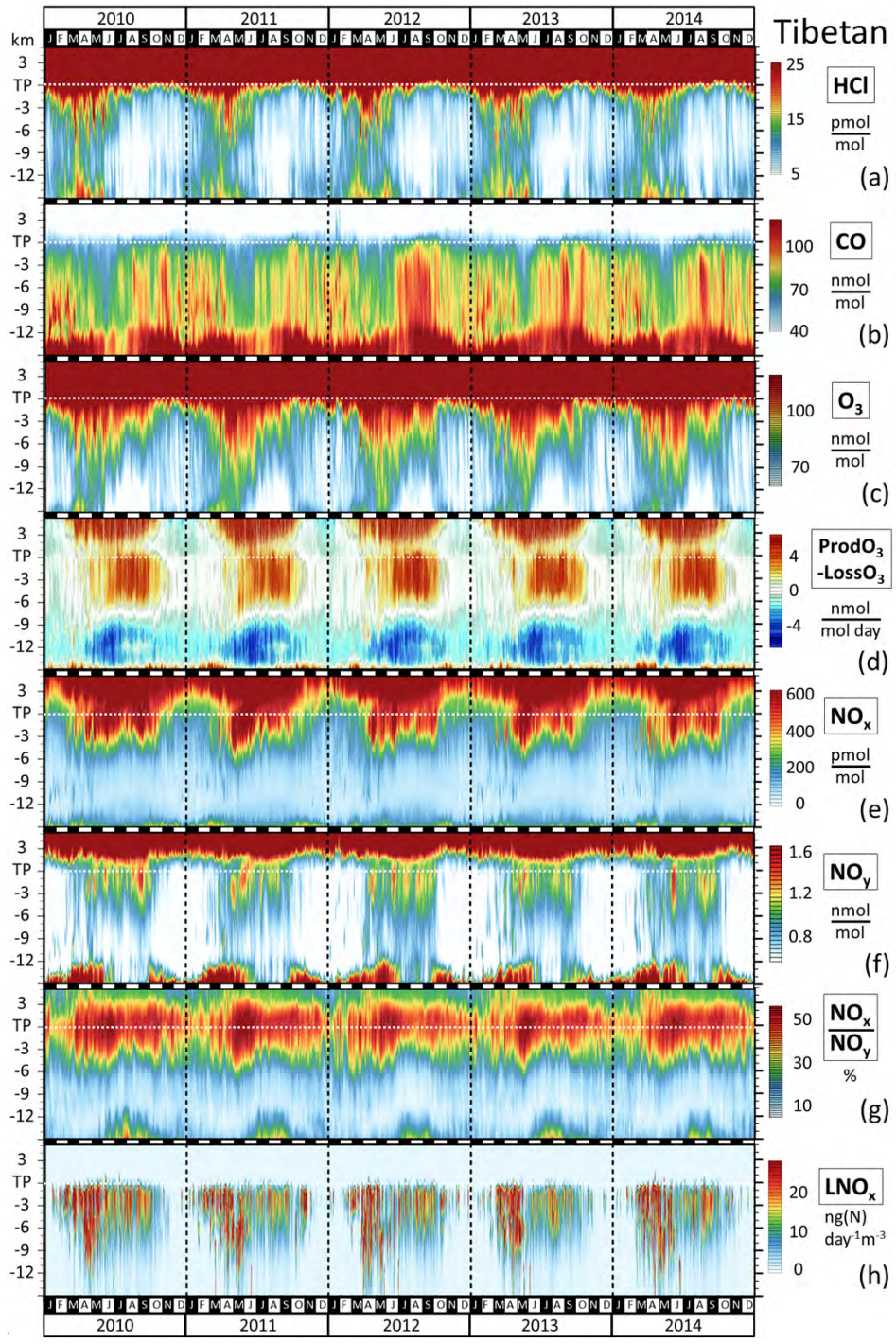

Figure S19. Evolution of simulated trace gas profiles and related diagnostics for the years 2010 – 2014 in the Tibetan ASMA region. The column for the year 2012 is identical to the corresponding panels in Figs. S4, S5.

References

Cecil, D. J.: LIS/OTD 2.5 Degree Low Resolution Monthly Climatology Time Series (LRMTS): Data set available online from the NASA Global Hydrology Resource Center DAAC, Huntsville, Alabama, U.S.A. doi: http://dx.doi.org/10.5067/LIS/LIS-OTD/DATA311, access: https://lightning.nsstc.nasa.gov/data/data_lis-otd-climatology.htm, 18. September 2017, 2006.

Santee, M. L., Manney, G. L., Livesey, N. J., Schwartz, M. J., Neu, J. L., and Read, W. G.: A comprehensive overview of the climatological composition of the Asian summer monsoon anticyclone based on 10 years of Aura Microwave Limb Sounder measurements, Journal of Geophysical Research: Atmospheres, 122, 5491-5514, 10.1002/2016jd026408, 2017.

Formatted: Font: +Body (Calibri), 10 pt

Formatted: Line spacing: 1,5 lines

Formatted: Font: +Body (Calibri), 10 pt

Formatted: Font: +Body (Calibri), 10 pt